

SPIN DECOHERENCE AND MANIPULATION IN
QUANTUM DOTS:
THE ROLE OF THE SPIN-ORBIT INTERACTION

INAUGURALDISSERTATION

zur

Erlangung der Würde eines Doktors der Philosophie

vorgelegt der

Philosophisch-Naturwissenschaftlichen Fakultät

der Universität Basel

von

Massoud Borhani

aus Yazd (Iran)

Basel, 2010

Genehmigt von der Philosophisch-Naturwissenschaftlichen Fakultät auf Antrag
von

Prof. Dr. Daniel Loss

Dr. Jörg Lehmann

Basel, den 9. Dezember 2008

Prof. Dr. Eberhard Parlow
Dekan

Acknowledgments

It is my pleasure to acknowledge here all of those who contributed to this thesis and made this work possible, however, I apologize if I have overlooked some names.

First of all, I would like to thank my advisor, Prof. Daniel Loss, for giving me a chance to join the Condensed Matter Theory group at the University of Basel. His enormous contribution to my thesis, in form of ideas and guidance, provided me with better understanding of the problems I encountered during my research time. Being part of this unique group and interacting with some of the best students and researchers in my field of study, has been always a great honor for me and I am deeply grateful to him. I would like also to thank Prof. Dirk Trautmann who accepted to chair my defense session, and Dr. Jörg Lehmann who agreed to co-referee this thesis and also for his valuable friendship.

During my PhD, working with Dr. Vitaly Golovach was a great opportunity for me; his physical intuition and skills in different mathematical techniques helped me a lot and I appreciate his patience in occasions when I repeated my questions over and over again. My special thanks go to Beat Röthlisberger who helped me to prepare this manuscript for publication and for being a good friend. I am also indebted to the, both current and former, members of the group: Fabian Bodoky, Luca Chirolli, Charles Doiron, Mathias Duckheim, Jan Fischer, Kevin van Hoogdalem, Philipp Traber, Mircea Trif, Robert Andrzej Zak, Oded Zilberberg, Dr. Audrius Alkauskas, Dr. Dan Bohr, Dr. Bernd Braunecker, Dr. Denis Bulaev, Dr. Veronica Cerletti, Dr. Oleg Chalaev, Dr. Stefano Chesi, Dr. Bill Coish, Dr. Hans-Andreas Engel, Dr. Sigurdur Erlingsson, Dr. Hanno Gassmann, Dr. Oliver Gywat, Dr. Tero Heikkilä, Dr. Daniel Klauser, Dr. Verena Koerting, Dr. Minchul Lee, Dr. Andriy Lyakhov, Dr. Joël Peguiron, Dr. Patrik Recher, Dr. Daniel Saraga, Dr. Manuel Schmidt, Dr. Thomas Schmidt, Dr. Christian Schroll, Dr. Dimitrije Stepanenko, Dr. Filippo Troiani, Dr. Oleksandr Tsyplyatyev, Dr. Mihaejlo Vanevic, Prof. Christoph Bruder, Prof. Guido Burkard, Prof. Mahn-Soo Choi, Prof. Jose Carlos Egues, Prof. Alexander Khaetskii, Prof. Dmitrii Maslov, Prof. John Schliemann, Prof. Pascal Simon, Prof. Björn Trauzettel, and the other members of the Physics Department particularly Alex Eichler, Andreas Kleine, Dr. Andreas Aste, Dr. Anthony Clark, Dr. Javad Farahani,

Dr. Reza Ghasemi, and Dr. Daniel Salem, for providing a warm and friendly environment, specially during our coffee breaks and Basel weekend nights from which I have got many unforgettable stories!

It is a great opportunity for me here to go a bit back in time, when I was still a teenager student, and thank my neighbor, Mr. Mohsen Askari, who convinced me not to hate Math, after a long evening discussion. He eventually persuaded me to study mathematics and physics instead of literature; Without his encouragement, I would not be here writing these lines. Furthermore, I am grateful to my former advisors at Sharif University in Iran, Prof. Mehdi Golshani and Prof. Reza Mansouri, who encouraged me to pursue theoretical physics.

Finally, I cordially thank all of my family members for their continuous support and for being there when I needed their help; When I look through these pages, I see them everywhere.

Summary

Solid state based quantum information processing is focused on physical implementation of all necessary elements of quantum computation and quantum information in solid state systems, mainly due to their scalability compared to e.g. optical systems. Among many proposals to realize these types of devices, such as quantum dots as charge qubits or Josephson junction circuits, we study here one of the most promising candidates, i.e., the spin of an electron confined to a quantum dot as a qubit. Experimentally, it has been shown that the relaxation rate of this two level system can be pushed above few seconds in low magnetic fields. Moreover, using spin echo techniques, the spin dephasing time can be maximized up to milliseconds with the current technology. This long spin decay time is one of the main reasons that make this system desirable for quantum computation and quantum information purposes.

In the first chapter of this thesis, we reexamine the recent measurement based proposal called *one-way quantum computation* which exploits entanglement and local measurements as tools to perform quantum computation on N qubits. Although it was suggested in the original work to entangle the qubits via the nearest neighbor Ising interaction, we investigate here how one can generate the so-called *cluster states* with the Heisenberg interaction. We extend our method to include more general forms of Heisenberg interaction such as asymmetric coupling of adjacent qubits. These forms of couplings, rather than Ising interaction, are more encountered in solid state devices, and therefore make it possible to perform one-way quantum computation with electron spins in quantum dots coupled via exchange interaction to their adjacent spins.

Chapters II, III, and IV are devoted to the study of the spin-orbit interaction in heterostructure quantum dots and its effect on the spin dynamics. We observe that one can actually use spin-orbit interaction to manipulate the spin state of an electron on time scales much smaller than the spin dephasing time. Specifically, in chapter II, we study the effect of a nearby functioning quantum point contact (QPC) on the relaxation of the electron spin and show that the charge fluctuations in QPC lead to spin relaxation of the confined electron in the presence of spin-orbit interaction and an applied magnetic field. We also address the relation of this rate to the microscopic parameters of the system and find some geometrical dependence of the spin relaxation time on the orientation of the QPC on the substrate. Moreover, we show in chapters

III and IV that the spin-orbit interaction can play a positive role, in order to rotate the spin around the Bloch sphere. We consider different mechanisms, particularly, Electron Dipole Spin Resonance (EDSR) and holonomic unitary gates in quantum dots. We verify that these mechanisms of spin manipulation can be realized in solid state systems with the state of the art semiconductor technologies.

Chapter V of this thesis covers a slightly different topic and focuses on the role of the Coulomb interaction in electronic transport. There, we review the non-analytic corrections to the Fermi liquid behavior and their consequences on the momentum occupation number of the electrons in a two dimensional electron gas (2DEG). As an example, we calculate the tunneling rate from an interacting electron reservoir onto a quantum dot and compare our result to the corresponding case for electron tunneling between bilayer 2DEGs. Moreover, within *RPA* approximation, we find that the electron-plasmon coupling leads to a quadratic frequency dependence of the electron self energy at low frequencies at the Fermi surface. This correction suppresses the same order corrections due to the particle-hole bubble.

Finally, the details of some calculations, which did not fit into the bulk of the thesis, and the collection of related references are presented at the end of this manuscript.

Contents

Acknowledgments	iii
Summary	v
1 Cluster States	1
1.1 Abstract	1
1.2 Introduction	1
1.3 Cluster states	2
1.4 Cluster states from Heisenberg interaction	3
1.4.1 One-dimensional case	4
1.4.2 Higher dimensions	4
1.4.3 Anisotropic Heisenberg Hamiltonian	5
1.5 Physical realization of the model	7
1.6 Concluding remarks	8
2 QPC-Induced Decay	9
2.1 Abstract	9
2.2 Introduction	9
2.3 The model	11
2.4 The effective Hamiltonian	12
2.5 Coupling constants $\epsilon_{ll'}$	16
2.5.1 Three limiting cases	17
2.5.2 Consistency check	18
2.6 Spin relaxation rate	19
2.6.1 k -independent case	19
2.6.2 k -dependent case	25
2.7 Concluding remarks	26
3 EDSR	27
3.1 Abstract	27
3.2 Introduction	27
3.3 EDSR setup	29
3.4 Spin-electric coupling	32
3.5 Spin dynamics and coherence	36

3.6	p^3 -Dresselhaus terms	37
3.7	Discussions	40
4	Holonomic Spin Rotator	45
4.1	Abstract	45
4.2	Introduction	45
4.3	The Model and Basic Relations	47
4.4	Single Qubit Rotation	52
4.5	Two-qubit gates, read out, and quantum computation	55
5	Momentum Distribution	57
5.1	Abstract	57
5.2	Introduction	57
5.3	Momentum distribution	58
5.4	Electron-Plasmon Coupling	61
5.5	Non-analytic part of the self energy	63
5.6	Tunneling Rate	66
A	Transformation matrix S	69
B	k-dependent coupling constants	71
C	Spin relaxation rate	73
D	Schrieffer-Wolff transformation	77
E	Spin rotation generator	81

Chapter 1

Cluster States From Heisenberg Interaction

1.1 Abstract

We show that a special type of entangled states, cluster states, can be created with Heisenberg interactions and local rotations in $2d$ steps where d is the dimension of the lattice. We find that, by tuning the coupling strengths, anisotropic exchange interactions can also be employed to create cluster states. Finally, we propose electron spins in quantum dots as a possible realization of a one-way quantum computer based on cluster states.

1.2 Introduction

Entanglement plays a crucial role in quantum information processing [1]. Quantum algorithms (in particular, Shor's algorithm, to find the prime factors of an n -bit integer) exploit entanglement to speed up computation. In addition, quantum communication protocols use entangled states as a medium to send information through quantum channels. However, creating entangled states is a great challenge for both theoretical and experimental physicists. Recently, Briegel and Raussendorf [2] introduced a special kind of entangled states, the so-called cluster states, which can be created via an Ising Hamiltonian [3]. These states are eigenstates of certain correlation operators (see Eqs. (1.5) and (1.6) below). It has been shown that via cluster states, one can implement a quantum computer on a lattice of qubits. In this proposal, which is known as "one way quantum computer", information is written onto the cluster, processed, and read out from the cluster by one-qubit measurements [4]. In other words, all types of quantum circuits and quantum gates can be implemented on the lattice of qubits by single-qubit measurements only. The entangled state of the cluster thereby serves as a universal resource for any quantum computation. However, in this model, cluster states are created with

an Ising interaction, which maybe difficult to realize, in particular in a solid state system. Here, we propose an alternative way to create the same states with a Heisenberg interaction (isotropic exchange interaction), but in several steps, where the number of steps depends on the dimension of the lattice of cubic symmetry. Furthermore, we consider some deviations from the Heisenberg Hamiltonian due, for example, to lattice asymmetry, and obtain the same cluster state by tuning the exchange coupling strengths. It turns out that if these coupling strengths satisfy certain conditions, which can be tuned experimentally, we can obtain a cluster state, up to an overall phase. Following Ref. [5], we propose a lattice of electron spins in quantum dots as a possible realization of this scheme in solid-state systems. In this system, electron spins in nearest-neighbor quantum dots are coupled via a Heisenberg exchange interaction.

This paper is organized as follows: Section II is devoted to a brief introduction to cluster states. In Section III we introduce an alternative way to create cluster states. Section III.C considers the anisotropic Heisenberg interaction between qubits on a lattice and how to get cluster states via this interaction. Finally, in Section IV, we propose electron spins in quantum dots as a physical realization of this proposal.

1.3 Cluster states

A cluster state [2] is an entangled state which has special features suitable for implementing a quantum computer on an array of qubits. According to this scheme, we can obtain a cluster state by applying an Ising Hamiltonian ($\hbar = 1$)

$$H = g(t) \sum_{\langle a, a' \rangle} \frac{1 - \sigma_z^{(a)}}{2} \frac{1 - \sigma_z^{(a')}}{2}, \quad (1.1)$$

on a special kind of initial state. Here, $\sigma_i^{(a)}$, $i \in \{x, y, z\}$ are Pauli matrices at lattice site a and $\langle a, a' \rangle$ denotes that a' is the nearest neighbor of a . Furthermore, $g(t)$ allows for a possible overall time dependence. To be specific, consider a qubit chain (see Fig. 1.a) prepared initially in a product state $|\phi_0\rangle = \bigotimes_a |+\rangle_a$, where index a refers to the sites of the qubits and $|+\rangle_a$ is eigenstate of $\sigma_x^{(a)}$ with eigenvalue 1. The time evolution operator for the qubit chain is then given by

$$U(\theta) = \exp \left(-i \theta \sum_a \frac{1 - \sigma_z^{(a)}}{2} \frac{1 - \sigma_z^{(a+1)}}{2} \right), \quad (1.2)$$

with $\theta = \int g(t) dt$. From now on we assume that $\theta = \pi$ [2]. Because the terms in the Ising Hamiltonian (1.1) mutually commute, we can decompose

the evolution operator $U(\pi)$ into two-particle operators as follows,

$$U \equiv U(\pi) = \prod_a U^{(a,a+1)}, \quad (1.3)$$

$$U^{(a,a+1)} = \frac{1}{2} (1 + \sigma_z^{(a)} + \sigma_z^{(a+1)} - \sigma_z^{(a)} \sigma_z^{(a+1)}). \quad (1.4)$$

Therefore, U is a product of two-qubit conditional phase gates [1]. More generally we can define the cluster states as the eigenstates of the following correlation operators

$$K^{(a)} |\phi_{\{\kappa\}}\rangle_{\mathcal{C}} = (-1)^{\kappa_a} |\phi_{\{\kappa\}}\rangle_{\mathcal{C}}, \quad (1.5)$$

$$K^{(a)} \equiv \sigma_x^{(a)} \bigotimes_{b \in nbgh(a)} \sigma_z^{(b)}, \quad (1.6)$$

with $\kappa \in \{0,1\}$. A cluster state is completely specified by the eigenvalue equation (1.5) and it can be shown [6] that all states $|\phi_{\{\kappa\}}\rangle_{\mathcal{C}}$ are equally suitable for computation. For simplicity we put $\kappa = 0$ for all lattice sites. The detailed proof of the above assertions and properties of cluster states, especially their application in implementing a one way quantum computer, have been given in Refs. [4] and [6]. We note that in one dimension a cluster is a qubit chain with nearest neighbor interaction. However, in more than one dimension, the cluster does not have a regular shape. In the latter case, qubits can be arranged in a multi-dimensional square lattice such that only some of the lattice sites are occupied by qubits. A cluster is then defined as a set of qubits where any two qubits are connected by a sequence of neighboring sites that are occupied by a qubit.

1.4 Cluster states from Heisenberg interaction

Cluster states are produced through Ising interactions. However, an ideal Ising interaction is difficult to obtain in nature especially in a solid state environment. So, how can such states be created? The usual spin-spin interaction is (nearly) isotropic in spin space and is described by the Heisenberg Hamiltonian [7],

$$H = -J \sum_{\langle ij \rangle} S_x^{(i)} S_x^{(j)} + S_y^{(i)} S_y^{(j)} + S_z^{(i)} S_z^{(j)}, \quad (1.7)$$

$$\vec{S}^{(i)} = (S_x^{(i)}, S_y^{(i)}, S_z^{(i)}) = \frac{1}{2} \vec{\sigma}^{(i)} \quad (\hbar = 1), \quad (1.8)$$

where $\vec{S}^{(i)}$ and $\vec{S}^{(j)}$ are spin- $\frac{1}{2}$ operators at lattice sites i and j , and J is the exchange coupling constant, which is assumed to be constant for all spin pairs and is positive (negative) for ferromagnetic (antiferromagnetic) coupling. Next we

describe a method to create cluster states via Heisenberg instead of Ising interaction. We start with one dimension and then generalize to higher dimensions.

1.4.1 One-dimensional case

Recall that all operators $U^{(a,a+1)}$ in U (Eqs. (4.13) and (1.4) above) mutually commute and they can therefore be applied in arbitrary order, i.e. at the same or different times. (see Fig. 1.a). Suppose we have a one-dimensional N -qubit chain where all qubits are prepared in the $|+\rangle$ state. The initial state of the cluster is then (as before) $\bigotimes_{a \in \mathcal{C}} |+\rangle_a$, and the index a refers to the lattice site. The idea is to apply first the sequence $U^{(1,2)} U^{(3,4)} U^{(5,6)} \dots$, and then in a second step, the sequence $U^{(2,3)} U^{(4,5)} U^{(6,7)} \dots$. In other words, first we let qubits 1-2, 3-4, 5-6, ... interact with each other, and then qubits 2-3, 4-5, 6-7, ... (Fig. 1.b). We obtain the same result (4.13), but now we have entangled the qubits in our chain *pairwise* in each step. This means that each qubit is entangled with only one of its nearest neighbors in each step. In one dimension, there are two nearest neighbors for each qubit, thus we entangle our chain in two steps.

We note that $U^{(a,a+1)}$, given by Eq.(1.4), describes a conditional phase shift. On the other hand, in Ref. [5] it was shown that this evolution operator can also be realized with a Heisenberg Hamiltonian (obtained e.g. via a Hubbard model) and local one-qubit rotations (see also next section). Therefore, the problem of generating a cluster state with a Heisenberg interaction has been solved provided in each step each qubit interacts with only one of its nearest neighbors.

1.4.2 Higher dimensions

In two dimensions, the minimum number of steps increases to four in a two dimensional square lattice. In general for a d -dimensional cubic lattice, the minimum number of steps required is $2d$. (Note that cluster states are only defined on lattices with cubic symmetry. See also the last paragraph in Section II).

However, in dimensions higher than one, there is no regular shape for an arbitrary cluster. How then, can we obtain cluster states with just $2d$ steps? There may be several optimal ways to do this but we mention only one. For simplicity, consider a two dimensional cluster and suppose that this cluster can be contained within a rectangle of n rows and m columns. Now, entangle all qubits in the cluster within each of these n rows independently (recall that each row requires two steps to be entangled). Then, do the same for the m columns. There is no need to worry about the qubits which are within the rectangle but not part of the cluster, since they are excluded automatically if

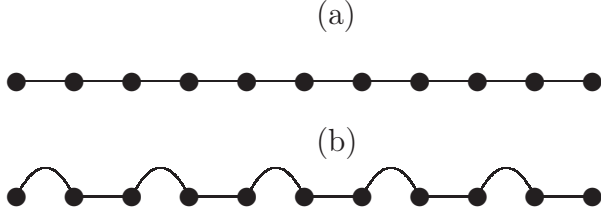


Figure 1.1: (a) A one-dimensional cluster (a qubit chain). The connecting lines represent the interaction between nearest neighbors. (b) An alternative way to entangle a one-dimensional cluster. The qubits which are connected by straight lines are entangled in the first step and those connected by semicircles are entangled in the subsequent step.

we do not entangle them to their nearest neighbors. The idea is the same for $d = 3$ cubic lattice, except that we would need 6 steps to entangle the cluster.

1.4.3 Anisotropic Heisenberg Hamiltonian

We do not consider the most general form of an anisotropic Heisenberg model since it is beyond the scope of this work. Here we introduce a special case, known as *symmetric* anisotropic Heisenberg model (SAH) which does not include the cross-spin terms. It has the following form in one dimension

$$H_{SAH} = \sum_a H_{SAH}^{(a,a+1)}, \quad (1.9)$$

$$H_{SAH}^{(a,a+1)} = \alpha(t) S_x^{(a)} S_x^{(a+1)} + \beta(t) S_y^{(a)} S_y^{(a+1)} + \gamma(t) S_z^{(a)} S_z^{(a+1)}. \quad (1.10)$$

This situation occurs for example, when our lattice does not have enough symmetry to use the isotropic interaction. However,

$$[S_p^{(a)} S_p^{(a+1)}, S_q^{(a)} S_q^{(a+1)}] = 0, \quad (1.11)$$

$$\forall p, q = x, y, z.$$

Therefore, these three terms in the Hamiltonian mutually commute and consequently when we write the unitary evolution operator for two adjacent qubits, $U_{SAH}^{(a,a+1)}$, it can be decomposed into three unitary operators. The order of application of these three operators does not matter

$$U_{SAH}^{(a,a+1)} = U_{xx}^{(a,a+1)} U_{yy}^{(a,a+1)} U_{zz}^{(a,a+1)}, \quad (1.12)$$

$$U_{xx}^{(a,a+1)} = \exp(-i J_{xx} S_x^{(a)} S_x^{(a+1)}), \quad (1.13)$$

$$U_{yy}^{(a,a+1)} = \exp(-i J_{yy} S_y^{(a)} S_y^{(a+1)}), \quad (1.14)$$

$$U_{zz}^{(a,a+1)} = \exp(-i J_{zz} S_z^{(a)} S_z^{(a+1)}). \quad (1.15)$$

Now, according to our alternative method to create cluster states, if the coefficients α , β and γ satisfy the following conditions,

$$J_{xx} = \int \alpha(t) dt = 4n\pi, \quad (1.16)$$

$$J_{yy} = \int \beta(t) dt = 4m\pi, \quad (1.17)$$

$$J_{zz} = \int \gamma(t) dt = (2k+1)\pi, \quad (1.18)$$

where n , m , and k are arbitrary integers, Then $U_{xx}^{(a,a+1)}$ and $U_{yy}^{(a,a+1)}$ are just *unity* operators (up to a minus sign) and do not affect the initial state ¹. If we could tune these coefficients properly in our lattice, we would get the same cluster states, up to some local (single-qubit) operations. The crucial point is that $U_{SAH}^{(a,a+1)}$ and $U_{SAH}^{(a+1,a+2)}$ do not commute and thereby, we can *not* decompose U_{SAH} , the total evolution operator of the cluster with an SAH interaction, into two-qubit evolution operators. This is why we need at least two steps to entangle the chain.

In general, when the Hamiltonian includes cross-spin terms, (the asymmetric anisotropic Heisenberg model (AAH)), the problem can not be solved exactly because the terms in the AAH Hamiltonian do not mutually commute. There is still a hope of solving this problem if we have the following interaction between spins ²:

$$H_{AAH}^{(a,a+1)} = \alpha'(t) S_x^{(a)} S_y^{(a+1)} + \beta'(t) S_y^{(a)} S_x^{(a+1)} + \gamma'(t) S_z^{(a)} S_z^{(a+1)}. \quad (1.19)$$

Again, the terms in this Hamiltonian mutually commute and we can decompose the two-qubit evolution operator like above. However, this Hamiltonian is related to the previous Hamiltonian (1.10) via a single-qubit unitary transformation (through $\pi/2$ -rotation of one of the spins about the z -axis) and therefore, both have the same structure. In the end, we emphasize that the basic cornerstone of this method is that in each step, each qubit can interact with *only* one of its nearest neighbors. Generalizing the above method to higher dimensions is straightforward (see previous section). Therefore we have shown that the problem of creating cluster states with more realistic interaction models other than Ising, can be solved exactly.

¹For the special case $n = m = 0$, the time evolution operator $U_{SAH}^{(a,a+1)}$ reduces to Eq. (1.4), up to a minus sign, depending on the value of k .

² x , y and z can be changed in cyclic permutation.

1.5 Physical realization of the model

In Refs. [5], [8] and [9], a detailed scenario has been proposed for how quantum computation may be achieved in a coupled quantum dots system. In this proposal, a qubit is realized as the spin of the excess electron on a single-electron quantum dot. A mechanism has been proposed there for two-qubit quantum-gate operation that operates by a purely electrical gating of the tunneling barrier between neighboring quantum dots, rather than by spectroscopic manipulation as in other models. Consider two quantum dots which are labeled by “1” and “2” and coupled to each other via exchange interaction (see below). If the barrier potential is “high”, tunneling is forbidden between dots, and the qubit states are held stably without evolution in time (t). If the barrier is pulsed to a “low” voltage, the usual physics of the Hubbard model [7] says that the spins will be subject to a transient Heisenberg coupling,

$$H = J(t)\vec{S}^{(1)} \cdot \vec{S}^{(2)} , \quad (1.20)$$

where $J(t)$ is the time-dependent exchange constant which is produced by the turning on and off of the tunneling matrix element [5, 8].

For instance, a quantum XOR gate is obtained by a simple sequence of operations [5]:

$$U_{XOR} = e^{i\frac{\pi}{2}S_z^{(1)}} e^{-i\frac{\pi}{2}S_z^{(2)}} U_{sw}^{\frac{1}{2}} e^{i\pi S_z^{(1)}} U_{sw}^{\frac{1}{2}} , \quad (1.21)$$

where U_{sw} is a swap gate, created in this model via Heisenberg interaction, and $e^{i\pi S_z^{(1)}}$ etc. are single-qubit operations only, which can be realized by applying local Zeeman interaction. (It has been established that XOR along with single-qubit operations may be assembled to do any quantum computation [10].) Note that the XOR of Eq. (1.21) is given in the basis where it has the form of a conditional phase-shift operation; the standard XOR is obtained by a simple basis change for qubit “2”. According to Eq. (1.21), we need 5 steps to realize an XOR gate. However, in Ref. [11] it has been shown that for a certain choice of system parameters (for example, opposite direction of the local B fields), we can generate an XOR gate in one step. The crucial observation now is that the XOR operation can be written as [5] $U_{XOR} = \frac{1}{2} + S_z^{(1)} + S_z^{(2)} - 2S_z^{(1)}S_z^{(2)}$, which has exactly the same form as $U^{(a,a+1)}$ in Eq. (1.4). In other words, we can generate the operation $U^{(a,a+1)}$ (and thus the cluster states) with the Heisenberg interaction as described e.g. by the sequence in Eq. (1.21). We finally note that an alternative way to achieve the XOR operation is given by [5] $U_{XOR} = e^{i\pi S_z^{(1)}} U_{sw}^{-\frac{1}{2}} e^{-i\frac{\pi}{2}S_z^{(1)}} U_{sw} e^{i\frac{\pi}{2}S_z^{(1)}} U_{sw}^{\frac{1}{2}}$. This form has the potential advantage that the single qubit operations involve only spin 1.

The mechanisms described above for performing gate operations with spin qubits are independent of the details of the pulse shape $P(t)$, where P stands for the exchange coupling J or the Zeeman interaction. It is only the value of the integral $\int_0^\tau P(t)dt \pmod{2\pi}$ which determines the quantum gate action.

This is true provided that the parameters $P(t)$ are switched adiabatically, guaranteeing the validity of the effective Hamiltonian Eq. (1.20). The unwanted admixture of a state with double occupation of a dot in the final state is found to be tiny if a suitable pulse is used and the adiabaticity criterion is fulfilled [12, 13].

We note that as long as an XOR (or CNOT) gate is realized, cluster states (and consequently, a one-way quantum computer) can be generated. This result does not depend on the type of interaction in the system. Therefore, other proposals such as trapped ion [14] and superconducting qubits [15], can be used as well, to create cluster states.

1.6 Concluding remarks

In summary, an alternative way, using Heisenberg interaction between qubits, was introduced to create cluster states which is useful for solid state systems. In this method the qubits in the cluster are entangled pairwise, leading to $2d$ steps in d -dimensional cubic lattices. Furthermore, by tuning the coupling strengths of the interaction, it is possible to create cluster states via anisotropic Heisenberg exchange interaction. Experimentally, these cluster states can be generated in coupled quantum dots or similar systems.

Chapter 2

Spin Decay in a Quantum Dot Coupled to a Quantum Point Contact

2.1 Abstract

We consider a mechanism of spin decay for an electron spin in a quantum dot due to coupling to a nearby quantum point contact (QPC) with and without an applied bias voltage. The coupling of spin to charge is induced by the spin-orbit interaction in the presence of a magnetic field. We perform a microscopic calculation of the effective Hamiltonian coupling constants to obtain the QPC-induced spin relaxation and decoherence rates in a realistic system. This rate is shown to be proportional to the shot noise of the QPC in the regime of large bias voltage and scales as a^{-6} where a is the distance between the quantum dot and the QPC. We find that, for some specific orientations of the setup with respect to the crystallographic axes, the QPC-induced spin relaxation and decoherence rates vanish, while the charge sensitivity of the QPC is not changed. This result can be used in experiments to minimize QPC-induced spin decay in read-out schemes.

2.2 Introduction

Recent progress in nanotechnology has enabled access to the electron spin in semiconductors in unprecedented ways [9, 16, 17], with the electron spin in quantum dots being a promising candidate for a qubit due to the potentially long decoherence time of the spin [5, 18]. Full understanding of the decoherence processes of the electron spin is thus crucial. On the other hand, as a part of a quantum computer, read-out systems play an essential role in determining the final result of a quantum computation. However, read-out devices, in general, affect the spin state of the system in an undesired way. Quantum point contacts

(QPCs) which are used as charge detectors [19–25], in particular, couple to the spin via the spin-orbit interaction. For small GaAs quantum dots, the spin-orbit length ($\lambda_{SO} \approx 8 \mu\text{m}$) is much larger than the dot size ($\lambda_d \approx 50 \text{ nm}$) and thus the spin-orbit interaction presents a small perturbation. Nevertheless, we will see that shot noise in the QPC can induce an appreciable spin decay via this weak spin-orbit coupling.

Quite remarkably, the number of electrons in quantum dots can be tuned starting from zero [26–28]. More recently, Zeeman levels have been resolved [29] and the spin relaxation time (T_1) has been measured, yielding times of the order of milliseconds in the presence of an in-plane magnetic field of 8 T [22, 23]. In these experiments, based on spin-charge conversion [5], use is made of a QPC located near the quantum dot as a sensitive charge detector to monitor changes of the number of electrons in the dot. The shot noise in the QPC affects the electron charge in the quantum dot via the Coulomb interaction, and therefore, it can couple to the electron spin as well, via the spin-orbit interaction. While charge decoherence in a quantum dot due to a nearby functioning QPC has been studied both experimentally [20, 21] and theoretically [30–32], we show here that the same charge fluctuations in the QPC introduce spin decay via spin-orbit and Zeeman interactions. Note that several read-out schemes utilizing a QPC have been considered before [33] in the context of the spin qubit. However, in Ref. [33] the QPC was used for charge read-out, while the spin state of the qubit was converted into the charge state of a *reference* dot [5]. Recently, a different read-out scheme has been implemented [22], in which the reference dot was replaced by a Fermi lead and the QPC was coupled directly to the spin qubit.

The effect of spin-orbit interaction on spin relaxation and decoherence was considered in Ref. [34]. There, it was shown that the decoherence time T_2 due to spin-orbit interaction approaches its upper bound [34], i.e. $T_2 = 2T_1$, determined by spin-flip processes [34, 35]. Measurements of T_1 have been performed on spins in electrostatically confined (lateral) quantum dots [22] ($T_1 \simeq 0.85 \text{ ms}$) and self-assembled quantum dots [36] ($T_1 \simeq 20 \text{ ms}$). The measured spin relaxation times T_1 in both cases agree well with the theory in Refs. [34] and [35]. In addition to the spin-orbit interaction, the hyperfine interaction plays an important role in quantum dots [37–50]. Measurements of the spin decoherence time T_2 have recently been performed in a self-assembled quantum dot [47] ($T_2^* \simeq 16 \text{ ns}$) as well as in a double-dot setup for singlet-triplet decoherence ($T_2 \simeq 10 \mu\text{s}$) [50]. Finally we note that a number of alternative schemes to measure the decoherence time of the electron spin in quantum dots have been proposed [51–53].

Motivated by these recent experiments, we study here the effect of the QPC on spin relaxation and decoherence in a quantum dot. For this, we first derive an effective Hamiltonian for the spin dynamics in the quantum dot and find a transverse (with respect to the external magnetic field) fluctuating

magnetic field. We calculate microscopically the coupling constants of the effective Hamiltonian by modeling the QPC as a one-dimensional channel with a tunnel barrier. We show that this read-out system speeds up the spin decay and derive an expression for the spin relaxation time T_1 . However, there are some regimes in which this effect vanishes, in the first order of spin-orbit interaction. The relaxation time will turn out to be strongly dependent on the QPC orientation on the substrate, the distance between the QPC and the quantum dot, the direction of the applied magnetic field, the Zeeman splitting E_Z , the QPC transmission coefficient \mathcal{T} , and the screening length λ_{sc} (see Fig. 2.1). Although this effect is, generally, not larger than other spin decay mechanisms (e.g. coupling of spin to phonons [34] or nuclear spins [44–46]), it is still measurable with the current setups under certain conditions. The following results could be of interest to experimentalists to minimize spin decay induced by QPC-based charge detectors.

The paper is organized as follows. In Section II we introduce our model for a quantum dot coupled to a quantum point contact and the corresponding Hamiltonian. Section III is devoted to the derivation of the effective Hamiltonian for the electron spin in the quantum dot. In Section IV we derive microscopic expressions for the coupling constants of the effective Hamiltonian and discuss different regimes of interest. Finally, in Section V, we calculate the electron spin relaxation time T_1 due to the QPC and make numerical predictions for typical lateral quantum dots.

2.3 The model

We consider an electron in a quantum dot and a nearby functioning quantum point contact (QPC), see Fig. 2.1, embedded in a two-dimensional electron gas (2DEG). We model the QPC as a one-dimensional wire coupled via the Coulomb interaction to the electron in the quantum dot. We also assume that there is only one electron inside the dot, which is feasible experimentally [22, 24, 26–29]. The Hamiltonian describing this coupled system reads $H = H_d + H_Z + H_{SO} + H_Q + H_{Qd}$, where

$$H_d = \frac{p^2}{2m^*} + U(\mathbf{r}), \quad (2.1)$$

$$H_Z = \frac{1}{2}g\mu_B\mathbf{B} \cdot \boldsymbol{\sigma} = \frac{1}{2}E_Z\mathbf{n} \cdot \boldsymbol{\sigma}, \quad (2.2)$$

$$H_{SO} = \beta(-p_x\sigma_x + p_y\sigma_y) + \alpha(p_x\sigma_y - p_y\sigma_x), \quad (2.3)$$

$$H_Q = \sum_{lk\sigma} \epsilon_k \bar{C}_{lk\sigma}^\dagger \bar{C}_{lk\sigma}, \quad (2.4)$$

$$H_{Qd} = \sum_{l'k'k'\sigma} \eta_{ll'}(\mathbf{r}) \bar{C}_{lk\sigma}^\dagger \bar{C}_{l'k'\sigma}. \quad (2.5)$$

Here, Q refers to the QPC and d to the dot, $\mathbf{p} = -i\hbar\nabla + (e/c)\mathbf{A}(\mathbf{r})$ is the electron 2D momentum, $U(\mathbf{r})$ is the lateral confining potential, with $\mathbf{r} = (x, y)$, m^* is the effective mass of the electron, and $\boldsymbol{\sigma}$ are the Pauli matrices. The 2DEG is perpendicular to the z direction. The spin-orbit Hamiltonian H_{SO} in Eq.(2.3) includes both Rashba [54] spin-orbit coupling (α), due to asymmetry of the quantum well profile in the z direction, and Dresselhaus [55] spin-orbit couplings (β), due to the inversion asymmetry of the GaAs lattice. The Zeeman interaction H_Z in Eq. (3.6) introduces a spin quantization axis along $\mathbf{n} = \mathbf{B}/B = (\cos\varphi\sin\vartheta, \sin\varphi\sin\vartheta, \cos\vartheta)$. The QPC consists of two Fermi liquid leads coupled via a tunnel barrier and is described by the Hamiltonian H_Q , where $\bar{C}_{lk\sigma}^\dagger$, with $l = L, R$, creates an electron incident from lead l , with wave vector k and spin σ . We use the overbar on, e.g., $\bar{C}_{lk\sigma}$ to denote the scattering states in the absence of electron on the dot. The Hamiltonian H_{Qd} in Eq. (2.5) describes the coupling between the quantum dot electron and the QPC electrons. We assume that the coupling is given by the screened Coulomb interaction,

$$\eta_W(\mathbf{r}) = \langle \bar{l}k | \frac{e^2}{\kappa|\mathbf{r} - \mathbf{R}|} \tilde{\delta}(\mathbf{R} - \mathbf{a}) | \bar{l}'k' \rangle, \quad (2.6)$$

where $\mathbf{R} = (X, Y)$ is the coordinate of the electron in the QPC and κ is the dielectric constant. The Coulomb interaction is modulated by a dimensionless screening factor $\tilde{\delta}(\mathbf{R} - \mathbf{a})$, where $\mathbf{a} = (0, a)$ gives the QPC position (see Fig. 2.1).¹ The quantum dot electron interacts with the QPC electrons mostly at the tunnel barrier; away from the tunnel barrier the interaction is screened due to a large concentration of electrons in the leads. For the screening factor we assume, in general, a function which is peaked at the QPC and has a width $2\lambda_{sc}$ (see Fig. 2.1). Note that λ_{sc} is generally different from the screening length in the 2DEG and depends strongly on the QPC geometry and size. Generally, η_W are k -dependent, however, their k -dependence turns out to be weak and will be discussed later.

2.4 The effective Hamiltonian

The quantum dot electron spin couples to charge fluctuations in the QPC via the spin-orbit Hamiltonian (2.3). The charge fluctuations are caused by electrons passing through the QPC. To derive an effective Hamiltonian for the coupling of spin to charge fluctuations, we perform a Schrieffer-Wolff transformation [56,57], $\tilde{H} = \exp(S)H\exp(-S)$, and remove the spin-orbit Hamiltonian in leading order. We thus require that $[H_d + H_Z, S] = H_{SO}$, under the condition $\lambda_d \ll \lambda_{SO}$, where λ_d is the quantum dot size and $\lambda_{SO} = \hbar/m^*(|\beta| + |\alpha|)$

¹Strictly speaking, the screening factor depends also on \mathbf{r} , $\tilde{\delta}(\mathbf{R} - \mathbf{a}, \mathbf{r})$. However, since usually $\lambda_d \lesssim \lambda_s$, we approximate $\tilde{\delta}(\mathbf{R} - \mathbf{a}, \mathbf{r}) \approx \tilde{\delta}(\mathbf{R} - \mathbf{a}, 0) \equiv \tilde{\delta}(\mathbf{R} - \mathbf{a})$, keeping in mind that $|\mathbf{r}| \lesssim \lambda_d$.

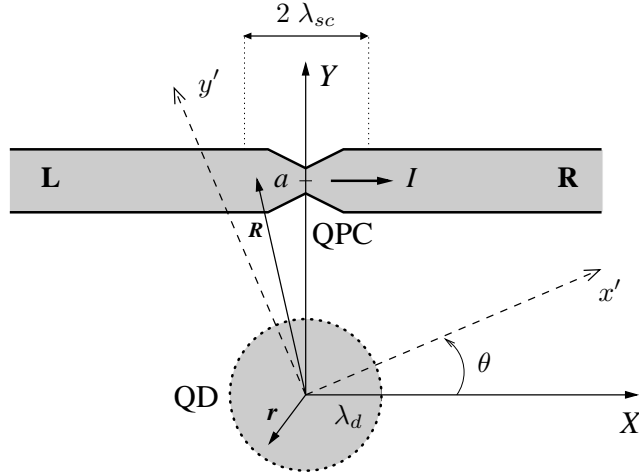


Figure 2.1: Schematic of the quantum dot (QD) coupled to a QPC. The (X, Y) frame gives the setup orientation, left (L) and right (R) leads, with respect to the crystallographic directions $x' \equiv [110]$ and $y' \equiv [\bar{1}10]$. The dot has a radius λ_d and is located at a distance a from the QPC. The vector \mathbf{R} describes the QPC electrons and \mathbf{r} refers to the coordinate of the electron in the dot. The noise of the QPC current I perturbs the electron spin on the dot via the spin-orbit interaction.

is the shortest spin-orbit length. The transformed Hamiltonian is then given by

$$\tilde{H} = H_d + H_Z + H_Q + H_{Qd} + [S, H_{Qd}], \quad (2.7)$$

$$S = \frac{1}{L_d + L_Z} H_{SO} = \frac{1}{L_d} \sum_{m=0}^{\infty} \left(-L_Z \frac{1}{L_d} \right)^m H_{SO}, \quad (2.8)$$

$$H_{SO} = iL_d(\boldsymbol{\sigma} \cdot \boldsymbol{\xi}), \quad (2.9)$$

where L is Liouville superoperator for a given Hamiltonian defined by $LA \equiv [H, A]$ and $\boldsymbol{\xi}$ is a vector in the 2DEG plane and has a simple form in the coordinate frame $x' = (x + y)/\sqrt{2}$, $y' = (y - x)/\sqrt{2}$, $z' = z$, namely, $\boldsymbol{\xi} = (y'/\lambda_-, x'/\lambda_+, 0)$, where $\lambda_{\pm} = \hbar/m^*(\beta \pm \alpha)$ are the spin-orbit lengths. For a harmonic dot confinement $U(r) = \frac{1}{2}m^*\omega_0^2 r^2$, we have

$$\frac{1}{L_d} x = \frac{-i}{\hbar m^* \omega_0^2} \left(p_x + \frac{eB_z}{c} y \right), \quad (2.10)$$

$$\frac{1}{L_d} y = \frac{-i}{\hbar m^* \omega_0^2} \left(p_y - \frac{eB_z}{c} x \right), \quad (2.11)$$

$$\frac{1}{L_d} p_j = \frac{im^*}{\hbar} r_j, \quad (j = x, y). \quad (2.12)$$

In addition, we have the following relations for the Zeeman Liouvillian

$$L_Z^m(\boldsymbol{\sigma} \cdot \boldsymbol{\xi}) = \begin{cases} iE_Z^m[\mathbf{n} \times \boldsymbol{\xi}] \cdot \boldsymbol{\sigma}, & \text{for odd } m > 0 \\ -E_Z^m[\mathbf{n} \times (\mathbf{n} \times \boldsymbol{\xi})] \cdot \boldsymbol{\sigma}, & \text{for even } m > 0, \end{cases} \quad (2.13)$$

where $E_Z = g\mu_B B$ is the Zeeman splitting. The last term in Eq. (2.7) gives the coupling of the dot spin to the QPC charge fluctuations. The transformation matrix S (to first order in spin-orbit interaction) can be derived by using the above relations (see Appendix A). We obtain

$$-iS = \boldsymbol{\xi} \cdot \boldsymbol{\sigma} + [\mathbf{n} \times \boldsymbol{\xi}_1] \cdot \boldsymbol{\sigma} - [\mathbf{n} \times [\mathbf{n} \times \boldsymbol{\xi}_2]] \cdot \boldsymbol{\sigma}, \quad (2.14)$$

$$\boldsymbol{\xi}_1 = ((\alpha_1 p_{y'} + \alpha_2 x')/\lambda_-, (\alpha_1 p_{x'} - \alpha_2 y')/\lambda_+, 0), \quad (2.15)$$

$$\boldsymbol{\xi}_2 = ((\beta_1 p_{x'} + \beta_2 y')/\lambda_-, (-\beta_1 p_{y'} + \beta_2 x')/\lambda_+, 0), \quad (2.16)$$

$$\alpha_1 = \frac{\hbar}{m^*} \frac{E_Z[E_Z^2 - (\hbar\omega_0)^2]}{(E_Z^2 - E_+^2)(E_Z^2 - E_-^2)}, \quad (2.17)$$

$$\alpha_2 = \frac{E_Z \hbar\omega_c (\hbar\omega_0)^2}{(E_Z^2 - E_+^2)(E_Z^2 - E_-^2)}, \quad (2.18)$$

$$\beta_1 = \frac{\hbar}{m^*} \frac{E_Z^2 \hbar\omega_c}{(E_Z^2 - E_+^2)(E_Z^2 - E_-^2)}, \quad (2.19)$$

$$\beta_2 = E_Z^2 \frac{(\hbar\omega_c)^2 + (\hbar\omega_0)^2 - E_Z^2}{(E_Z^2 - E_+^2)(E_Z^2 - E_-^2)}, \quad (2.20)$$

where $E_{\pm} = \hbar\omega \pm \hbar\omega_c/2$, with $\omega = \sqrt{\omega_0^2 + \omega_c^2/4}$ and $\omega_c = eB_z/m^*c$. Here, we assume $E_{\pm} - |E_Z| \gg |E_Z \lambda_d/\lambda_{SO}|$, which ensures that the lowest two levels in the quantum dot have spin nature. Below, we consider low temperatures T and bias $\Delta\mu$, such that $T, \Delta\mu \ll E_{\pm} - |E_Z|$, (hence only the orbital ground state is populated so that its Zeeman sublevels constitute a two level system) and average over the dot ground state in Eq. (2.7). We obtain, using Eqs. (2.10)-(2.13), the following effective spin Hamiltonian

$$H_{\text{eff}} = \frac{1}{2} g\mu_B [\mathbf{B} + \delta\mathbf{B}(t)] \cdot \boldsymbol{\sigma}, \quad (2.21)$$

and the effective fluctuating magnetic field $\delta\mathbf{B}(t)$ is then given by the operator

$$\delta\mathbf{B}(t) = 2\mathbf{B} \times [\boldsymbol{\Omega}_1(t) + \mathbf{n} \times \boldsymbol{\Omega}_2(t)], \quad (2.22)$$

$$\boldsymbol{\Omega}_1 = \frac{e\hbar^2 \gamma_1}{m^*} (\lambda_-^{-1} \mathcal{E}_{y'}, \lambda_+^{-1} \mathcal{E}_{x'}, 0),$$

$$\boldsymbol{\Omega}_2 = \frac{e\hbar^2 \gamma_2}{m^*} (-\lambda_-^{-1} \mathcal{E}_{x'}, \lambda_+^{-1} \mathcal{E}_{y'}, 0),$$

$$\gamma_1 = \frac{m^*}{\hbar E_Z} \alpha_1 = \frac{E_Z^2 - (\hbar\omega_0)^2}{(E_+^2 - E_Z^2)(E_-^2 - E_Z^2)},$$

$$\gamma_2 = \frac{m^*}{\hbar E_Z} \beta_1 = \frac{E_Z \hbar\omega_c}{(E_+^2 - E_Z^2)(E_-^2 - E_Z^2)},$$

where we have gone to the interaction picture with respect to the lead Hamiltonian $H'_Q = H_Q + \langle H_{Qd} \rangle_d$ and omitted a spin-independent part. Note that the coordinate-dependent part of S drops out and thus α_2, β_2 do not enter. Here and below, we use $\langle \dots \rangle_d$ to denote averaging over the dot ground state. Note that H'_Q describes the QPC, while it is electrostatically influenced by the quantum dot with one electron in the ground state. Obviously, H'_Q can be rewritten in the same form as H_Q in Eq. (2.4), but with a different scattering phase in the scattering states. To denote the new scattering states, we omit the *overbar* sign in our notations. We have introduced an effective electric field operator $\mathcal{E}(t)$ in the interaction picture, [57]

$$\begin{aligned} \mathcal{E}(t) &= \frac{1}{e} \langle \nabla H_{Qd}(t) \rangle_d \\ &= \sum_{ll'kk'\sigma} \varepsilon_{ll'} e^{i(\mu_l - \mu_{l'})t/\hbar} C_{lk\sigma}^\dagger(t) C_{l'k'\sigma}(t), \end{aligned} \quad (2.23)$$

$$\varepsilon_{ll'} = \frac{1}{e} \langle \nabla \eta_{ll'}(\mathbf{r}) \rangle_d, \quad (2.24)$$

where the fermionic operators $C_{l'k'\sigma}$ correspond to scattering states in the leads with the dot being occupied by one electron (H'_Q is diagonal in $C_{l'k'\sigma}$). Here, $\mu_l, l = L, R$, are the chemical potentials of the left (L) and right (R) leads, with $\Delta\mu = \mu_L - \mu_R$ being the voltage bias applied to the QPC driving a current I . Note that in the absence of screening ($\tilde{\delta}(\mathbf{R} - \mathbf{a}) = 1$ in Eq. (2.6)), \mathcal{E} coincides with the electric field that the quantum dot electron exerts on the QPC electrons.

As a first result, we note that the fluctuating quantum field $\delta\mathbf{B}(t)$ is transverse with respect to the (classical) applied magnetic field \mathbf{B} (*cf.* Ref. [34]). The magnetic field fluctuations originate here from orbital fluctuations that couple to the electron spin via the spin-orbit interaction. The absence of time reversal symmetry, which is removed by the Zeeman interaction, is crucial for this coupling. We assume no fluctuations in the external magnetic field \mathbf{B} . In our model, the dot electron spin couples to a bath of fermions, in contrast to Ref. [34] where the bath (given by phonons) was bosonic.

To calculate the coupling constants $\varepsilon_{ll'}$ in Eq. (2.23), it is convenient to first integrate over the coordinates of the dot electron. We thus obtain $\mathcal{E}(\mathbf{R}) = \mathcal{E}_0(\mathbf{R})\tilde{\delta}(\mathbf{R} - \mathbf{a})$, see Eq. (2.6), where \mathbf{R} refers to the location of the electrons in the QPC and the bare (unscreened) electric field is given by

$$\begin{aligned} \mathcal{E}_0(\mathbf{R}) &= \frac{e}{\kappa} \left\langle \frac{\mathbf{R} - \mathbf{r}}{|\mathbf{R} - \mathbf{r}|^3} \right\rangle_d \\ &= \frac{e\mathbf{R}}{\kappa R^3} \left(1 + \frac{3}{4} \frac{\lambda_d^2}{R^2} + \dots \right). \end{aligned} \quad (2.25)$$

Consequently, the coupling constants in Eq. (2.23) read $\varepsilon_{ll'} = \langle lk | \mathcal{E}(\mathbf{R}) | l'k' \rangle$, where $|lk\rangle$ denote the scattering states in the leads. Here, we have assumed a

parabolic confinement for the electron in the dot, set the origin of coordinates in the dot center ($\langle \mathbf{r} \rangle_d = 0$) and averaged with the dot wave function

$$\Psi_d(\mathbf{r}) = \exp(-r^2/2\lambda_d^2)/\lambda_d\sqrt{\pi}, \quad (2.26)$$

which is the ground state of the electron in a symmetric harmonic potential in two dimensions. While we choose a very special form for the ground state wave function, this does not affect substantially the final result, i.e. the relaxation time T_1 . This is because any circularly symmetric wave function leads to the same form for $\mathcal{E}_0(\mathbf{R})$ except that it just alters the second term in Eq. (2.25) which is very small compared to the first term (about one hundredth) and negligible. An analogous argument applies to asymmetric wave functions.

2.5 Coupling constants $\varepsilon_{ll'}$

To proceed further, we construct the scattering states out of the exact wave functions of an electron in the QPC potential. While this is a generic method, we consider for simplicity a δ -potential tunnel barrier for the QPC,

$$V(X) = \frac{\hbar^2 b}{m^*} \delta(X), \quad (2.27)$$

where b gives the strength of the delta potential. Then, the electron wave functions in the even and odd channels are given by

$$\psi_e(X) = \sqrt{2} \begin{cases} \cos(kX + \phi), & X < 0, \\ \cos(kX - \phi), & X > 0, \end{cases} \quad (2.28)$$

$$\psi_o(X) = \sqrt{2} \sin kX, \quad (2.29)$$

where $\phi = \arctan(b/k)$, $k = \sqrt{2m^*E/\hbar^2}$ and, for convenience, the sample length is set to unity. Note that $\phi = \pi/2 - \delta$, where $\delta \equiv \delta_e - \delta_o$ is the relative scattering phase between the even (e) and odd (o) channels. The transmission coefficient \mathcal{T} through the QPC is related to ϕ by $\mathcal{T}(k) = \cos^2 \phi$. We construct the scattering states in the following way

$$\begin{pmatrix} \psi_{sc}^L \\ \psi_{sc}^R \end{pmatrix} = \mathcal{U} \begin{pmatrix} \psi_e \\ \psi_o \end{pmatrix}, \quad \mathcal{U} = \frac{-i}{\sqrt{2}} \begin{pmatrix} e^{i\delta} & -1 \\ e^{i\delta} & 1 \end{pmatrix}. \quad (2.30)$$

Up to a global phase, Eq. (2.30) is valid for any symmetric tunnel barrier.

2.5.1 Three limiting cases

We calculate now the matrix elements of $\mathcal{E}(\mathbf{R})$ using the wave functions (2.28) and (2.29). Three interesting regimes are studied in the following.

(i) $\lambda_{sc} \ll k_F^{-1} \ll a$, where λ_{sc} is the screening length in the QPC leads and k_F is the Fermi wave vector. In this case, we set $\tilde{\delta}(\mathbf{R} - \mathbf{a}) = 2\lambda_{sc}\delta(X)$. By calculating the matrix elements of ε with respect to the eigenstates of the potential barrier, Eqs. (2.28) and (2.29), we obtain

$$\varepsilon_{ee} = 4\lambda_{sc}\mathcal{T}\mathcal{E}_0(\mathbf{a}), \quad \varepsilon_{oo} = \varepsilon_{eo} = 0, \quad (2.31)$$

where we used the odd and even eigenstates and $\int dY|\Phi(Y)|^2\mathcal{E}(X, Y) = \mathcal{E}(X, a)$. Here, $\Phi(Y)$ is the QPC wave function in the transverse direction with width $\ll \lambda_{sc}$. Going to the Left-Right basis, Eq. (2.30), which is more suitable for studying transport phenomena, we obtain

$$\begin{pmatrix} \varepsilon_{LL} & \varepsilon_{LR} \\ \varepsilon_{RL} & \varepsilon_{RR} \end{pmatrix} = \frac{1}{2}\varepsilon_{ee} \begin{pmatrix} 1 & 1 \\ 1 & 1 \end{pmatrix}. \quad (2.32)$$

Note that in this case we have $\varepsilon_{ll'} \propto \mathcal{T}$, where $l, l' = L, R$, see Eqs. (2.31) and (2.32).

(ii) $k_F^{-1} \ll \lambda_{sc} \ll a$. In this case, we set $\tilde{\delta}(\mathbf{R} - \mathbf{a}) = \Theta(X + \lambda_{sc}) - \Theta(X - \lambda_{sc})$, where $\Theta(X)$ is the step function, and we obtain in leading order in $1/k_F\lambda_{sc}$

$$\varepsilon_{ee} = \varepsilon_{oo} = \frac{2e\lambda_{sc}}{\kappa a^2} \left(1 + \frac{3\lambda_d^2}{4a^2} - \frac{\lambda_{sc}^2}{2a^2} + \dots \right) \mathbf{e}_Y, \quad (2.33)$$

$$\varepsilon_{eo} = \frac{e\lambda_{sc}^2 \cos \delta}{\kappa a^3} \left(1 + \frac{3\lambda_d^2}{4a^2} - \frac{3\lambda_{sc}^2}{4a^2} + \dots \right) \mathbf{e}_X. \quad (2.34)$$

In the above equations, \mathbf{e}_Y is a unit vector parallel to \mathbf{a} and \mathbf{e}_X is a unit vector perpendicular to \mathbf{a} (see Fig. 2.1). Further, we assumed that $\hbar v_F \Delta k \leq E_Z \ll \hbar v_F \lambda_{sc}^{-1} \ll E_F$, where $\Delta k = k - k'$, v_F is the Fermi velocity, and $E_F = \hbar v_F k_F$ is the Fermi energy. Going as before to the Left-Right basis, we obtain

$$\begin{pmatrix} \varepsilon_{LL} & \varepsilon_{LR} \\ \varepsilon_{RL} & \varepsilon_{RR} \end{pmatrix} = \begin{pmatrix} \varepsilon_{ee} - \varepsilon_{eo} \cos \delta & i\varepsilon_{eo} \sin \delta \\ -i\varepsilon_{eo} \sin \delta & \varepsilon_{ee} + \varepsilon_{eo} \cos \delta \end{pmatrix}. \quad (2.35)$$

Note that in this case we have $\varepsilon_{LR} \propto \sqrt{\mathcal{T}(1 - \mathcal{T})}$, see Eqs. (2.34) and (2.35). Since typically $\lambda_{sc} \gtrsim k_F^{-1}$, we expect case (ii) to describe realistic setups. A more general case, $k_F^{-1}, \lambda_{sc} \ll a$, is studied in Appendix B.

(iii) $k_F^{-1}, a \ll \lambda_{sc}$. In this regime, we neglect the screening ($\tilde{\delta}(\mathbf{R} - \mathbf{a}) = 1$ in Eq. (2.6)). Then, we obtain the following expressions for the coupling constants

$$\begin{aligned} \varepsilon_{oe} = \varepsilon_{eo} &= \frac{4ke}{\kappa} \left\{ K_0(2ka) \sin \delta \right. \\ &\quad \left. + \frac{\pi}{2} \cos \delta [I_0(2ka) - L_0(2ka)] \right\} \mathbf{e}_X, \end{aligned} \quad (2.36)$$

$$\begin{aligned} \varepsilon_{ee} &= \frac{2e}{\kappa} \left\{ \frac{1}{a} - 2k \cos(2\delta) K_1(2ka) \right. \\ &\quad \left. + \frac{\pi}{2} k \sin(2\delta) \left[\frac{2}{\pi} - 2I_1(2ka) + L_1(2ka) + L_{-1}(2ka) \right] \right\} \mathbf{e}_Y, \end{aligned} \quad (2.37)$$

$$\varepsilon_{oo} = \frac{2e}{\kappa} \left\{ \frac{1}{a} - 2k K_1(2ka) \right\} \mathbf{e}_Y, \quad (2.38)$$

where I_n and K_n are the modified Bessel functions and L_n is the modified Struve function. Here, we assumed $\Delta k \ll a^{-1} \ll \lambda_{sc}^{-1}$.

Since usually $ka \gg 1$, the k -dependence of the coupling constants in Eqs. (2.36)-(2.38) is suppressed. One can use the following asymptotic expressions for $a \gg k_F^{-1}$,

$$\varepsilon_{oe} = \varepsilon_{eo} \approx \frac{2e \cos \delta}{\kappa a} \mathbf{e}_X, \quad (2.39)$$

$$\varepsilon_{ee} \approx \varepsilon_{oo} \approx \frac{2e}{\kappa a} \mathbf{e}_Y. \quad (2.40)$$

In this case, the transformation to the Left-Right basis is given in Eq. (2.35) and we obtain $\varepsilon_{LR} \propto \sqrt{\mathcal{T}(1 - \mathcal{T})}$ as in case (ii).

2.5.2 Consistency check

Next we would like to verify whether our model predicts a realistic charge sensitivity of the QPC exploited in recent experiments [20, 28, 58]. For this we estimate the change in transmission $\delta\mathcal{T}$ through the QPC due to adding an electron to the quantum dot. The coupling in Eq. (2.5) (with coupling constants $\eta_{ll'}(\mathbf{r})$ given in Eq. (2.6)) is responsible for this transmission change $\delta\mathcal{T}$. It is convenient to view this coupling as a potential $\delta V(X)$ induced by the dot electron on the QPC. From Eq. (2.6), we obtain

$$\delta V(X) = \frac{e^2}{\kappa \sqrt{X^2 + a^2}} \tilde{\delta}(X), \quad (2.41)$$

where we have integrated over the dot coordinates $\mathbf{r} = (x, y)$ and the QPC coordinate Y , neglecting terms $\mathcal{O}(\lambda_d^2/a^2)$. The screening factor $\tilde{\delta}(X)$ is peaked around $X = 0$ with a halfwidth λ_{sc} . We consider two regimes.

(i) $\delta V(X)$ is a smooth potential. In this regime, $\hbar^2/m^*\bar{a}^2 \ll \delta V(0) \ll E_F$, with $\bar{a} = \min(\lambda_{sc}, a)$ being the width of $\delta V(X)$. Therefore, the dot electron provides a constant potential (like a back gate) to the QPC, implying that $\delta V(X)$ merely shifts the origin of energy for the QPC electrons by a constant amount, $\delta V(0)$. From the geometry of the current experimental setups [20, 28, 58] it appears reasonable to assume that this is the regime which is experimentally realized. The transmission change $\delta\mathcal{T}$ can then be estimated as

$$\delta\mathcal{T} \approx -\delta V(0) \left. \frac{\partial\mathcal{T}(E)}{\partial E} \right|_{E_F} = -\frac{\delta V(0)}{E_F} \mathcal{T}(1 - \mathcal{T}), \quad (2.42)$$

$$\mathcal{T}(E) = \cos^2 \phi = \frac{E}{E + \hbar^2 b^2 / 2m^*}, \quad (2.43)$$

where $\mathcal{T} = \mathcal{T}(E = E_F)$. By inserting typical numbers in Eq. (2.42), i.e. $\mathcal{T} = 1/2$, $E_F = 10$ meV, and $\delta V(0) = e^2/\kappa a$ [$\tilde{\delta}(0) = 1$], with $a = 200$ nm and $\kappa = 13$, we obtain $\delta\mathcal{T}/\mathcal{T} \approx 0.02$, which is consistent with the QPC charge sensitivity observed experimentally [28].

(ii) $\delta V(X)$ is a sharp potential. In this regime, adding an electron onto the quantum dot modifies the shape of the existing tunnel barrier in the QPC. Assuming sharp potentials, we obtain

$$\delta\mathcal{T} \approx -\frac{2\delta A}{A} \mathcal{T}(1 - \mathcal{T}), \quad (2.44)$$

where $\delta A = \int \delta V(X) dX$ and $A = \int V(X) dX = \hbar^2 b / m^*$. In deriving Eq. (2.44), we assumed that $\delta A \ll A$. Additionally, we assumed that both potentials $\delta V(X)$ and $V(X)$ are sharp enough to be replaced by δ -potentials. Redefining \bar{a} such that $\delta A = \bar{a}\delta V(0)$, we quantify the latter assumption as $\bar{a} \ll 1/b$, where b is the strength of $V(X)$ in Eq. (2.27). Note that for this regime the screening is crucial, because $\delta A \rightarrow \infty$ for $\lambda_{sc} \rightarrow \infty$.

2.6 Spin relaxation rate

2.6.1 k -independent case

Next we use the effective Hamiltonian (2.21) with Eqs. (2.22), (2.23) and (2.35) to calculate the spin relaxation time T_1 of the electron spin on the dot in lowest order in $\delta\mathbf{B}$. In the Born-Markov approximation [59], the spin relaxation rate is given by [34]

$$\Gamma_1 \equiv 1/T_1 = n_i n_j \Gamma_{ij}^r, \quad (2.45)$$

where $\mathbf{n} = \mathbf{B}/B$ is the unit vector along the applied magnetic field, Γ_{ij}^r is the spin relaxation tensor (see appendix C), and we imply summation over repeating indices. To evaluate T_1 , it is convenient to use the following expression,

obtained in Ref. [34],

$$\frac{1}{T_1} = \mathcal{J}_{ii}^+(\omega_Z) - n_i n_j \mathcal{J}_{ij}^+(\omega_Z) - \varepsilon_{kij} n_k \mathcal{J}_{ij}^-(\omega_Z), \quad (2.46)$$

where ε_{ijk} is the antisymmetric tensor and $\omega_Z = |E_Z|/\hbar$ is the Zeeman frequency (for detailed derivation of Eq. (2.46) see appendix C). $\mathcal{J}_{ij}^\pm(\omega_Z)$ are Fourier transforms of anticommutators of the fluctuating fields (with $\langle \delta \mathbf{B}(t) \rangle = 0$)

$$\begin{aligned} \mathcal{J}_{ij}^+(w) &= \frac{g^2 \mu_B^2}{4\hbar^2} \int_{-\infty}^{+\infty} \langle \{\delta B_i(0), \delta B_j(t)\} \rangle \cos(wt) dt, \\ \mathcal{J}_{ij}^-(w) &= \frac{g^2 \mu_B^2}{4\hbar^2} \int_{-\infty}^{+\infty} \langle \{\delta B_i(0), \delta B_j(t)\} \rangle \sin(wt) dt, \end{aligned} \quad (2.47)$$

which are evaluated in Eq. (2.46) at the Zeeman frequency ω_Z . Here and below, $\langle C \rangle \equiv \text{Tr}(\rho_L \rho_R C)$ where ρ_L (ρ_R) refers to the grand-canonical density matrix of the left (right) lead at the chemical potential μ_L (μ_R), and Tr is the trace over the leads. In our particular case, the second and third terms in Eq. (2.46) vanish. The reason for vanishing of the second term is the transverse nature of $\delta \mathbf{B}(t)$ in Eq. (2.22), *i.e.* $n_i \delta B_i(t) = 0$. The third term vanishes because each of the $\varepsilon_{i\ell\nu}$ in Eq. (2.35) is either real or imaginary. The time dependence of the anticommutators of fluctuating fields at zero temperature, together with their Fourier transforms (at finite temperature T) are given by the following expressions

$$\langle \{\delta B_i(0), \delta B_j(t)\} \rangle \propto \frac{A(t)}{t^2}, \quad (2.48)$$

$$\mathcal{J}_{ij}^+(w) \propto E_Z^2 \mathcal{S}(\hbar w), \quad \Delta\mu = 0, \quad (2.49)$$

$$\mathcal{S}(x) = x \coth(x/2k_B T), \quad (2.50)$$

where $A(t)$ is an oscillatory function of t with period $\Delta\mu$ and $\mathcal{S}(\hbar w)$ is the spectral function of the QPC which is linear in frequency at zero temperature. This time behavior shows that the QPC leads behave like an Ohmic bath. This Ohmic behavior results from bosonic-like particle-hole excitations in the QPC leads, possessing a density of states that is linear in frequency close to the Fermi surface. In the spin-boson model, having an Ohmic bath is sometimes problematic and needs careful study because of the non-Markovian effects of the bath [60]. However, we find that the Born-Markov approximation is still applicable since the non-Markovian corrections are not important in our case, due to the smallness of the spin-orbit interaction.²

²In the spin-boson model an appreciable non-Markovian contribution emerges for coupling constants $\alpha = \hbar/T_1 E_Z \gtrsim 10^{-2}$ [60]. Since typically $\hbar/T_1 E_Z \lesssim 10^{-4}$ in the case we studied here [*cf.* Tables (2.1) and (2.2)], we see that non-Markovian effects are negligible.

For the fluctuating field $\delta\mathbf{B}(t)$, we use the Born-Markov approximation [59] and obtain from Eqs. (2.46) and (2.47) the spin relaxation rate

$$\begin{aligned} \frac{1}{T_1} &= 4\pi\hbar\nu^2 (M_{LL} + M_{RR}) \mathcal{S}(E_Z) \\ &\quad + 4\pi\hbar\nu^2 M_{LR} [\mathcal{S}(E_Z + \Delta\mu) + \mathcal{S}(E_Z - \Delta\mu)], \end{aligned} \quad (2.51)$$

where $\nu = 1/2\pi\hbar v_F$ is the density of states per spin and mode in the leads and the coefficients $M_{ll'}$ read

$$\begin{aligned} M_{ll'} &= \boldsymbol{\omega}^{ll'} \cdot \boldsymbol{\omega}^{ll} - (\mathbf{n} \cdot \boldsymbol{\omega}^{ll'}) (\mathbf{n} \cdot \boldsymbol{\omega}^{ll}), \\ \boldsymbol{\omega}^{ll'} &= \boldsymbol{\Omega}_1^{ll'} + \mathbf{n} \times \boldsymbol{\Omega}_2^{ll'}, \\ \boldsymbol{\Omega}_1^{ll'} &= \frac{e\hbar\gamma_1 E_Z}{m^*} (\lambda_-^{-1} \varepsilon_{y'}^{ll'}, \lambda_+^{-1} \varepsilon_{x'}^{ll'}, 0), \\ \boldsymbol{\Omega}_2^{ll'} &= \frac{e\hbar\gamma_2 E_Z}{m^*} (-\lambda_-^{-1} \varepsilon_{x'}^{ll'}, \lambda_+^{-1} \varepsilon_{y'}^{ll'}, 0), \end{aligned} \quad (2.52)$$

where $\boldsymbol{\Omega}_i^{ll'}$ ($i = 1, 2$ and $l, l' = L, R$) are matrix elements of the operators $\boldsymbol{\Omega}_i$ with respect to the leads. In addition, in deriving Eq. (2.51) we assumed $T, \Delta\mu \ll E_F$. Note that, if the transmission coefficient of the QPC is zero or one ($\mathcal{T} = 0, 1$), then Eq. (2.51) reduces to

$$\frac{1}{T_1} = 4\pi\hbar\nu^2 (M_{LL} + M_{RR}) E_Z, \quad T \ll E_Z. \quad (2.53)$$

On the other hand, the equilibrium part of the relaxation time is obtained by assuming $\Delta\mu = 0$,

$$\frac{1}{T_1} = 4\pi\hbar\nu^2 (M_{LL} + M_{RR} + 2M_{LR}) E_Z, \quad T \ll E_Z. \quad (2.54)$$

Therefore, even with zero (or one) transmission coefficient or in the absence of the bias, the spin decay rate is non-zero due to the equilibrium charge fluctuations in the leads.

Another case of interest is the large bias regime $E_Z \ll \Delta\mu \ll \hbar\omega_0$, which simply means that only the second term in Eq. (2.51) appreciably contributes to the relaxation rate. Therefore, the non-equilibrium part of Eq. (2.51) is given by

$$\frac{1}{T_1} \approx 8\pi\hbar\nu^2 M_{LR} \Delta\mu, \quad E_Z, T \ll |\Delta\mu \pm E_Z| \ll \hbar\omega_0. \quad (2.55)$$

To estimate the relaxation time, we use typical experimental parameters for GaAs quantum dots (see, *e.g.*, Ref. [22]). We consider an in-plane magnetic field \mathbf{B} which leads to $\boldsymbol{\Omega}_2 = 0$ ($\gamma_2 = 0$) and, for simplicity, assume that \mathbf{B} is directed along one of the spin-orbit axes (say x' , see Fig. 2.1). In this

Table 2.1: Equilibrium ($\Delta\mu = 0$) relaxation time T_1 (ms) with \mathbf{B} along x' , see Fig. 2.1.

$T_1 (B = 14 T)$	$T_1 (B = 10 T)$	$T_1 (B = 8 T)$	$T_1 (B = 6 T)$	θ	\mathcal{T}
0.9	2.77	5.64	13.78	0	0
1.85	5.57	11.3	27.57	0	0.5
∞	∞	∞	∞	0	1
0.1	0.32	0.66	1.62	$\pi/4$	0
0.1	0.33	0.68	1.67	$\pi/4$	0.5
0.11	0.34	0.7	1.72	$\pi/4$	1
0.06	0.17	0.35	0.86	$\pi/2$	0
0.06	0.17	0.35	0.86	$\pi/2$	0.5
0.06	0.17	0.35	0.86	$\pi/2$	1

Table 2.2: Non-equilibrium ($E_Z \ll \Delta\mu = 1$ meV) relaxation time T_1 (ms) with \mathbf{B} along x' , see Fig. 2.1.

$T_1 (B = 14 \text{ T})$	$T_1 (B = 10 \text{ T})$	$T_1 (B = 8 \text{ T})$	$T_1 (B = 6 \text{ T})$	θ	\mathcal{T}
0.9	2.77	5.64	13.78	0	0
0.95	2.25	3.8	7.32	0	0.5
∞	∞	∞	∞	0	1
0.1	0.32	0.66	1.62	$\pi/4$	0
0.1	0.32	0.64	1.54	$\pi/4$	0.5
0.11	0.34	0.7	1.72	$\pi/4$	1
0.06	0.17	0.35	0.86	$\pi/2$	0
0.06	0.17	0.35	0.86	$\pi/2$	0.5
0.06	0.17	0.35	0.86	$\pi/2$	1

special case we obtain the following expression for $k_F^{-1} \ll \lambda_{sc} \ll a$ (case (ii) of Sec. 2.5.1),

$$M_{LR} \simeq \frac{e^4 \hbar^2}{m^{*2} \kappa^2} \frac{\lambda_{sc}^4}{\lambda_+^2 a^6} \frac{E_Z^2 \cos^2 \theta}{(\hbar^2 \omega_0^2 - E_Z^2)^2} \mathcal{T}(1 - \mathcal{T}), \quad (2.56)$$

or equivalently, the relaxation rate is given in terms of the QPC shot noise

$$\frac{1}{T_1} \approx \frac{8\pi^2 e^2 \hbar^4}{m^{*2} \kappa^2} \frac{\nu^2 \lambda_{sc}^4}{a^6 \lambda_+^2} \frac{E_Z^2 \cos^2 \theta}{(\hbar^2 \omega_0^2 - E_Z^2)^2} S_{LL}, \quad (2.57)$$

$$S_{LL} = \frac{e^2 \Delta\mu}{\pi \hbar} \mathcal{T}(1 - \mathcal{T}), \quad (2.58)$$

where S_{LL} is the current shot noise in the left lead of the QPC, and due to current conservation, $S_{LL} = S_{RR} = -S_{LR} = -S_{RL}$ [61]. We note that Eq. (2.57) is the non-equilibrium part of the relaxation rate. Thus, even if the constant equilibrium part ($\sim M_{LL}, M_{RR}$ in Eq. (2.51)) is of comparable magnitude, the non-equilibrium part can still be separated, owing to its bias dependence. Moreover, at low temperatures and large bias voltages, the relaxation rate is linear in the bias $\Delta\mu$ and proportional to the current shot noise in the QPC, $1/T_1 \propto \mathcal{T}(1-\mathcal{T})\Delta\mu$. The latter relation holds in cases (ii) and (iii) of Sec. 2.5.1, whereas in case (i) we have $1/T_1 \propto \mathcal{T}^2 \Delta\mu$.

The lifetime T_1 of the quantum dot spin strongly depends on the distance a to the QPC. For the regime (ii) in Sec. 2.5.1, the non-equilibrium part of $1/T_1$ depends on a as follows, $1/T_1 \propto a^{-6}$. A somewhat weaker dependence on a occurs in the regimes (i), $1/T_1 \propto a^{-4}$, and in the regime (iii), $1/T_1 \propto a^{-2}$. On the other hand, the charge sensitivity of the QPC scales as a^{-1} , which allows one to tune the QPC into an optimal regime with reduced spin decoherence but still sufficient charge sensitivity.

The spin lifetime T_1 strongly depends on the QPC orientation on the substrate (the angle θ between the axes x' and X in Fig. 2.1). For example, in the regimes (ii) and (iii) (with $ka \gg 1$), the non-equilibrium part of the relaxation rate vanishes at $\theta = \pi/2$, for an in-plane magnetic field \mathbf{B} along x' . Analogously, in the regime (i), both the equilibrium and the non-equilibrium parts of the relaxation rate vanish at $\theta = 0$, for $\mathbf{B} \parallel x'$.

We summarize our results in Tables (2.1) and (2.2), where we have evaluated the relaxation time T_1 (Eqs. (2.54) and (2.51)) for a QPC located at $a = 200$ nm away from the center of a GaAs quantum dot with $\lambda_d \approx 30$ nm, assuming $\lambda_{sc} = 100$ nm, $\lambda_{SO} = 8 \mu\text{m}$, and $k_F = 10^8 \text{ m}^{-1}$. Here, we use coupling constants derived for the regime (ii) in Sec. 2.5.1.

Finally, we remark that, for a perpendicular magnetic field ($\mathbf{B} = (0, 0, B)$), we have

$$M_{ll'} = \boldsymbol{\omega}^{ll'} \cdot \boldsymbol{\omega}^{ll'}, \quad \mathbf{n} = \mathbf{e}_z, \quad (2.59)$$

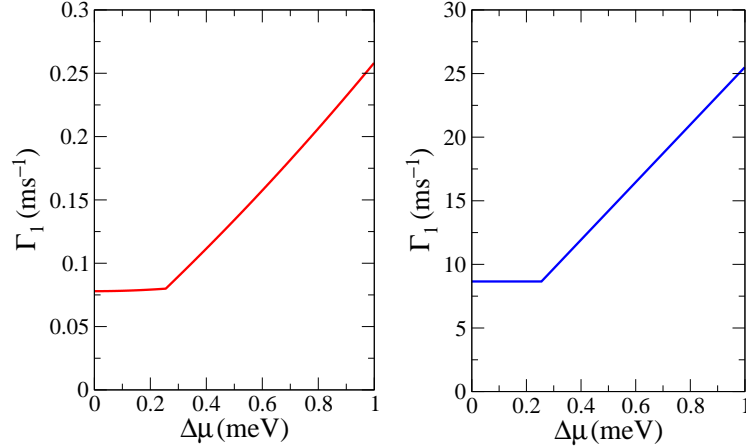


Figure 2.2: Relaxation rate $\Gamma_1 = 1/T_1$ as a function of the bias $\Delta\mu$ applied to the QPC for cases (ii) and (iii), see Sec. IV.A. The magnetic field \mathbf{B} is along x' with magnitude $B = 10$ T.

and the relaxation rate can be calculated analogously. The only difference is that $\mathbf{\Omega}_2$ is no longer zero and the matrix elements $M_{ll'}$ are given by more complicated expressions.

2.6.2 k -dependent case

In this regime we use the k -dependent coupling constants which are given in Eqs. (2.36)-(2.38) and in Appendix B. Using Eq. (2.46), the relaxation rate is given now by the following expression

$$\begin{aligned} \frac{1}{T_1} = & -\varepsilon_{kij} n_k \mathcal{J}_{ij}^-(\omega_Z) \\ & + 4\pi \hbar \nu^2 \sum_{ll'} \int dE \int dE' M_{ll'}(E, E') f(E) [1 - f(E')] \\ & \times \{ \delta(\Delta E + \mu_{l'} - \mu_l - \hbar\omega_Z) + \delta(\Delta E + \mu_{l'} - \mu_l + \hbar\omega_Z) \}, \end{aligned} \quad (2.60)$$

where $\Delta E = E' - E$ and $f(E) = [\exp(E/k_B T) + 1]^{-1}$ is the Fermi distribution function and the energies are measured from the Fermi level μ_l in each lead. The matrix elements $M_{ll'}(E, E')$ are given by Eq. (2.52), however, in this case they are k -dependent through $E = \hbar v_F k$. Fig. 2.2 shows the numerical results for the relaxation rate $\Gamma_1 = 1/T_1$ as a function of the bias $\Delta\mu$ for an in-plane magnetic field \mathbf{B} of 10 T in both cases. We note that the relaxation rate in case (iii) is typically two orders of magnitude larger than in case (ii), which underlines the important role played by the screening length λ_{sc} in the QPC-induced spin relaxation in a quantum dot.

2.7 Concluding remarks

In conclusion, we have shown that charge read-out devices (e.g. a QPC charge detector) induces spin decay in quantum dots due to the spin-orbit interaction (both Rashba and Dresselhaus). Due to the transverse nature of the fluctuating quantum field $\delta\mathbf{B}(t)$, we found that pure dephasing is absent and the spin decoherence time T_2 becomes twice the relaxation time T_1 , i.e. $T_2 = 2T_1$. Finally, we showed that the spin decay rate is proportional to the shot noise of the QPC in the regime of large bias ($\Delta\mu \gg E_Z$) and scales as a^{-6} (see Fig. 2.1). Moreover, we have shown that this rate can be minimized by tuning certain geometrical parameters of the setup. Our results should also be useful for designing experimental setups such that the spin decoherence can be made negligibly small while charge detection with the QPC is still efficient.

Chapter 3

Electric Dipole Induced Spin Resonance in Quantum Dots

3.1 Abstract

An alternating electric field, applied to a quantum dot, couples to the electron spin via the spin-orbit interaction. We analyze different types of spin-orbit coupling known in the literature and find two efficient mechanisms of spin control in quantum dots. The linear in momentum Dresselhaus and Rashba spin-orbit couplings give rise to a fully transverse effective magnetic field in the presence of a Zeeman splitting at lowest order in the spin-orbit interaction. The cubic in momentum Dresselhaus terms are efficient in a quantum dot with non-harmonic confining potential and give rise to a spin-electric coupling proportional to the orbital magnetic field. We derive an effective spin Hamiltonian, which can be used to implement spin manipulation on a timescale of 10 ns with the current experimental setups.

3.2 Introduction

Coherent manipulation of electron spin is at the heart of spintronics [9, 16] and quantum computing with spins [5]. In the proposal of Ref. [5], the spin of an electron confined to a quantum dot is used as qubit to store and process quantum information. A quantum register consisting of an array of such spin-1/2 quantum dots is operated by a set of quantum gates that act on single spins and pairs of neighboring spins [5]. Among the simplest quantum gates are the spin rotations on the Bloch sphere. With the help of only a static magnetic field and an electron-spin-resonance (ESR) pulse, one can change the state of the spin qubit at will. It is important, however, that the ESR pulse can be applied locally to each of the quantum dots, ensuring that the spins are accessed independently from one another. For an ESR [51, 62, 63] to occur, usually, the electron is exposed to an alternating magnetic field of a

frequency ω_{ac} that matches the electron Zeeman splitting. However, because strong local electric fields are easier to obtain than strong local magnetic fields, interest arises in spin resonance induced by electric fields.

Recently, Kato *et al.* [64] have demonstrated three-dimensional control of spins in a GaAs/Al_xGa_{1-x}As heterostructure with the use of an alternating electric field. The mechanism of spin coupling to the electric field relies on a specially engineered Landé g tensor in the heterostructure, achieved by modulating the Al content during the MBE growth [65]. The resulting g tensor is both anisotropic and space-dependent, and allows control over the direction and magnitude of the spin precession frequency [64, 66]. A g -factor modulation resonance (g -TMR) occurs similarly to an ESR, when the frequency of the electric field matches the Zeeman splitting [64]. Rashba and Efros [67–69] have further proposed to use the standard (Dresselhaus [55] and Rashba [54]) spin-orbit couplings to achieve an electric dipole induced spin resonance (EDSR) in quantum wells. Rashba and Efros [67–69] have shown that the EDSR is highly efficient in quantum wells, promising electron spin control on a timescale $\omega_R^{-1} \simeq 100$ ps, where ω_R is the Rabi frequency [62]. These results have important practical implications in spintronics, where spins of extended electrons are used as a resource to accomplish information processing. In the context of quantum computing, however, interest arises in the spin of a localized electron. A natural question is, therefore, “What is the microscopic mechanism of EDSR in quantum dots and how strong is the EDSR effect?”

EDSR has nearly half-a-century long history. It has been first observed for extended electrons in bulk semiconductors, [70, 71] and studied more recently for donor-bound electrons in Cd_{1-x}Mn_xSe [72, 73] and extended electrons in two-dimensional electron gases [74, 75] and epilayers [76]. The “forbidden” electric-dipole transition between the electron spin-up and spin-down states becomes possible in the presence of spin-orbit interaction. Absorption spectra of EDSR provide information about the value of the electron g factor and the strength of the spin-orbit coupling. In two-dimensional electron systems, one expects the Dresselhaus spin-orbit interaction [55] to be enhanced compared to bulk semiconductors, because of the confinement of electron motion in one direction. Furthermore, the Rashba spin-orbit interaction [54] arises in heterostructures lacking inversion symmetry, such as, e.g., heterojunctions. In some systems, the Rashba coupling constant can be efficiently tuned by electric fields [77].

In quantum dots [78], the spin-orbit interaction is generally suppressed due to complete localization of electron motion [79–81]. Typically, the quantum dot lateral size λ_d is smaller than the spin-orbit length λ_{SO} , and any effect of the spin-orbit interaction is suppressed as a power of λ_d/λ_{SO} and therefore is expected to be weak. This expectation contrasts with the case of electrons in quantum wells, where the EDSR meets most favorable conditions [67–69]. The Zeeman interaction in quantum dots plays an important role for observing spin-

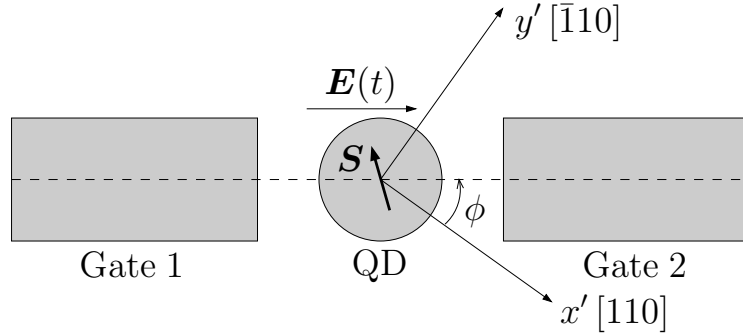


Figure 3.1: Schematic of a setup for electric field control of spin via the spin-orbit interaction. The quantum dot (QD) contains a single electron with spin $\mathbf{S} = (\hbar/2)\boldsymbol{\sigma}$, deep in the Coulomb blockade valley. The gates 1 and 2 are used to generate an alternating electric field $\mathbf{E}(t)$, which acts via the spin-orbit interaction on the electron spin. As a result, an electric dipole spin resonance (EDSR) occurs if the frequency of $\mathbf{E}(t)$ is tuned to match the Larmor frequency $\omega_Z = E_Z/\hbar$.

orbit effects [34, 35]. Without the Zeeman interaction, the Rashba and linear in momentum Dresselhaus spin-orbit terms do not contribute to spin-related phenomena at the first order of spin-orbit interaction. This “absence of spin-orbit” at the leading order in quantum dots has been discussed extensively in the literature [34, 35, 79–81]. Below, we show that a similar result arises also for the cubic in momentum Dresselhaus terms in the case when the dot confining potential is quadratic and the perturbation is linear in the electron coordinates.

In this paper, we consider the use of EDSR for control of individual electron spins in quantum dots. We derive an effective spin Hamiltonian for a quantum-dot electron, subject to *ac* electric fields. We show that there are two major mechanisms of EDSR in quantum dots. One arises from the linear in momentum Dresselhaus and Rashba spin-orbit couplings in combination with the Zeeman interaction. The other arises from the cubic Dresselhaus terms in combination with the cyclotron frequency. We estimate the strengths of both EDSR effects and compare them to the ordinary ESR. We find that despite a strong suppression, compared to quantum wells, the EDSR in quantum dots is still an efficient mechanism of spin manipulation and can be used alone or together with ESR to achieve control of spin on a timescale $\omega_R^{-1} \simeq 10$ ns.

3.3 EDSR setup

We consider a quantum dot containing a single electron with charge $-e$ and spin $\mathbf{S} = (\hbar/2)\boldsymbol{\sigma}$, where $\boldsymbol{\sigma} = (\sigma_x, \sigma_y, \sigma_z)$ are the Pauli matrices. The quantum dot is in the Coulomb blockade regime with extraction (U_-) and addition

(U_+) energies that are large compared to the temperature, so that the dot occupation remains constant. An external electric field $\mathbf{E}(\mathbf{r}, t)$ is applied to the quantum dot. In practice, $\mathbf{E}(\mathbf{r}, t)$ can be generated by a pair of gates, as sketched in Fig. 3.1, to which an ac signal of frequency ω_{ac} is supplied from an external circuit (not shown). The Hamiltonian describing the quantum dot electron in the external alternating field reads

$$H = H_0 + V(\mathbf{r}, t), \quad (3.1)$$

where $V(\mathbf{r}, t) = e \int^{\mathbf{r}} d\mathbf{r}' \cdot \mathbf{E}(\mathbf{r}', t)$ is the potential energy of the electron in the external electric field and H_0 is the “unperturbed” Hamiltonian (see further). In particular, for an electric field constant in space $\mathbf{E}(\mathbf{r}, t) = \mathbf{E}(t)$, the potential energy reads $V(\mathbf{r}, t) = e\mathbf{E}(t) \cdot \mathbf{r}$.

For practical applications, it is a good idea to use two gates, as shown in Fig. 3.1, because this allows larger amplitudes of $\mathbf{E}(t)$ to be applied to the quantum dot, while still maintaining the dot within the same Coulomb blockade valley. Ideally, the ac voltage drop is distributed between the two gates symmetrically and the dot potential is kept constant by counteracting potential shifts quadratic in the electric field. For a harmonic quantum dot, the desired ac potential reads

$$V(\mathbf{r}, t) = e\mathbf{E}(t) \cdot \mathbf{r} + \frac{(eE(t))^2}{2m_e\omega_0^2}, \quad (3.2)$$

where m_e is the electron effective mass and ω_0 is the oscillator frequency. Then the only effect of the ac signal on the dot confinement is shifting the dot center as a function of time by the amount

$$\mathbf{r}_0(t) = -\frac{e\mathbf{E}(t)}{m_e\omega_0^2}. \quad (3.3)$$

The amplitude of $\mathbf{r}_0(t)$ is going to be a relevant parameter in our following analysis. Therefore, setups in which the dot can be easily moved on the substrate by gates are particularly interesting in the context of this paper. We discuss the case of $r_0 \sim \lambda_{SO}$ in Sec. 3.7, whereas for the bulk of the chapter we restrict ourself to $r_0 \ll \lambda_{SO}$.

The Hamiltonian H_0 consists of several terms,

$$H_0 = H_d + H_Z + H_{SO}, \quad (3.4)$$

where H_d is the Hamiltonian of a confined electron,

$$H_d = \frac{p^2}{2m_e} + U(\mathbf{r}), \quad (3.5)$$

with $\mathbf{p} = -i\hbar\partial/\partial\mathbf{r} + (e/c)\mathbf{A}(\mathbf{r})$ being the electron momentum, c the speed of light in vacuum, and $U(\mathbf{r})$ the quantum dot confining potential. We restrict

our consideration to quantum dots with strong confinement along one axis, such as, e.g., quantum dots defined in a two-dimensional electron gas (2DEG). For GaAs, the 2DEG lies, typically, in the crystallographic plane (001) and has a width $d \simeq 5$ nm, which ensures a strong size quantization along $z \parallel [001]$. The in-plane motion of the electron is described by the Hamiltonian (3.5), where $\mathbf{r} = (x, y)$ is the electron in-plane coordinate; whereas the transverse motion (along z) has already been integrated out in Eqs. (3.1)-(3.5). In the absence of external time-dependent fields, $\mathbf{A}(\mathbf{r})$ accounts for the orbital effect of a static magnetic field \mathbf{B} . Assuming that \mathbf{B} is constant in space, we have $\mathbf{A}(\mathbf{r}) = B_z(-y/2, x/2, 0)$ in the symmetric gauge. Note that the in-plane components B_x and B_y are not present in $\mathbf{A}(\mathbf{r})$, because the motion along z is strongly quantized ($d \ll \sqrt{\hbar c / e B_{x(y)}}$).

The magnetic field \mathbf{B} also induces a Zeeman splitting $E_Z = g\mu_B B$ and a spin quantization axis $\mathbf{n} = \mathbf{B}/B$ via the Zeeman interaction,

$$H_Z = \frac{1}{2}g\mu_B \mathbf{B} \cdot \boldsymbol{\sigma} = \frac{1}{2}E_Z \mathbf{n} \cdot \boldsymbol{\sigma}, \quad (3.6)$$

where g is the electron g -factor and μ_B is the Bohr magneton. In GaAs, the magnitude of the g -factor is anomalously small ($g \approx -0.44$) compared to other $A_{\text{III}}B_{\text{V}}$ semiconductors. The Zeeman energy is, therefore, much smaller than the cyclotron energy $\hbar\omega_c = \hbar e B_z / m_e c$ by a factor $g m_e / m \ll 1$ (with m being the electron mass in vacuum), for magnetic fields applied transversely to the 2DEG. In Sec. 3.6, we derive an efficient spin-electric coupling that is proportional to $\hbar\omega_c$, but present only in non-harmonic quantum dots. We remark that the magnetic field is an important ingredient in our EDSR scheme, since at $B = 0$ no spin-electric coupling can be obtained at the first order of the spin-orbit interaction (see further).

In Eq. (3.4), H_{SO} stands for the spin-orbit Hamiltonian. We start with considering the so-called ‘‘linear in p ’’ spin-orbit interaction,

$$H_{SO} = \alpha(p_x \sigma_y - p_y \sigma_x) + \beta(-p_x \sigma_x + p_y \sigma_y), \quad (3.7)$$

which is the sum of the Rashba (α) [54] and 2D Dresselhaus (β) [55, 82] spin-orbit interactions. This type of spin-orbit interaction gives rise to a sizable phonon-induced spin relaxation rate $1/T_1$ [34, 35], of the same order of magnitude as experimentally measured [22, 36, 83]. Moreover, in the 2D limit the linear in p spin-orbit interaction is dominant, because $\beta \propto 1/d^2$.

In the standard EDR scheme, an alternating magnetic field is generated by a current in a nearby conductor. In our setup, see Fig. 3.1, no charge flow is ideally present between the gates. However, the alternating electric field $\mathbf{E}(\mathbf{r}, z, t)$ gives rise to a displacement current, with the current density

$$\mathbf{J}_D(\mathbf{r}, z, t) = \frac{\kappa}{4\pi} \frac{\partial \mathbf{E}(\mathbf{r}, z, t)}{\partial t}, \quad (3.8)$$

where κ is the electric permittivity. The external magnetic field \mathbf{B} acquires, thus, an ac -component, $\mathbf{B} \rightarrow \mathbf{B} + \mathbf{B}(t)$, where $\mathbf{B}(t) = \nabla \times \mathcal{A}(t)$. The vector potential $\mathcal{A}(\mathbf{r}, z, t)$ is obtained as usual from Ampere's law [84]

$$\nabla^2 \mathcal{A} = -\frac{4\pi\mu}{c} (\mathbf{J} + \mathbf{J}_D), \quad (3.9)$$

where μ is the magnetic permittivity and \mathbf{J} is the charge flow density (in our case $J = 0$). In Eq. (3.9), we adopted the Coulomb gauge $\nabla \cdot \mathcal{A} = 0$ and used the notation $\nabla = (\partial/\partial \mathbf{r}, \partial/\partial z)$.

The magnetic field $\mathbf{B}(t)$ couples to the electron spin via the Zeeman interaction in Eq. (3.6) [with $\mathbf{B} \rightarrow \mathbf{B} + \mathbf{B}(t)$], giving rise to an ESR source, which can be used, in principle, for spin manipulation in quantum dots. However, the amplitude of $\mathbf{B}(t)$ is, in practice, extremely small; it is proportional to $1/c$, as expected from the relativistic nature of $\mathbf{B}(t)$. Furthermore, the proximity of the top gates to the 2DEG decrease the displacement current enclosed by the magnetic field lines penetrating the quantum dot. Using Eq. (3.9), we estimate $\mathbf{B} = \mu\kappa c^{-1} L_z \partial E / \partial t \approx 10^{-6}$ G, for a quantum dot which is $L_z = 100$ nm below the gates plane and an electric field $E(t) = E_0 \sin(\omega_{ac} t)$, with amplitude $\mu\kappa E_0 = 10^2$ V/cm and frequency $\omega_{ac}/2\pi = 10^9$ Hz. As we show below, a much stronger effective magnetic field arises from the EDSR effect in the present setup, and therefore, the displacement current can be safely ignored.

Recently, a sizable ESR effect has been obtained with the help of a wire placed on top of a GaAs double dot [85]. In this case, $J \neq 0$ and the magnitude of $\mathbf{B}(t)$ is estimated from Eq. (3.9) to be $\mathbf{B} = \pi\mu c^{-1} I / (L_y + L_z)$, where I is current in the wire and $2L_y$ is the lateral size of the wire. For $L_y = L_z = 100$ nm and $I = 1$ mA, the magnetic field obtained in this setup is on the order of $\mathbf{B} \sim 10$ G.

3.4 Spin-electric coupling

Now, we focus on the electric-field component of the ac -signal and show that, together with the spin-orbit interaction H_{SO} and Zeeman splitting H_Z , it suffices to generate a sizable EDSR field in the quantum dot. For simplicity, we set $\mathbf{B}(t) \rightarrow 0$ from now on and choose $\mathcal{A}(t) = 0$. As a result, we retain only a constant in space and time magnetic field $\mathbf{B} = B(\cos \varphi \sin \vartheta, \sin \varphi \sin \vartheta, \cos \vartheta)$ and an alternating electric field $\mathbf{E}(\mathbf{r}, t) = (1/e)\nabla V(\mathbf{r}, t)$. Thus, we consider further the Hamiltonian in Eq. (3.1), assuming that H_0 is time-independent and describes the dot in the absence of ac fields.

We aim at diagonalizing H_0 using a Schrieffer-Wolff transformation, similar to Ref. [34]. We thus look for a transformation matrix S such that the transformed Hamiltonian $\tilde{H}_0 = \exp(S)H_0 \exp(-S)$ is fully diagonal, see Appendix D. At $B = 0$, the ground state of H_0 (and also of \tilde{H}_0) is a Kramers doublet, because the spin-orbit interaction is always time-reversal symmetric

(at $B = 0$). We therefore choose to encode the qubit into the ground state Kramers doublet of the quantum dot. Owing to the mixed spin and orbital nature of the states an alternating potential $V(\mathbf{r}, t)$, such as in Eq. (3.1), couples to the qubit. We proceed to derive this coupling, by calculating the transformation matrix S at the leading order of spin-orbit interaction,

$$S = \frac{1 - \mathcal{P}}{\hat{L}_d + \hat{L}_Z} H_{SO} + \mathcal{O}(H_{SO}^2), \quad (3.10)$$

where \hat{L}_d and \hat{L}_Z are Liouville superoperators, *i.e.* $\hat{L}_d A = [H_d, A]$ and $\hat{L}_Z A = [H_Z, A]$, $\forall A$. The projector \mathcal{P} projects onto the diagonal (or degenerate) part of the Hilbert space of $H_d + H_Z$, which ensures applicability of “non-degenerate” perturbation theory. The coupling of spin to electric fields is then found by applying the same Schrieffer-Wolff transformation to the potential $V(\mathbf{r}, t)$. We obtain the following effective Hamiltonian for our qubit in the presence of an alternating potential $V(\mathbf{r}, t)$, to leading order in the spin-orbit interaction,

$$H_{\text{eff}} = H_Z + \langle \psi_0 | [S, V(\mathbf{r}, t)] | \psi_0 \rangle, \quad (3.11)$$

where S is the transformation matrix in Eq. (3.10) and $|\psi_0\rangle$ is the quantum dot ground state. For a quantum dot with a harmonic confining potential, $U(\mathbf{r}) = m_e \omega_0^2 r^2 / 2$, the transformation matrix S was calculated in Ref. [86] to all orders of the Zeeman interaction and the first order of the “linear in p ” spin-orbit interaction. For simplicity, we consider here only the linear in B terms,

$$\begin{aligned} S &= i\boldsymbol{\xi} \cdot \boldsymbol{\sigma} - \frac{E_Z}{m_e \omega_0^2} [\mathbf{n} \times \boldsymbol{\zeta}] \cdot \boldsymbol{\sigma}, \\ \boldsymbol{\xi} &= (\lambda_-^{-1} y', \lambda_+^{-1} x', 0), \\ \boldsymbol{\zeta} &= (\lambda_-^{-1} \partial / \partial y', \lambda_+^{-1} \partial / \partial x', 0), \end{aligned} \quad (3.12)$$

where $\lambda_{\pm} = \hbar / m_e (\beta \pm \alpha)$ are the spin-orbit lengths, and the vectors $\boldsymbol{\xi}$ and $\boldsymbol{\zeta}$ are given in the coordinate frame (see Fig. 3.1)

$$x' = (x + y) / \sqrt{2}, \quad (3.13)$$

$$y' = -(x - y) / \sqrt{2}, \quad (3.14)$$

$$z' = z. \quad (3.15)$$

The first term in Eq. (3.12) commutes with scalar potentials and therefore drops out in Eq. (3.11). More generally, for arbitrary confining potential, the first term is replaced by $i(1 - \mathcal{P})\boldsymbol{\xi} \cdot \boldsymbol{\sigma}$, resulting nevertheless in no coupling of spin to electric fields. The second term in Eq. (3.12), however, allows us to express the coupling of spin to charge via the electric field

$$\mathbf{E}(t) = (1/e) \langle \psi_0 | \nabla V(\mathbf{r}, z, t) | \psi_0 \rangle \quad (3.16)$$

that acts on the quantum dot electron. For the harmonic confining potential, we obtain

$$H_{\text{eff}} = \frac{1}{2}g\mu_B\mathbf{B} \cdot \boldsymbol{\sigma} + \frac{1}{2}\mathbf{h}(t) \cdot \boldsymbol{\sigma}, \quad (3.17)$$

$$\mathbf{h}(t) = 2g\mu_B\mathbf{B} \times \boldsymbol{\Omega}(t), \quad (3.18)$$

$$\boldsymbol{\Omega}(t) = \frac{-e}{m_e\omega_0^2} (\lambda_-^{-1}E_{y'}(t), \lambda_+^{-1}E_{x'}(t), 0). \quad (3.19)$$

The dimensionless field $\boldsymbol{\Omega}(t)$ describes a combined effect of the spin-orbit interaction and electric fields (or more generally potential fluctuations) on the qubit. $\boldsymbol{\Omega}(t)$ was calculated in Ref. [34] for the phonon potential and in Ref. [86] for the shot-noise of a QPC nearby the quantum dot. In our case, $\boldsymbol{\Omega}(t)$ is merely a classical driving field generated by the ac -signal.

Considering further a constant in space (at least on the scale of the quantum dot), alternating electric field $\mathbf{E}(t) = \mathbf{E}_0 \sin(\omega_{ac}t)$ of amplitude $\mathbf{E}_0 = E_0(\cos\phi, \sin\phi, 0)$, where ϕ is the angle of \mathbf{E}_0 with respect to the axis x' , see Fig. 3.1, we obtain explicitly $\boldsymbol{\Omega}(t) = \boldsymbol{\Omega}_0 \sin(\omega_{ac}t)$, with

$$\boldsymbol{\Omega}_0 = \frac{-eE_0}{m_e\omega_0^2} (\lambda_-^{-1} \sin\phi, \lambda_+^{-1} \cos\phi, 0). \quad (3.20)$$

To give an estimate for the amplitude Ω_0 in GaAs quantum dots, we assume $\lambda_+ \approx \lambda_- \approx \lambda_{SO} = 8\mu\text{m}$, $\hbar\omega_0 = 1\text{meV}$, and $E_0 = 10^2\text{V/cm}$, which yields $\Omega_0 \sim 10^{-3}$.

The amplitude of the resulting effective magnetic field due to EDSR is found from Eq. (3.18) to be

$$\delta\mathbf{B}_0 = 2\mathbf{B} \times \boldsymbol{\Omega}_0. \quad (3.21)$$

The maximal amplitude is obtained for $\mathbf{B} \perp \boldsymbol{\Omega}_0$, which in experiment can easily be arranged for by, e.g., choosing $\mathbf{B} \parallel z$. In-plane magnetic fields can also be used, provided $\mathbf{E}(t)$ is linearly polarized. For example, an electric field $\mathbf{E}(t)$ aligned with x' generates, according to Eq. (3.19), a dimensionless field $\boldsymbol{\Omega}(t)$ along y' . In this case, \mathbf{B} should be chosen along x' for maximal spin-electric coupling.

Using our previous estimate for $\Omega_0 \sim 10^{-3}$, we obtain from Eq. (3.21) that $\delta B_0 \sim 1\text{mT}$ for a magnetic field $B = 1\text{T}$ oriented transversely to $\boldsymbol{\Omega}_0$. In principle, the dimensionless factor Ω_0 can be increased up to $\Omega_0 \sim 1$. However, this requires a specially designed setup, where the value of the electron displacement r_0 in Eq. (3.3) approaches the spin-orbit length λ_{SO} .

Next we remark that $\boldsymbol{\Omega}(t)$ in Eq. (3.19) can be written by the order of magnitude as $\Omega(t) \sim r_0(t)/\lambda_{SO}$. More rigorously, we rewrite Eq. (3.19) in the following form

$$\Omega_i(t) = \sum_j (\lambda_{SO}^{-1})_{ij} r_{0j}(t), \quad (3.22)$$

where $(\lambda_{SO}^{-1})_{ij}$ is a tensor of inverse spin-orbit lengths,

$$(\lambda_{SO}^{-1})_{ij} = \begin{pmatrix} 0 & 1/\lambda_- \\ 1/\lambda_+ & 0 \end{pmatrix}, \quad (3.23)$$

with $1/\lambda_{\pm} = m_e(\beta \pm \alpha)/\hbar$ and the frame (x', y') was used to represent the tensor. For order of magnitude estimates, it is useful to introduce the scalar

$$\frac{1}{\lambda_{SO}} = \frac{1}{\sqrt{2}} \|\lambda_{SO}^{-1}\|, \quad (3.24)$$

where $\|\lambda_{SO}^{-1}\|$ is the Frobenius norm of $(\lambda_{SO}^{-1})_{ij}$. In the case of Eq. (3.23), we have $1/\lambda_{SO} = (m_e/\hbar)\sqrt{\alpha^2 + \beta^2}$.

Despite the fact that Eq. (3.22) was obtained considering the harmonic confining potential as an example, its generality suggests that it should remain valid for quantum dots of arbitrary confinement, provided, to a good approximation, the ac -signal merely displaces the quantum dot parallel to itself by a vector $\mathbf{r}_0(t)$ as a function of time. Note that $\mathbf{r}_0(t)$ is the only available parameter to be compared with λ_{SO} in the limit of strong confinement ($\lambda_d \rightarrow 0$). We extend the class of Hamiltonians considered here to any combination of confinement and ac -voltage potential that can be rewritten in the form

$$U(\mathbf{r}) + V(\mathbf{r}, t) = U(\mathbf{r} - \mathbf{r}_0(t)) + V_0(t), \quad (3.25)$$

where $V_0(t)$ is independent of \mathbf{r} . We note that, as before, the electron wave function extension λ_d is assumed to be small compared to the spin-orbit length λ_{SO} at each moment in time. Equation (3.25) need not be satisfied exactly. Note that λ_d enters only in the definition of $\mathbf{r}_0(t)$ and does appear alone as a parameter in Eq. (3.22). Therefore, defining $\mathbf{r}_0(t)$ as the average electron position, $\mathbf{r}_0(t) = \int \mathbf{r} |\psi(\mathbf{r}, t)|^2 d^2r$, we expect Eq. (3.22) to be valid to leading order also when the electron probability density $|\psi(\mathbf{r}, t)|^2$ changes shape, but the dot size changes weakly.

Equations (3.17), (3.18), and (3.22) form the basis of EDSR in quantum dots and can be used to efficiently manipulate the electron spin by electrical gates. Finally, we remark that Eqs. (3.17)-(3.19) have been derived under the assumption $r_0 \ll \lambda_{SO}$, and therefore, can be used only for $\Omega_0 \ll 1$. In Sec. 3.7 we discuss the case of $\Omega_0 \sim 1$ in more detail. A further assumption in deriving Eqs. (3.17)-(3.19) was that the frequency spectrum of $\mathbf{E}(t)$ lies well below the size-quantization energy $\hbar\omega_0$. This adiabaticity constraint is generic to the spin-based quantum computation [5, 9]; it guarantees that the electron is not excited to higher in energy orbital levels.

3.5 Spin dynamics and coherence

The electron spin obeys the Bloch equation [87–90]

$$\langle \dot{\mathbf{S}} \rangle = [\boldsymbol{\omega}_Z + \delta\boldsymbol{\omega}(t)] \times \langle \mathbf{S} \rangle - \Gamma \langle \mathbf{S} \rangle + \boldsymbol{\Upsilon}, \quad (3.26)$$

where $\boldsymbol{\omega}_Z = g\mu_B \mathbf{B}/\hbar$ is the Larmor spin-precession frequency and $\delta\boldsymbol{\omega}(t) = \mathbf{h}(t)/\hbar$. The spin relaxation tensor Γ_{ij} and the inhomogeneous part Υ_i are due to the environment and can be derived microscopically [34, 87–89] within the Born-Markov approximation. Strictly speaking, Γ_{ij} and Υ_i in Eq. (3.26) depend also on the driving. In particular, Γ_{ij} acquires, in general, a time-dependent part. However, we neglect these effects here since the energy scales are well separated. Indeed, from experiments [22, 36, 83] and theory [34, 35], we infer that $\Gamma_{ij}, \Upsilon_i \sim (10^2 - 10^6) \text{ s}^{-1}$, *i.e.* they are very small, so that the regime $\Gamma_{ij}, \Upsilon_i \ll \delta\omega \ll \omega_Z$ holds. In this regime, the rotating wave approximation [90] is valid. We consider a completely general driving field

$$\delta\boldsymbol{\omega}(t) = \delta\boldsymbol{\omega}_a \sin(\omega_{ac}t) + \delta\boldsymbol{\omega}_b \cos(\omega_{ac}t), \quad (3.27)$$

which can be realized in practice by implementing two independent electric fields at the quantum dot site. This is, however, by no means necessary for our EDSR scheme.

The Rabi frequency then reads

$$\boldsymbol{\omega}_R = \frac{1}{2} (\delta\boldsymbol{\omega}_a \times \mathbf{n} - [\delta\boldsymbol{\omega}_b \times \mathbf{n}] \times \mathbf{n}). \quad (3.28)$$

Here, we assume that ω_{ac} is not far from resonance, *i.e.* $|\omega_{ac} - \omega_Z| < \omega_{ac}/2$. In a coordinate frame (X, Y, Z) with $Z \parallel \mathbf{B}$, the spin dynamics is approximated as follows

$$\langle S_{\pm}(t) \rangle \approx \tilde{S}_{\pm}(t) e^{\pm i\omega_{ac}t} \quad (3.29)$$

$$\langle S_Z(t) \rangle \approx \tilde{S}_Z(t), \quad (3.30)$$

where $S_{\pm} = S_X \pm iS_Y$. The spin $\tilde{\mathbf{S}}(t)$ obeys a simpler (static) Bloch equation

$$\dot{\tilde{\mathbf{S}}} = (\boldsymbol{\delta} + \boldsymbol{\omega}_R) \times \tilde{\mathbf{S}} - \tilde{\Gamma} \tilde{\mathbf{S}} + \tilde{\boldsymbol{\Upsilon}}, \quad (3.31)$$

where $\boldsymbol{\delta} = (\omega_Z - \omega_{ac})\mathbf{n}$ gives the detuning from resonance. The relaxation tensor $\tilde{\Gamma}_{ij}$ is diagonal, with $\tilde{\Gamma}_{XX} = \tilde{\Gamma}_{YY} = 1/T_2$ and $\tilde{\Gamma}_{ZZ} = 1/T_1$, and $\tilde{\Upsilon}_i$ assumes $\tilde{\Upsilon}_i = \tilde{\Gamma}_{ij} S_j^T$. Here, T_1 and T_2 are the relaxation and decoherence times in the absence of driving measured in experiment [22, 36, 83], and $\mathbf{S}^T = -(\mathbf{n}g/2|g|) \tanh(E_Z/2k_B T)$ is the thermodynamic value of spin, with T being the temperature.

The time-evolution of $\tilde{\mathbf{S}}$ in Eq. (3.31) is simplest in a coordinate frame (X', Y', Z') , with $Z' \parallel (\boldsymbol{\delta} + \boldsymbol{\omega}_R)$, and reads

$$\begin{aligned}\tilde{S}_{X'}(t) &= S_{\perp}^0 e^{-t/\tilde{T}_2} \sin\left(t\sqrt{\delta^2 + \omega_R^2} + \phi\right), \\ \tilde{S}_{Y'}(t) &= S_{\perp}^0 e^{-t/\tilde{T}_2} \cos\left(t\sqrt{\delta^2 + \omega_R^2} + \phi\right), \\ \tilde{S}_{Z'}(t) &= \tilde{S}_T + (S_{Z'}^0 - \tilde{S}_T)e^{-t/\tilde{T}_1},\end{aligned}\tag{3.32}$$

where S_{\perp}^0 , $S_{Z'}^0$, and ϕ give the initial spin state, $\langle \mathbf{S}(0) \rangle \equiv \tilde{\mathbf{S}}(0) = (S_{\perp}^0 \sin \phi, S_{\perp}^0 \cos \phi, S_{Z'}^0)$, in the coordinate frame (X', Y', Z') . Furthermore, the decay times \tilde{T}_1 and \tilde{T}_2 read

$$\begin{aligned}\frac{1}{\tilde{T}_1} &= \frac{1}{\delta^2 + \omega_R^2} \left(\frac{\delta^2}{T_1} + \frac{\omega_R^2}{T_2} \right), \\ \frac{1}{\tilde{T}_2} &= \frac{1}{2(\delta^2 + \omega_R^2)} \left(\frac{\omega_R^2}{T_1} + \frac{2\delta^2 + \omega_R^2}{T_2} \right).\end{aligned}\tag{3.33}$$

The stationary value of spin $\tilde{\mathbf{S}}_T := \tilde{\mathbf{S}}(t \rightarrow \infty)$ to leading order reads

$$\tilde{\mathbf{S}}_T = -\frac{g}{2|g|} \frac{(\boldsymbol{\delta} + \boldsymbol{\omega}_R)\delta}{\delta^2 + (T_1/T_2)\omega_R^2} \tanh(E_Z/2k_B T).\tag{3.34}$$

Note that at resonance ($\delta = 0$), the right-hand side in Eq. (3.34) vanishes. Therefore, in the vicinity of resonance, $\tilde{\mathbf{S}}_T$ is determined by the subleading order term, which can be obtained from Eq. (3.34) by replacing the numerator $(\boldsymbol{\delta} + \boldsymbol{\omega}_R)\delta \rightarrow (1/T_2)[\boldsymbol{\omega}_R \times \mathbf{n}]$. Measurement of $\tilde{\mathbf{S}}_T$ in the presence of driving provides information about the spin lifetimes $T_{1,2}$. For instance, at resonance the relaxation time T_1 can be accessed at the leading order of $\Gamma_{ij}/\omega_R \ll 1$,

$$\tilde{\mathbf{S}}_T(\delta = 0) = -\frac{g}{|g|} \frac{\boldsymbol{\omega}_R \times \mathbf{n}}{2T_1\omega_R^2} \tanh(E_Z/2k_B T).\tag{3.35}$$

Finally, we estimate the Rabi frequency ω_R using Eq. (3.28) and the parameters from Sec. 3.4. For $\Omega_0 \sim 10^{-3}$, $|g| = 0.44$, and $B = 10$ T we obtain $\omega_R \sim 10^8$ s $^{-1}$. We conclude that, with the present quantum-dot setups, EDSR enables one to manipulate the electron spin on a time scale of 10 ns, which is considerably shorter than the spin lifetimes, for which values between 1 and 150 ms (depending on the applied magnetic field) in gated GaAs quantum dots have been reported recently [22, 83].

3.6 p^3 -Dresselhaus terms

Next we consider the so-called p^3 terms of the Dresselhaus spin-orbit interaction [82],

$$H_{SO} = \frac{\gamma}{2} (p_y p_x p_y \sigma_x - p_x p_y p_x \sigma_y),\tag{3.36}$$

where $\gamma = \alpha_c/\sqrt{2m_e^3 E_g}$ is the spin-orbit coupling constant, with α_c (≈ 0.07 for GaAs [82]) being a dimensionless constant defined in Ref. [91] and E_g the band gap. For simplicity, we impose here the dipolar approximation for the ac -signal,

$$V(\mathbf{r}, t) = e \int_0^{\mathbf{r}} d\mathbf{r}' \cdot \mathbf{E}(\mathbf{r}', t) \approx e\mathbf{E}(t) \cdot \mathbf{r}. \quad (3.37)$$

Quite remarkably, if the quantum dot potential is harmonic, $U(\mathbf{r}) = \sum_{ij} u_{ij} r_i r_j$, then the spin does not couple to $\mathbf{E}(t)$ at the first order of H_{SO} and zeroth order of E_Z . Indeed, the second term in Eq. (3.11) vanishes for $V(\mathbf{r}, t) = e\mathbf{E}(t) \cdot \mathbf{r}$ and $S = \hat{L}_d^{-1} H_{SO}$ because of the following two identities

$$\langle \psi_0 | [\hat{L}_d^{-1} H_{SO}, \mathbf{r}] | \psi_0 \rangle = \langle \psi_0 | [\hat{L}_d^{-1} \mathbf{r}, H_{SO}] | \psi_0 \rangle, \quad (3.38)$$

$$[\hat{L}_d^{-1} \mathbf{r}, H_{SO}] = 0, \quad \forall H_{SO}(\mathbf{p}). \quad (3.39)$$

The latter is specific to H_d in Eq. (3.5) with a harmonic $U(\mathbf{r})$, for which the operator $\hat{L}_d^{-1} \mathbf{r}$ can be expressed via the components of $\mathbf{p} - (e/c)\mathbf{B}_z \times \mathbf{r}$. Note that, generally, $[\mathbf{p}, H_{SO}] = (e/c)[\mathbf{B}_z \times \mathbf{r}, H_{SO}]$ for any H_{SO} that is a function of only $\mathbf{p} = (p_x, p_y)$. Thus, for a harmonic confining potential, one is left with the same dominant mechanism as considered above for the "linear in p " terms. Expanding in terms of the Zeeman interaction, we recover Eqs. (3.17) and (3.18) with $\boldsymbol{\Omega}(t)$ given now by

$$\Omega_i(t) = -\frac{e}{m_e \omega_0^2} \sum_j (\lambda_{SO}^{-1})_{ij} E_j(t), \quad (3.40)$$

$$(\lambda_{SO}^{-1})_{ij} = \frac{m_e}{\hbar} \langle \psi_0 | \frac{\partial^2 H_{SO}}{\partial \sigma_i \partial p_j} | \psi_0 \rangle, \quad (3.41)$$

where $(\lambda_{SO}^{-1})_{ij}$ is a tensor of inverse spin-orbit lengths, and as before we consider $U(\mathbf{r}) = m_e \omega_0^2 r^2 / 2$. For H_{SO} in Eq. (3.36), we obtain explicitly $(\lambda_{SO}^{-1})_{ij} = \frac{1}{4} \gamma \omega_0 m_e^2 \delta_{ij}$ and $\Omega_i(t) = -\gamma e m_e E_i(t) / 4\omega_0$. To estimate the strength of the resulting EDSR, we note that $\gamma \sim \beta d^2 / \hbar^2$, and therefore the amplitude of $\mathbf{h}(t) = 2g\mu_B \mathbf{B} \times \boldsymbol{\Omega}(t)$ is down now by a factor $d^2 / \lambda^2 \ll 1$ compared to the p -terms.

Next we consider a quantum dot with non-harmonic potential $U(\mathbf{r})$ and show that the p^3 -terms in Eq. (3.36) give rise to a spin-electric coupling proportional to the cyclotron frequency $\omega_c = eB_z / m_e c$. Since $\hbar\omega_c$ differs parametrically from E_Z ($E_Z / \hbar\omega_c = gm_e B / 2mB_z$), the p^3 -terms can be as significant as the p -terms, provided $E_Z / \hbar\omega_c \lesssim d^2 / \lambda^2$, which is realistic for GaAs quantum dots. Note that for the p -terms no spin-electric coupling proportional to ω_c arises at the first order of H_{SO} . We thus leave out \hat{L}_Z in Eq. (3.10) and consider a confining potential $U(\mathbf{r})$ that differs from a harmonic one by a function $W(\mathbf{r})$,

$$U(\mathbf{r}) = \sum_{ij} u_{ij} r_i r_j + W(\mathbf{r}) \equiv U_H(\mathbf{r}) + W(\mathbf{r}), \quad (3.42)$$

where u_{ij} are real coefficients and $W(\mathbf{r}) = \mathcal{O}(r^3)$. While in general $W(\mathbf{r})$ need not be small compared to $H_H = p^2/2m_e + U_H(\mathbf{r})$, in the following we expand the denominator of Eq. (3.10) in terms of $W \ll H_H$, considering therefore only small deviations of $U(\mathbf{r})$ from harmonic potentials. Then, using Eqs. (3.11), (3.17), and (3.37), we obtain at leading order in ω_c

$$\frac{h_i(t)}{\omega_c} = e\mathbf{E}(t) \cdot \langle \psi_0 | [\mathbf{R}(\mathbf{r}), \frac{\partial^2 S_H}{\partial \omega_c \partial \sigma_i}] | \psi_0 \rangle \Big|_{\omega_c=0}, \quad (3.43)$$

where we set $\omega_c \rightarrow 0$ in the right-hand side of Eq. (3.43) after evaluating $\partial S_H / \partial \omega_c$ in the symmetric gauge, with S_H defined as $[H_H, S_H] = H_{SO}$. The linear relationship between h_i and ω_c holds for $\omega_c \ll \omega_0$, where $\omega_0 \equiv 2\sqrt{\det(u)/m_e \text{Tr}(u)}$. In Eq. (3.43), the perturbation $W(\mathbf{r})$ enters via the function $\mathbf{R}(\mathbf{r})$ defined as follows

$$R_i(\mathbf{r}) = \sum_j (u^{-1})_{ij} \frac{\partial W(\mathbf{r})}{\partial r_j}. \quad (3.44)$$

Note that $\langle R/r \rangle \sim W_0 \lambda_d / \hbar \omega_0 \lambda_W$ is the small parameter of our expansion in terms of $W(\mathbf{r})$, with W_0 and $\lambda_W \lesssim \lambda_d$ being, respectively, the characteristic amplitude and length scale of the variation of $W(\mathbf{r})$ over the quantum dot size. It is important to note that the antisymmetric part of $W(\mathbf{r})$ drops out in Eq. (3.43) because H_{SO} is also antisymmetric with respect to $\mathbf{r} \rightarrow -\mathbf{r}$.

Next, as an example, we consider $U_H(\mathbf{r}) = m_e \omega_0^2 r^2 / 2$ and $W(\mathbf{r}) = \eta r^4$, and obtain

$$\frac{1}{2} \mathbf{h}(t) \cdot \boldsymbol{\sigma} = \frac{e\gamma\eta\hbar^2\omega_c}{9m_e\omega_0^4} (E_y(t)\sigma_x + E_x(t)\sigma_y). \quad (3.45)$$

Here, we have used the deformation quantization theory [92, 93], which allowed us to considerably simplify the derivation of Eq. (3.45) by performing most of the calculation in classical mechanics and only at the final stage come back to quantum mechanics. We have also carried out a fully quantum derivation of Eq. (3.45) and recovered the same result.

To estimate the strength of the resulting EDSR, we note that

$$h \sim \hbar\omega_c (\lambda_d / \lambda_{SO}) (e\lambda_d E_0 / \hbar\omega_0) \langle R/r \rangle, \quad (3.46)$$

where $\lambda_{SO} = 4/\gamma\omega_0 m_e^2$ ($\approx \lambda_d^2 / [0.01 \text{ nm}]$ for GaAs) is the spin-orbit length of the p^3 -terms and the parameter $\langle R/r \rangle \sim W(\lambda_d) / \hbar\omega_0$ characterizes the deviation of the quantum dot confinement from harmonic. In practice, $\langle R/r \rangle$ can be as large as unity, but here we assume $\langle R/r \rangle \sim \eta\lambda_d^4 / \hbar\omega_0 = 0.1$. For an electric field with amplitude $E_0 = 10^2 \text{ V/cm}$ and a GaAs quantum dot with $\hbar\omega_0 = 1 \text{ meV}$, we obtain the equivalent of an *ac* magnetic field $\delta\mathbf{B}(t) = \mathbf{h}(t) / g\mu_B$ that has an amplitude $\delta B_0 \approx 1 \text{ mT}$ at $B_z = 1 \text{ T}$ and $|g| = 0.44$. In contrast to the previous mechanism, $\delta\mathbf{B}(t)$ can have here also a finite longitudinal component $\delta\mathbf{B}_{\parallel}(t) = \mathbf{n}(\mathbf{n} \cdot \delta\mathbf{B}(t))$, which however vanishes if $\mathbf{B} \parallel z$.

Finally, we note that the p^3 -terms can also be relevant for spin relaxation in quantum dots with non-harmonic confining potential. Of course, the magnetic field has to have an out-of-plane component for this spin-electric coupling to dominate over the one considered in Sec. 3.4.

3.7 Discussions

The coupling of spin to electric fields that we have derived above can be used in a variety of ways to access and manipulate the electron spin in experiments. The effective Hamiltonian in Eq. (3.17) has the same form as the Hamiltonian of an ESR effect. This shows that ESR and EDSR are mutually interchangeable and the choice of the effect to be used depends on the particular experimental setup. In GaAs quantum dots, the spin-orbit interaction is weak enough to ensure long coherence times and, at the same time, strong enough to allow room for spin manipulation on an experimentally accessible timescale of ~ 10 ns. Much shorter timescales can be achieved in InAs quantum dots, because of a much stronger spin-orbit coupling and a larger electron g -factor. In contrast, the EDSR effect is of little use in materials with very weak or nearly absent spin-orbit interaction, such as, e.g., carbon-nanotube quantum dots. To make order-of-magnitude estimates easier, we draw an analogy between the EDSR and ESR effects in terms of the particular way the \mathbf{B} and \mathbf{E} fields couple to the electron spin $\mathbf{S} = (\hbar/2)\boldsymbol{\sigma}$.

We recall that the ESR effect occurs as a result of the Zeeman interaction of the electron spin with an *ac* magnetic field. It is convenient to write this interaction in the form of a magnetic dipole interaction,

$$H_{\text{ESR}} = -\boldsymbol{\mu} \cdot \mathbf{B}(t), \quad (3.47)$$

where $\mathbf{B}(t)$ is the *ac* magnetic field and $\boldsymbol{\mu}$ is the electron magnetic moment,

$$\boldsymbol{\mu} = -\frac{1}{2}g\mu_B\boldsymbol{\sigma}, \quad (3.48)$$

where g is, in general, a tensor, see Eq. (D.18).

By analogy with the ESR effect, the EDSR effect can be viewed as arising from an interaction between the *ac* electric field $\mathbf{E}(t)$ and a spin-electric moment $\boldsymbol{\nu}$. The respective spin-electric interaction is then analogous to Eq. (3.47) and reads

$$H_{\text{EDSR}} = -\boldsymbol{\nu} \cdot \mathbf{E}(t), \quad (3.49)$$

where the spin-electric moment $\boldsymbol{\nu}$ is due to an interplay between the spin-orbit interaction and some time-reversal breaking interaction, such as the Zeeman interaction. This analogy is not complete. Equation (3.49) is valid only for *ac* electric fields $\mathbf{E}(t)$ that oscillate around zero, whereas Eq. (3.47) holds also

for static B -fields. The reason why a static electric field \mathbf{E} cannot be used in Eq. (3.49) will become clear after we explain the origin of $\boldsymbol{\nu}$ in Eq. (3.49).

The spin-electric moment $\boldsymbol{\nu}$ arises because the dipolar transitions in the quantum dot become allowed, e.g., for the ground state

$$\langle \psi_{0\uparrow} | \mathbf{r} | \psi_{0\downarrow} \rangle \neq 0. \quad (3.50)$$

The electron charge density operator $\rho(\mathbf{r}) = -e\delta(\mathbf{r} - \mathbf{r}_{el})$, where \mathbf{r}_{el} is the electron coordinate, acquires spin-dependent terms in the transformed basis,

$$|\psi_{ns}\rangle = e^{-S} |\psi_n\rangle |\chi_s\rangle, \quad (3.51)$$

$$\tilde{\rho}(\mathbf{r}) = e^S \rho(\mathbf{r}) e^{-S}, \quad (3.52)$$

where e^{-S} is the transformation used in Section 3.4 and studied in detail in Appendix D. One can present $\tilde{\rho}(\mathbf{r})$ as a sum of two terms,

$$\tilde{\rho}(\mathbf{r}) = \bar{\rho}(\mathbf{r}) + \delta\rho(\mathbf{r}), \quad (3.53)$$

where $\bar{\rho}(\mathbf{r})$ is spin independent and $\delta\rho(\mathbf{r})$ is proportional to the spin. Then the spin-electric moment can be written as follows,

$$\boldsymbol{\nu} = \int \mathbf{r} \delta\rho(\mathbf{r}) dv, \quad (3.54)$$

where dv is the elementary volume of integration. Equation (3.54) unveils the physical meaning of the spin-electric moment $\boldsymbol{\nu}$: due to the mixed spin and orbit nature of the electron density, the electron spin couples to the first moment (dipole moment) of the electron.

While oscillating around an equilibrium position, the electron produces a time-dependent dipole moment, part of which is proportional to the electron spin. Obviously, in a static electric field, one can set to zero the electron dipole moment, because the new electron position can be taken as the equilibrium one. Therefore, only the change of the moment as a function of time has a physical meaning for single electrons (as for any other monopoles). In contrast, the electron magnetic moment $\boldsymbol{\mu}$ couples to static magnetic fields, because one can view $\boldsymbol{\mu}$ as arising from a pair of Dirac monopoles of opposite signs, for which the relative distance between them has an absolute meaning.

Equation (3.54) is written in a very general (operator) form. After taking the expectation value in the orbital ground state $|\psi_0\rangle$, we obtain

$$\boldsymbol{\nu} = -\frac{1}{2} \bar{\bar{\nu}} \boldsymbol{\sigma}, \quad (3.55)$$

$$\bar{\bar{\nu}}_{ij} = 2e \frac{\partial}{\partial \sigma_j} \langle \psi_0 | e^S r_i e^{-S} | \psi_0 \rangle, \quad (3.56)$$

where the derivative with respect to σ_j is defined as a usual derivative of an expression that is linear in $\boldsymbol{\sigma}$. Note that Eq. (3.55) is analogous to Eq. (3.48)

where the role of $g\mu_B$ is played by the tensor $\bar{\nu}$. Using Eqs. (3.17)-(3.19) we obtain for the linear in momentum spin-orbit interaction,

$$\bar{\nu}_{ij} = -\frac{2eg\mu_B}{m_e\omega_0^2}\varepsilon_{jkl}B_k(\lambda_{SO}^{-1})_{li}. \quad (3.57)$$

Similarly, for the p^3 Dresselhaus terms we obtain from Eq. (3.45)

$$\bar{\nu}_{ij} = \frac{2e\gamma\eta\hbar^2\omega_c}{9m_e\omega_0^4} \begin{pmatrix} 0 & 1 \\ 1 & 0 \end{pmatrix}, \quad (3.58)$$

where we use the coordinate frame (x, y) to represent the tensor. Note that in both cases $\bar{\nu}_{ij}$ is proportional to the magnetic field (or one of its components). The spin-orbit interaction produces no spin-electric coupling at $B = 0$, because of the time-reversal symmetry of spin-orbit interaction.

The analogy between $\boldsymbol{\mu}$ and $\boldsymbol{\nu}$ is also seen in the pairwise interaction between spins in separate (not tunnel coupled) quantum dots [94]. For an unscreened Coulomb interaction between electrons, the spin-spin interaction is analogous to the magnetic dipole-dipole interaction [94],

$$H_{\text{dd}} = \sum_{i<j} \frac{\boldsymbol{\nu}_i \cdot \boldsymbol{\nu}_j r_{ij}^2 - 3(\boldsymbol{\nu}_i \cdot \mathbf{r}_{ij})(\boldsymbol{\nu}_j \cdot \mathbf{r}_{ij})}{\kappa r_{ij}^5}, \quad (3.59)$$

where $\mathbf{r}_{ij} = \mathbf{r}_i - \mathbf{r}_j$ is the distance between two quantum dots ($r_{ij} \gg \lambda_d$) and κ is the electric permittivity of the material. For further detail and a microscopic derivation of Eq. (3.59) we refer the reader to Ref. [94].

Next we discuss the limitations of our theory. Throughout the paper, we have assumed that the spin orbit interaction is weak compared to the dot level spacing, or, in other words, that $\lambda_d/\lambda_{SO} \ll 1$. This assumption allowed us to use the perturbation theory to find the unitary transformation $\exp(-S)$, see Appendix D. Of course, this restriction was not necessary, if, e.g., we were to apply numerical methods to diagonalize the Hamiltonian. In particular, note that Eq. (3.54) is meaningful whenever the unitary transformation $\exp(-S)$ exists. The latter is always the case, including also extended states. Our perturbative results are qualitatively correct for $\lambda_d \lesssim \lambda_{SO}$ and can be used in experiments to estimate the strength of the EDSR effect. The case $\lambda_d \gg \lambda_{SO}$ is more seldom and requires a separate theoretical investigation.

As a second limitation, we would like to mention the adiabaticity criterion. In Sections 3.4 and 3.6, we have derived effective Hamiltonians for the low energy subspace of the quantum dot Hilbert space. For the validity of this effective description, it is important that the switching (on and off) of the effective interaction occurs on a time scale that is larger than the inverse level spacing in the quantum dot. Obviously, this criterion excludes applicability of

our theory to extended states. In practice, however, the finite temperature T imposes a more stringent criterion on the confinement energy, $\hbar^2/m_e\lambda_d^2 \gg k_B T$.

The third limitation of our theory is a small amplitude of oscillation of the quantum dot, $r_0/\lambda_{SO} \ll 1$. We have shown in Section 3.4 that the EDSR effect is proportional to this small parameter. Thus, for breaking the time-reversal symmetry by the Zeeman interaction we have (by order of magnitude)

$$\omega_R \sim \omega_Z \frac{r_0}{\lambda_{SO}}, \quad (3.60)$$

where $\omega_Z = E_Z/\hbar$. Similarly, for breaking the time-reversal symmetry by the orbital B -field effect (Section 3.6), we have

$$\omega_R \sim \omega_c \frac{r_0}{\lambda_{SO}} \langle R/r \rangle, \quad (3.61)$$

where $\langle R/r \rangle$ is the small parameter of deviation of the quantum dot confinement from harmonic. We remark that our theory remains qualitatively valid also for $r_0/\lambda_{SO} \sim 1$ and for $\langle R/r \rangle \sim 1$. Beyond these limits, we do not expect the Rabi frequency to grow indefinitely. The Rabi frequency is bound in the case of Eq. (3.60) by $\omega_R \leq \omega_Z$, and in the case of Eq. (3.61) by $\omega_R \leq \omega_c$. We conclude that, by designing quantum dot setups that allow for large oscillation amplitudes $r_0 \lesssim \lambda_{SO}$, the EDSR effect can be strongly enhanced, beyond the numeric estimates made in Sections 3.4, 3.5, and 3.6.

In conclusion, the EDSR mechanisms presented above provides a means of implementing local electrical control of electron spins in quantum dots.

Chapter 4

Non-Abelian Spin Rotator

4.1 Abstract

With the help of the spin-orbit interaction, we propose a scheme to perform holonomic single qubit gates on the electron spin confined to a quantum dot. The manipulation is done in the absence (or presence) of an applied magnetic field. By adiabatic changing the position of the confinement potential, one can rotate the spin state of the electron around the Bloch sphere in semiconductor heterostructures. The dynamics of the system is equivalent to employing an effective non-Abelian gauge potential whose structure depends on the type of the spin-orbit interaction. As an example, we find an analytic expression for the electron spin dynamics when the dot is moved around a circular path (with radius R) on the two dimensional electron gas (2DEG), and show that all single qubit gates can be realized by tuning the radius and orientation of the circular paths. Moreover, using the Heisenberg exchange interaction, we demonstrate how one can generate two-qubit gates by bringing two quantum dots near each other, yielding a scalable scheme to perform quantum computing on arbitrary N qubits. This proposal shows a way of realizing holonomic quantum computers in solid-state systems.

4.2 Introduction

The emergence of geometrical phases in quantum mechanical systems and their physical and geometrical consequences were first recognized by Berry and Simon in their works on cyclic quantum evolution [95, 96]. Soon after that, Wilczek and Zee discovered the connection between (non-Abelian) gauge fields and the adiabatic dynamics of such systems, where the dimension of non-Abelian geometric phases is given by the n -fold degeneracy of the eigenstates of the Hamiltonian [97]. Moreover, Aharonov and Anandan [98] generalized Berry's idea to non-adiabatic evolutions, however, the resulting geometric

phase is not given anymore by the holonomy in the parameter space of the Hamiltonian but in the projective Hilbert space. Although, at the time, geometrical phases were already known in classical systems [99], their quantum mechanical counterparts are physically richer and more subtle.

Based on the above mentioned ideas, a variety of schemes for holonomic (HQC) and geometric (GQC) quantum computation have been proposed, which recently attained a considerable attention, and believed to be promising candidates to implement quantum computers using topological transformations as qubit gates [100, 101]. In HQC, for example, one can perform quantum computing by encoding quantum information in the degenerate levels of the Hamiltonian and adiabatically traversing closed loops (holonomies) in the parameter space of the Hamiltonian. So far, many theoretical (and experimental) investigations have been made to implement such Hamiltonians in physical systems, for example, confined ions in a linear Pauli trap [102]. The experiment by Jones *et al.* [103] was the first attempt in this direction where they realized geometric two-qubit gates between a pair of nuclear spins. Note that geometrical phases are generally small compared to dynamical phases. Being a small effect on top of a large effect, makes it challenging for the experimentalists to identify and employ them for quantum computation.

Among several proposals for HQC and GQC, solid state matrix is usually more desirable due to its potential in realizing large scale qubit systems. Specifically, spin of an electron in a quantum dot, as a two level system, has been shown to be a suitable qubit [5], meanwhile, rapid experimental progress in the field of semiconductor spintronics made it possible to access individual electron spin in low dimensional systems [9]. Manipulating the spin of the electrons/holes in semiconductors is, therefore, one of the objectives of spintronics [9, 104]. Among different tools to achieve this goal is to apply an external magnetic field, in combination with the spin-orbit interaction, in a controlled way. Recently, there has been a great progress in developing techniques to manipulate electrically the electron/hole spins in two dimensional electron/hole gases (2DEGs/2DHGs) and quantum dots (QDs) [64, 66–68, 75–77, 105–107]. However, most of the previous works on confined electrons are based on the assumption that the quantum dot itself is almost frozen in real space. Moreover, the presence of an applied magnetic field is usually assumed in order to break the time reversal symmetry, which is essential in electron spin resonance (ESR) schemes. The question is: what is the dynamics of the spin sector if we move the quantum dot in the absence (or presence) of the magnetic field? If time reversal symmetry is not broken, a convenient way to study the dynamics of such a system is to employ *non-Abelian* gauge fields [97]. In spite of the fact that the origin of non-Abelian gauge fields in classical/quantum field theories and the current problem is somewhat different, as long as the dynamics is concerned, they play the same role.

Using an effective non-Abelian gauge potential [97, 104, 108], we propose

a novel technique to manipulate topologically the spin of an electron inside a quantum dot without using any *applied* magnetic field. Although the rotation of the the electron spin in a moving quantum dot has been studied in previous works [104, 108], our goal here is to implement systematically *all* necessary single qubit gates for quantum information processing. We consider a setup, where the quantum dot can be moved on the substrate at distances comparable to λ_{SO} , the spin-orbit length. In addition, we assume that the electron is strongly confined to the quantum dot at a length scale $\lambda_d \ll \lambda_{SO}$, where λ_d is the dot size. We study the case which the confining potential is only displaced parallel to itself by a vector $\mathbf{r}_0(t)$ without changing its shape, see Fig. 4.2. Moreover, we assume that the driving electric field is classical and only quantize the electron dynamics (for the discussion of the quantum fluctuations of the electromagnetic fields which lead to the decoherence of the Kramers doublets, see Ref. [108]). For a moving quantum dot around a circular path, we derive an exact solution of the Schrödinger equation for the spin sector, in the first order in spin-orbit interaction. In addition, we show how one can generate different single- and two-qubit rotations and perform quantum computing on N spins.

4.3 The Model and Basic Relations

We consider a lateral quantum dot [78] formed by depleting the 2DEG via a set of metallic gates that allow the quantum dot position \mathbf{r}_0 to be changed at will to distances comparable to the spin-orbit length in the 2DEG. Such rolling quantum dots can be defined using, for example, a set of gates shown in Fig. 4.1. Two layers of finger-like gates (separated by an insulator) form a grid, which construct the dot confining potential at virtually any position under the grid by simultaneously pulsing several gates. A relatively different setup is shown in Fig. 4.3, which makes use of a quantum ring and allows the quantum dot to be moved along a circular trajectory.

The electron motion in the plane of the 2DEG, and in the presence of a time-dependent dot confining potential, is governed by the Hamiltonian

$$H(t) = H_d(t) + H_Z + H_{SO}, \quad (4.1)$$

where $H_d(t)$ describes the moving dot with one electron,

$$H_d(t) = \frac{p^2}{2m_e} + U(\mathbf{r} - \mathbf{r}_0(t)), \quad (4.2)$$

with $\mathbf{p} = -i\hbar\partial/\partial\mathbf{r} + (e/c)\mathbf{A}(\mathbf{r})$ and $\mathbf{r} = (x, y)$ being the electron momentum and coordinates, respectively. For the vector potential $\mathbf{A}(\mathbf{r})$, we choose the cylindric gauge, $\mathbf{A}(\mathbf{r}) = B_z(-y/2, x/2, 0)$, where B_z is the component

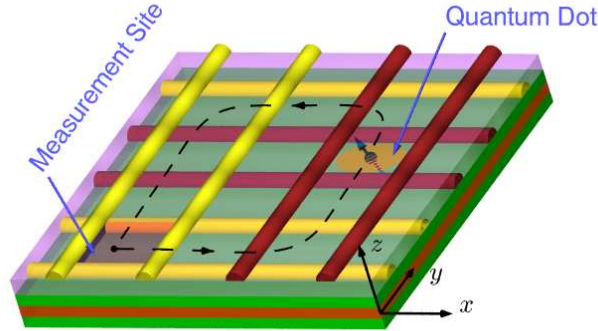


Figure 4.1: A set of metallic gates, deposited on top of the heterostructure, control the quantum dot position in the (x,y) -plane. The gates that define the current dot position are highlighted in a darker color. The superimposed gates are separated from each other by an insulating layer. The measurement site is used to initialize and read out the spin state of the quantum dot with the help of additional controls (not shown here). By applying time-dependent voltages to the gates, one is able to move the quantum dot along a desired trajectory, thus forming, for instance, a *Wilson loop* (dashed line) [97].

of the magnetic field normal to the 2DEG plane. The dot confinement potential $U(\mathbf{r}, t) = U(\mathbf{r} - \mathbf{r}_0(t))$ changes adiabatically with respect to the size-quantization energy in the dot and, thus, no transitions between orbital levels occur. For simplicity, we also assume that the shape of the dot confinement does not change in time, while the dot is moved along its trajectory $\mathbf{r}_0(t)$. In Eq. (4.1), the Zeeman interaction reads $H_Z = \frac{1}{2} \mathbf{E}_Z \cdot \boldsymbol{\sigma}$, with $|\mathbf{E}_Z|$ being the Zeeman energy and $\boldsymbol{\sigma} = (\sigma_x, \sigma_y, \sigma_z)$ the Pauli matrices. We note that the quantization axis is generally not along the magnetic field and one has $E_{Zi} = \mu_B g_{ij} B_j$, where μ_B is the Bohr magneton, g_{ij} is the g-factor tensor in the 2DEG, and \mathbf{B} is the magnetic field. The last term in Eq. (4.1), H_{SO} , denotes the spin-orbit interaction which has the following general form $H_{SO} = \frac{1}{2} \mathbf{h}(\mathbf{p}) \cdot \boldsymbol{\sigma}$, where $\mathbf{h}(\mathbf{p}) = -\mathbf{h}(-\mathbf{p})$ is an odd-power polynomial in \mathbf{p} . In GaAs 2DEG with the [001] growth direction, for example, the leading order (lowest power in \mathbf{p}) spin-orbit interaction terms read

$$H_{SO} = \alpha(p_x \sigma_y - p_y \sigma_x) + \beta(-p_x \sigma_x + p_y \sigma_y), \quad (4.3)$$

where α and β are the Rashba and Dresselhaus coupling constants, respectively [54, 55].

Considering first a stationary quantum dot potential $U(\mathbf{r})$, we set $\mathbf{r}_0(t) \rightarrow 0$ in Eq. (4.2) and denote the time-independent Hamiltonian by H with the

following eigenvalue equation, $H|\psi_{ns}\rangle = E_{ns}|\psi_{ns}\rangle$, where $n = 0, 1, 2, \dots$ and $s = \pm 1/2$ are the orbital and spin quantum numbers, respectively.

The eigenstates of H are related to the eigenstates of $H_d + H_Z$ via a unitary transformation (see Appendices D and E)

$$|\psi_{ns}\rangle = e^{-S} |\psi_n\rangle |\chi_s\rangle, \quad (4.4)$$

where $|\psi_n\rangle$ and $|\chi_s\rangle$ are obtained by solving $H_d|\psi_n\rangle = E_n|\psi_n\rangle$ and $H_Z|\chi_s\rangle = sE_Z|\chi_s\rangle$, respectively.

We are mainly interested here in spin dynamics in the *absence* of the applied magnetic field, therefore, we set $\mathbf{A}(\mathbf{r}) = 0$, and focus on the lowest-in-energy subspace $n = 0$ (for the discussion of the spin dynamics in the presence of an applied magnetic field, see Appendix E). The suitable qubit is then defined as $|\uparrow\rangle = |\psi_{0,1/2}\rangle$ and $|\downarrow\rangle = |\psi_{0,-1/2}\rangle$. In the absence of magnetic fields, the quantization axis can, therefore, be chosen arbitrarily. However, once it is chosen, all subsequent spin rotations are then with respect to this axis.

Given a linear in momentum spin-orbit interaction in Eq. (4.3), and a symmetric confining potential $U(\mathbf{r}) = U(-\mathbf{r})$, we have explicitly found the generator of the rotation for the Kramers doublet (see Appendix E), as one moves the dot along a given path

$$\Delta = \mathbb{1} - i\boldsymbol{\sigma} \cdot \boldsymbol{\lambda}_{SO}^{-1} \cdot \delta\mathbf{r}_0, \quad (4.5)$$

$$\boldsymbol{\lambda}_{SO}^{-1} \equiv \begin{pmatrix} 0 & 1/\lambda_- \\ 1/\lambda_+ & 0 \end{pmatrix}, \quad \lambda_{\pm} = \frac{\hbar}{m_e(\beta \pm \alpha)}, \quad (4.6)$$

where $\boldsymbol{\sigma}$ are Pauli matrices acting on the Kramers doublet states and $S = i\boldsymbol{\sigma} \cdot \boldsymbol{\lambda}_{SO}^{-1} \cdot \mathbf{r}$ [105]. According to Eq. (4.5), the electron state, in the space of a Kramers doublet, is rotated during the displacement by an angle $\sim \delta r_0/\lambda_{SO}$. This interpretation of the spin-orbit interaction effect is identical to the standard interpretation given to semiclassical electrons. In the latter, the electron with the momentum p travels a distance $l = pt/m_e$ during a time t and changes its spin by an angle proportional to l/λ_{SO} . This coincidence is not accidental, because in the semiclassical picture one also assumes that the electron moves in a wave packet of an extension that is much smaller than λ_{SO} . The speed at which the electron moves is unimportant at $B = 0$, because the path $\mathbf{r}_0(t)$ is the only information that determines the spin rotation. In particular, if the electron travels along some path forward and then returns the same way, but not necessarily at the same speed, then the initial and final spin states coincide.

We note that, for the linear in momentum H_{SO} , the tensor $\boldsymbol{\lambda}_{SO}^{-1}$ in Eq. (4.6) is independent of the electron orbital state $|\psi_n\rangle$, which means Eq. (4.5) is valid for all symmetric wave packets at the zeroth order of λ_d/λ_{SO} . Therefore,

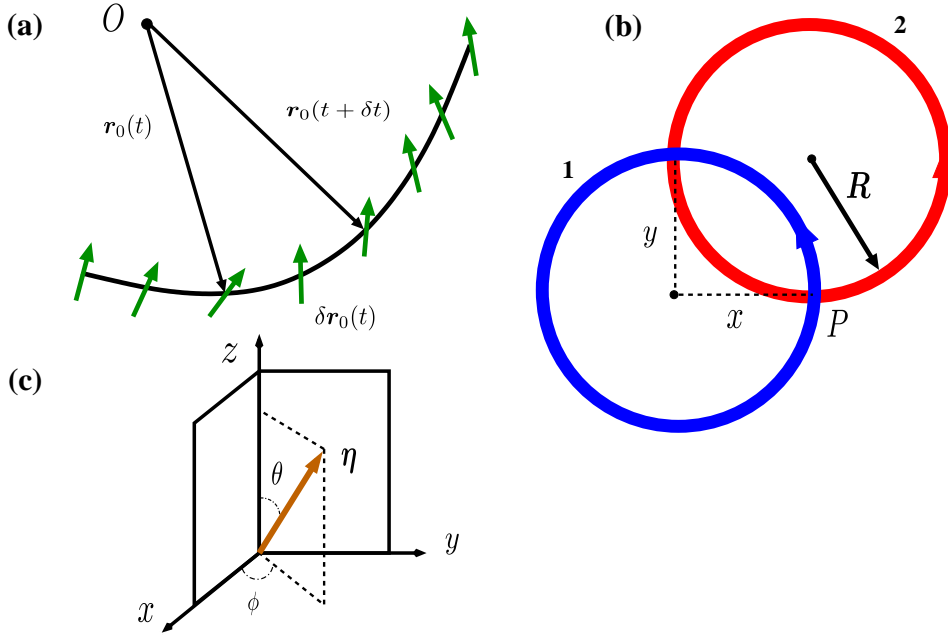


Figure 4.2: (a) Trajectory of the quantum dot center $\mathbf{r}_0(t)$ and the evolution of the spin state due to displacement. The spin state changes when going from \mathbf{r}_0 to $\mathbf{r}_0 + \delta \mathbf{r}_0$, due to the infinitesimal transformation (E.17). Since the directions of $\delta \mathbf{r}_0$ can be different in different parts of the curve, the infinitesimal transformations do not commute with each other and have to be ordered along the path of integration. (b) Two oriented circles with the same radii R but different centers (with their corresponding holonomic rotations at P) show the typical paths for the quantum dot on the 2DEG. (c) Moving the dot along the circles will rotate the spin of the electron around the $\boldsymbol{\eta}$ axis. For instance, blue (1) and red (2) circles in (b) correspond to $\phi = 0$ and $\phi = -\frac{\pi}{2}$, respectively.

we can consider also a point-like electron, for which the orbital wave function reads $\psi_{\mathbf{r}_0}(\mathbf{r}) = \delta(\mathbf{r} - \mathbf{r}_0)$. Integrating Eq. (4.5) over an arbitrary path we obtain an exact expression for this case,

$$\psi_{\mathbf{r}_0 s}(\mathbf{r}, \sigma) = e^{-i \int \boldsymbol{\sigma} \cdot \boldsymbol{\lambda}_{SO}^{-1} \cdot d\mathbf{r}_0} \delta(\mathbf{r} - \mathbf{r}_0) \chi_s(\sigma), \quad (4.7)$$

where the exponent is ordered (to the left) along the path of integration. To simplify notations, we use $\int d\mathbf{r}_0$ to denote the contour integral $\int_0^{\mathbf{r}_0} d\mathbf{r}'$ and agree that any exponent of an integral to be ordered along the path of integration. The radius vector $\mathbf{r}_0(t)$ gives us the path where we choose the beginning of the path at $\mathbf{r}_0 = 0$, and denote the running (present) point of the path by \mathbf{r}_0 . Eq. (4.7) determines how the spin of an electron is transformed (at $B = 0$) as the electron is moved along an arbitrary path. The difference between the spin and the Kramers doublet disappears here, since for point-like electrons we can take $S \rightarrow 0$. However, the transformation rule in Eq. (4.7) arises from the fact that $\partial S / \partial \mathbf{r}$ remains constant while taking $S \rightarrow 0$. Moreover, it holds exactly for the linear in momentum spin-orbit interaction, because $\boldsymbol{\lambda}_{SO}^{-1}$ is independent of the orbital state. For the p^3 terms, $1/\lambda_{SO}$ is proportional to the electron energy and Eq. (4.7) can be written only if H_{SO} is first linearized around a given energy.

We developed a code to calculate numerically the spin dynamics for an arbitrary path, however as an example, we consider a point like quantum dot (strong confining potential) moving around a circle with radius R (see Fig. 4.3). Using Eq. (4.5), the dynamical equation for the electron spin is then given by

$$\frac{d}{d\phi} \chi_s(\phi) = i \mathcal{M}_{DR} \chi_s(\phi), \quad (4.8)$$

$$\mathcal{M}_{DR} \equiv R \left(\frac{\sin \phi}{\lambda_+} \sigma_y - \frac{\cos \phi}{\lambda_-} \sigma_x \right), \quad (4.9)$$

where $\chi_s(\phi) = (v_1, v_2)$ is the spinor, ϕ is the angle between the starting point vector $\mathbf{r}_0(0)$ and the x axis, and \mathcal{M}_{DR} is a Hermitian matrix due to both Dresselhaus (\mathcal{M}_D) and Rashba (\mathcal{M}_R) spin orbit interaction (e.g. for the only Rashba interaction we have $\mathcal{M}_{DR} = \mathcal{M}_R = -\mathcal{M}_D^*$). In addition to trivial solutions for a linear path in Eq. (4.7), there are also simple analytical solutions for any elliptic or hyperbolic path ($x^2/a^2 \pm y^2/b^2 = 1$, where a and b are conic section parameters), provided $a/\lambda_+ = b/\lambda_-$. We show here the solution for a $\phi = 2\pi$ rotation, counterclockwise along the blue (1) circle in Fig. 4.2, for Dresselhaus only where $\mathcal{M}_{DR} = \mathcal{M}_D$ and $\lambda_+ = \lambda_- \equiv \lambda R$

$$\chi_s(2\pi) = \exp\left(-\frac{i}{2} \boldsymbol{\eta} \cdot \boldsymbol{\sigma}\right) \chi_s(0), \quad (4.10)$$

$$\begin{aligned} \boldsymbol{\eta} &= 2\pi \left(1 - \frac{1}{\epsilon}\right) \left(\frac{2}{\lambda}, 0, 1\right), \\ \epsilon &= \sqrt{1 + 4/\lambda^2}. \end{aligned} \quad (4.11)$$

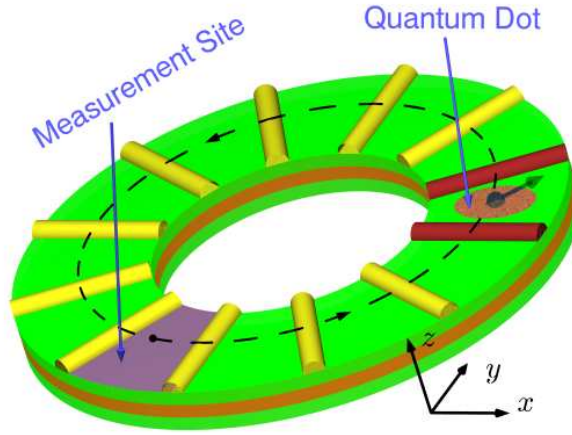


Figure 4.3: Same as in Fig. 4.1, except that the quantum dot is defined using a single layer of metallic gates deposited on top of a ring. The ring can be obtained out of a heterostructure by means of etching or defined with the help of an atomic force microscope using the oxidation technique of Refs. ([110], [111]).

Mathematically speaking, transformation (4.10) is an element of the holonomy group of point P , generated by the non-Abelian vector potential [100, 109], where this non-Abelian feature is a direct consequence of the Kramers degenerate doublets. Therefore, in the absence of any time reversal symmetry breaking interactions (like e.g. an applied magnetic field or magnetic impurities), the Kramers doublets are robust degenerate states and we are able to use the non-Abelian feature of the effective gauge potential to manipulate the spin.

4.4 Single qubit rotations: Hadamard and phase gates

The transformation (4.10) is nothing but a rotation along the vector $\boldsymbol{\eta}$ at point P which is in the x - z plane and makes an angle $\theta = \arctan(\frac{2}{\lambda})$ with the z axis, see Fig. 4.2. Therefore, for large values of λ (small circles), $\theta \approx 0$ and one would be able to realize arbitrary rotations around z axis (phase gate) with reasonable precision. Moreover, moving counterclockwise along the red (2) circle in Fig. 4.2 leads to the same result as in the blue (2) circle, but now the rotation takes place in the y - z plane. Therefore, depending on the orientation of the circles and their corresponding radii, we can, in principle, achieve all kinds of rotations around the Bloch sphere.

To be more specific, we show how to generate the Hadamard gate by rotations around two non-orthogonal axes (in our case z and $\boldsymbol{\eta}$ directions) [112] and, for convenience, we only consider the Dresselhaus term ($\alpha = 0$). As shown in Eq. (4.10), circles with different radii and/or orientations lead to different rotations. In particular, if we go counterclockwise along a full circle from point P which makes an angle ϕ with x axis (see Fig. 4.2), the electron spin will transform as follows

$$\begin{aligned} U_{11} &= -\cos \pi\epsilon + \frac{i}{\epsilon} \sin \pi\epsilon, \\ U_{12} &= \frac{2ie^{i\phi}}{\lambda\epsilon} \sin \pi\epsilon, \\ U_{11} &= U_{22}^*, \quad U_{12} = -U_{21}^*, \end{aligned}$$

where U_{ij} is the unitary transformation which acts on the initial spin state. Geometrically, U is the matrix corresponding to a rotation around $\boldsymbol{\eta}$ axis which lies in the same plane as z axis and P (see Fig. 4.2.c).

Hadamard gate can be achieved (up to a global phase) by a clockwise $\frac{\pi}{2}$ rotation around y axis followed by a counterclockwise π rotation around z axis,

$$H = \frac{1}{\sqrt{2}} \begin{pmatrix} 1 & 1 \\ 1 & -1 \end{pmatrix} = i U_z(\pi) U_y(-\frac{\pi}{2}). \quad (4.12)$$

The rotation around z with an arbitrary angle has already been discussed above, therefore, we show here how one can implement $U_y(\frac{\pi}{2})$. The main problem is that, according to Eqs. (4.10,4.11), the magnitude and the direction of the vector $\boldsymbol{\eta}$ are not independent variables (both are functions of the variable λ). Moreover, the vector $\boldsymbol{\eta}$ is not in general orthogonal to z axis. To obtain an arbitrary rotation around, say, y axis, we need to perform 3 rotations (two around $\boldsymbol{\eta}$ and one around z axis). Specifically, we want to know for which values of λ , $\pm\frac{\pi}{2}$ rotations around y axis can be achieved. One can show that [112]

$$\begin{aligned} U_y(\gamma) &= U_\eta(\theta)U_z(\phi)U_\eta(\theta), \\ \cos \eta &= \frac{\cos^2 \theta \sin^2 \frac{\gamma}{2} \pm \cos \frac{\gamma}{2} \sqrt{1 - \cot^2 \theta \sin^2 \frac{\gamma}{2}}}{\cos^2 \theta \sin^2 \frac{\gamma}{2} - 1}, \\ \tan \left(\frac{\phi}{2} \right) &= -\frac{\sin \eta \cos \theta}{\sin^2 \theta + \cos \eta \cos^2 \theta}, \quad \eta = |\boldsymbol{\eta}|, \end{aligned} \quad (4.13)$$

where for our purpose, $U_y(\frac{\pi}{2})$, we need to evaluate Eq. (4.13) at $\gamma = \pi/2$. Obviously, there are an infinite number of solutions corresponding to different values of λ . Therefore, the $\pi/2$ rotation around y axis, and consequently the

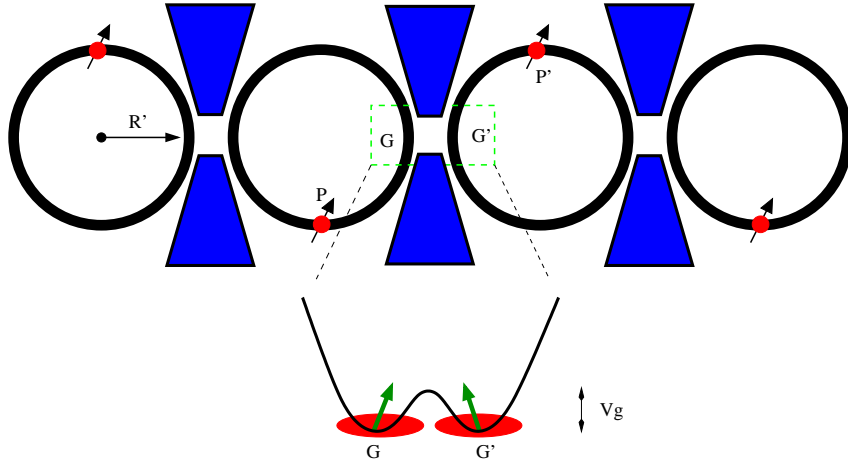


Figure 4.4: Schematic of the two-qubit rotation setup. The confined electrons are brought together at the intersection of the circular paths (with their potential profile shown in the inset at this point), where they interact via Heisenberg exchange interaction. The (holonomic) single-qubit operations are done at position P (P') while the (exchange) two-qubit gates are performed at position G (G').

Hadamard gate, is achievable in our scheme. Together with the phase gate (arbitrary rotation around z axis), all single qubit operations can be realized.

We note that the quantum fluctuations of the driving field will lead to the decoherence of the Kramers doublets even in the absence of the applied magnetic field, however, this rate saturates at the zero field strength [108]. For typical lateral GaAs quantum dots with the size $\lambda_d \sim 50$ nm which corresponds to the orbital quantization $\omega_0 \sim 1$ meV, the estimated decoherence rate $\Gamma \sim \mu s^{-1}$ [108]. Obviously, to implement efficient single qubit gates by using a ring of tunnel-coupled quantum dots, the pulsing and the total travel time of the quantum dot should be then much smaller than the decoherence time Γ^{-1} . On the other hand, the adiabaticity criterion puts a limit on the velocity v of the moving quantum dot in order to keep the electron in its ground state doublet. Therefore, one needs to satisfy $\Gamma \lambda_{SO} \ll |v| \ll \lambda_d \omega_0$ at any moment in time for a quantum dot which is displaced on the scale of λ_{SO} . Recent experiments on tunnel-coupled quantum dots show the ability to transfer the electron wave function over few hundreds of nm (from one dot to the other) in 1 ns [78]. We observe that, for instance, for the spin-orbit length $\lambda_{SO} \sim 3 \mu m$, this pulsing time is perfectly within the range of the above mentioned condition and our scheme is, therefore, experimentally feasible.

4.5 Two-qubit gates, read out, and quantum computation

For quantum computing, in addition to single qubit rotations, two qubit operations are needed as well (e.g. CNOT gate). Here, we propose a scalable setup to perform quantum computation on arbitrary N qubits (see. Fig. 4.4). To this end, we move two quantum dots around a circular path and bring them close to each other, e.g. from the position P (P') to G (G'), as shown in Fig. 4.4. The top gates are introduced to control over the wave functions of the confined electrons at the touching points of the circles. By lowering the potential barrier (V_g) between two quantum dots, the residing electron spins can couple to each other (due to the overlap of their orbital wave functions) via the Heisenberg exchange interaction [5, 37]. It has already been shown that by electrically engineering the gate potentials, one can generate the SWAP gate, and eventually the CNOT gate, between two spins [5]. However, this additional step, i.e. moving two quantum dots towards each other to perform two-qubit gates, leads to a spin rotation of each electron, see Eqs. (4.8, 4.9), and therefore this partial spin dynamics should also be taken into account. For practical purposes, we assume that the radius of the (holonomic) single-qubit gates (R) is smaller than the radius of the two-qubit circles (R'), to avoid spatial overlap of different local single-qubit operations, see Figs. 4.2.b and 4.4. The read-out part of the scheme is accomplished by applying an external magnetic field, using different techniques such as spin-to-charge conversion [78].

As an example, we observe that our scheme is able to produce the so called *cluster states* on N qubits [2]. The peculiar properties of cluster states made them a suitable candidate for realizing quantum computers in quantum optical and solid state systems [2, 4, 113, 114]. One of the main advantages of one-way quantum computation is that these set of entangled states (cluster states) are produced once, and then quantum computation is done by local (adaptive) measurements of the qubits. Therefore, there is no need to perform two-qubit gates during the information processing. In Fig. 4.4, we showed a one dimensional linear chain of qubits, however, this scheme can be easily generalized to higher dimensional lattices, and in principal be used to generate cluster states and perform *holonomic one-way* quantum computing in solid state environments.

Chapter 5

Momentum Distribution Function of the Two-Dimensional Electron Liquid: Non-analytic Corrections to the Fermi Liquid Behavior

5.1 Abstract

We compute the momentum distribution function for the electrons in a two-dimensional electron liquid. The dominant contribution to the electron self energy comes from the non-analytic corrections to the Fermi liquid. We employ the leading low-frequency terms in the self-energy expansion to calculate the electron momentum occupation number $n_{\mathbf{k}}$. Furthermore, within the *Rapid Phase Approximation* (RPA), we show that the electron-plasmon coupling at the Fermi surface leads to a quadratic frequency term in the self energy which scales as the inverse of the density. Finally, we derive an expression for the electron tunneling from an interacting lead onto a single-level quantum dot.

5.2 Introduction

Long after Landau's seminal work on interacting fermions [115], this topic is still pursued by many condensed matter physicists and there are many problems yet to be solved in fermionic systems. According to his theory, there is a one-to-one mapping between the low-energy single-particle excitations of a Fermi liquid and the corresponding excitations of a Fermi gas. However, one needs to renormalize certain physical quantities, such as mass, charge and spin susceptibilities, due to the inter-particle interactions. The aim of this chapter is not to give an introduction to Landau's Fermi liquid theory (we refer the interested reader to the classic book by Pines and Nozierés [116]), but instead to

study a handful of problems which are interested in mesoscopic physics, more specifically the role of the electron-electron interaction in 2DEG on electronic transport. One of the main quantities of interest is the electron momentum distribution which approaches the Fermi function in the absence of Coulomb interaction. To this end, one needs to know the real and imaginary parts of the exact electron Green's function. However, this is a formidable task and one is only able to calculate this function approximately. Until now, there have been many efforts to include exchange and correlation effects (beyond RPA) in calculations of the electron self energy, e.g. by introducing local field factors [57, 117–119]. However, the final result of different methods (like the effective mass and the renormalization factor Z_F) are not generally in agreement with each other and depend on the different approximation schemes. On the other hand, Monte Carlo calculations are widely considered as a consistency check, nevertheless, they suffer from the finite-size corrections which fail to produce the thermodynamic limit in certain density regimes [120].

We follow here the approach presented first by Chubukov and Maslov [121] to calculate the first leading terms in the (on-shell and off-shell) electron self energy. It has been noted that the on-shell self energy does not have a regular analytic perturbative expansion for small frequencies ω and the subleading correction is logarithmic in frequency [121]. However, having a regular expansion in frequency for the on-shell self energy is not a requirement of a generic Fermi liquid theory. We use their result to calculate the electron momentum occupation number $n_{\mathbf{k}}$ and show that the non-analytic corrections to the self energy lead to a deviation of $n_{\mathbf{k}}$ from the Fermi distribution (step function) at zero temperature. However, to observe this small change is experimentally challenging. We believe that the remaining contributions to the self energy, such as short-range correlation effects or larger frequency terms, can explain the discrepancy between our calculations and previous works. Next, we investigate the electron coupling to the collective modes of the medium, the plasmons. We show that there is a ω^2 correction to the electron self energy at the Fermi surface which is a direct consequence of the absence of the plasmonic gap in the spectrum of the electrons in two dimensions. Finally, we calculate the tunneling rate of electrons from an interacting two-dimensional electron lead onto a single-level quantum dot. We find that there is no linear dependence on the bias voltage V for the tunneling rate, even in low bias regime.

5.3 Momentum distribution

We start with the calculation of the momentum distribution function of an interacting two-dimensional electron gas, or equivalently, electron liquid. Throughout this chapter, we consider only zero-temperature properties of a Fermi liquid. The momentum occupation number for the electrons (not quasi-particles)

is generally given by the following expression [57]

$$n_{\mathbf{k}} = \frac{1}{2\pi} \int_{-\infty}^{+\infty} A(\mathbf{k}, \omega) n_F(\omega) d\omega, \quad (5.1)$$

$$G(\mathbf{k}, \omega) = \frac{1}{\omega - \epsilon_{\mathbf{k}} - \Sigma(\mathbf{k}, \omega)}, \quad (5.2)$$

$$A(\mathbf{k}, \omega) = -2 \operatorname{Im} G(\mathbf{k}, \omega) = -\frac{2\Sigma''(\mathbf{k}, \omega)}{(\omega - \tilde{\epsilon}_{\mathbf{k}})^2 + \Sigma''(\mathbf{k}, \omega)^2}, \quad (5.3)$$

$$\tilde{\epsilon}_{\mathbf{k}} = \epsilon_{\mathbf{k}} + \Sigma'(\mathbf{k}, \omega), \quad (5.4)$$

where $n_F(\omega)$ is the Fermi function, $A(\mathbf{k}, \omega)$ is the spectral function of the system, and Σ' and Σ'' are the real and imaginary part of the self energy Σ , respectively. Eq. (5.1) has a clear physical interpretation: the spectral function is simply the probability of having a particle with momentum \mathbf{k} and energy ω ($\hbar = 1$), and the Fermi function $n_F(\omega)$ gives the probability of the corresponding levels to be occupied. Therefore, the integration over frequency leads to the electron momentum distribution. Note that in the limit of weak interaction (high densities), the spectral function $A(\mathbf{k}, \omega)$ has a very sharp peak at the single quasi-particle excitations and its width is given by the imaginary part of the self energy. However, in the regime of strong interaction (low densities), the spectral function is generally broadened and has a much more complicated form.

The electron self energy $\Sigma(\mathbf{k}, \omega)$, or *mass operator*, is defined via a Dyson equation which relates the exact (interacting) single-particle Green's function $G(\mathbf{k}, \omega)$ to its corresponding free particle $G_0(\mathbf{k}, \omega)$

$$G = G_0 + G_0 \Sigma G. \quad (5.5)$$

At zero temperature, the Fermi function reduces to the step function $\Theta(-\omega)$, and the momentum distribution is given by

$$n_{\mathbf{k}} = \frac{1}{2\pi} \int_{-\infty}^0 A(\mathbf{k}, \omega) d\omega. \quad (5.6)$$

We recall that the imaginary part of the self energy is directly related to the lifetime, or equivalently, the mean free path of the quasi-particles on the mass shell

$$\frac{1}{\tau_{\mathbf{k}}} = -2\Sigma''(\mathbf{k}, \omega_{\mathbf{k}}). \quad (5.7)$$

In two dimensions, the on-shell lifetime of the quasi-particles reads [117]

$$\frac{1}{\tau_{\mathbf{k}}} = f(r_s) \frac{\epsilon_{\mathbf{k}}^2}{4\pi E_F} \ln \frac{4 E_F}{|\epsilon_{\mathbf{k}}|}, \quad (5.8)$$

$$f(r_s) = 1 + \frac{1}{2} \left(\frac{r_s}{r_s + \sqrt{2}} \right), \quad (5.9)$$

$$A(\mathbf{k}, \omega) \simeq -2 \operatorname{Im} \frac{Z_{\mathbf{k}}}{\omega - \epsilon_{\mathbf{k}} + i/2\tau_{\mathbf{k}}}, \quad (5.10)$$

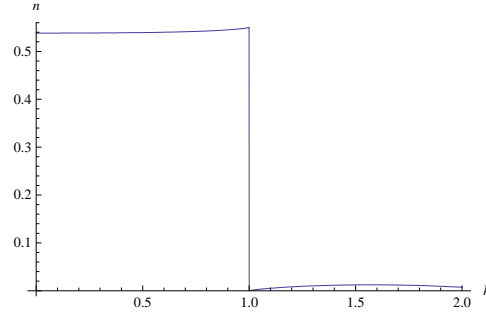


Figure 5.1: Momentum distribution for fermions calculated according to Eq. (5.11) for $r_s = 1$. The clear deviation from the expected result for fermionic distribution is due to the fact that we chose an on-shell (frequency-independent) form of the self energy.

where r_s is a dimensionless parameter which is inversely proportional to the density [117], and we assume that the renormalization factor $Z_{\mathbf{k}} = Z_F$ is constant. The momentum distribution function $n_{\mathbf{k}}$ is then given by

$$n_{\mathbf{k}} = Z_F \left[\frac{1}{2} + \frac{1}{\pi} \arctan(-2\tau_{\mathbf{k}}\epsilon_{\mathbf{k}}) \right]. \quad (5.11)$$

As it is shown in Fig. 5.1, the behavior of the function disagrees with the previous theoretical and experimental works. This is mainly due to the fact that we neglected the frequency dependence of the imaginary part of the self energy and just used the mass-shell expression for $\tau_{\mathbf{k}}$.

Furthermore, if one uses the zero-frequency RPA form of the dielectric function $\epsilon^{RPA}(q)$ to screen the Coulomb potential $V_c = 2\pi e^2/q$, the self energy will be given by

$$\Sigma(\mathbf{k}, i\omega_n) = -k_B T \sum_{\mathbf{q}, iq_m} V^{RPA}(q) G_0(\mathbf{q} + \mathbf{k}, iq_m + i\omega_n) \quad (5.12)$$

$$= -k_B T \sum_{\mathbf{q}} V^{RPA}(q) \sum_{iq_m} \frac{1}{i\omega_n + iq_m - \epsilon_{\mathbf{q}+\mathbf{k}}} \quad (5.13)$$

$$= \sum_{\mathbf{q}} V^{RPA}(q) [1 - n_F(\epsilon_{\mathbf{q}+\mathbf{k}})], \quad (5.14)$$

$$V^{RPA}(q) \equiv \frac{V_c(q)}{\epsilon^{RPA}(q)} = \frac{2\pi e^2}{q + q_{TF}}, \quad (5.15)$$

where $i\omega_n$ (iq_m) are Matsubara frequencies [57] and q_{TF} is the Thomas-Fermi screening wavelength. Therefore, the static RPA (or any other static screening of the Coulomb interaction) gives no frequency dependence for the self energy. This is due to the fact that the exchange (Fock) self energy is only a function of the electron momentum. However, we realize that the frequency dependence

of the self energy plays the major role in obtaining the correct momentum distribution, and therefore, we need to go beyond the static model.

To this end, we study the finite-frequency RPA model given by the following potential

$$V^{RPA}(q, \omega) \equiv \frac{V_c(q)}{\epsilon^{RPA}(q, \omega)} = \frac{V_c(q)}{1 - V_c(q)\chi^0(q, \omega)}, \quad (5.16)$$

where $\chi^0(q, \omega)$ is the Lindhard function for non-interacting electrons [117]. The self energy then reads

$$\Sigma(\mathbf{k}, i\omega_n) = -k_B T \sum_{\mathbf{q}, i\Omega_m} \frac{V^{RPA}(q)}{\epsilon^{RPA}(q, i\Omega_m)} \frac{1}{i\omega_n + i\Omega_m - \epsilon_{\mathbf{q}+\mathbf{k}}} \quad (5.17)$$

$$= -\frac{1}{(2\pi)^3} \int d^2q V_c(q) \int \frac{d\Omega}{\epsilon^{RPA}(q, i\Omega)} \frac{1}{i(\Omega + \omega_n) - \epsilon_{\mathbf{q}+\mathbf{k}}}, \quad (5.18)$$

where we used the zero-temperature limit

$$k_B T \sum_{\Omega_m} \rightarrow \frac{1}{2\pi} \int d\Omega. \quad (5.19)$$

5.4 Electron-plasmon coupling: The electron self energy

To calculate the retarded self energy, it is more convenient to use the method proposed by Quinn and Ferrell [57, 122]: one first does the analytic continuation of the self energy (on the complex frequency plane to the real axis), and Matsubara summation is performed afterwards,

$$\Sigma^{ret}(\mathbf{k}, \omega) = \Sigma_l^{ret}(\mathbf{k}, \omega) + \Sigma_r^{ret}(\mathbf{k}, \omega), \quad (5.20)$$

where Σ_l^{ret} is the part (the so-called *line term*) which we obtain by changing the order of the integration and the analytic continuation, and Σ_r^{ret} is the error part (*residue term*) by doing so. It can be shown that Σ_l^{ret} is a real function, however, we are interested here in the imaginary part of the self energy. Therefore, we present only the calculation for Σ_r^{ret} , given by the following expression [57]

$$Im \Sigma^{ret}(\mathbf{k}, \omega) = Im \Sigma_r^{ret}(\mathbf{k}, \omega), \quad (5.21)$$

$$\Sigma_r^{ret}(\mathbf{k}, \omega) = \frac{1}{(2\pi)^2} \int d^2q \frac{V_c(q)}{\epsilon^{RPA}(q, \epsilon_{\mathbf{k}+\mathbf{q}} - \omega)} \times [\Theta(\omega - \epsilon_{\mathbf{k}+\mathbf{q}}) - \Theta(-\epsilon_{\mathbf{k}+\mathbf{q}})]. \quad (5.22)$$

We observe that the main contribution to this integral comes from the poles of the integrand, which are the zeros of $\epsilon^{RPA}(q, \epsilon_{\mathbf{k}+\mathbf{q}} - \Omega)$. However, these poles

are nothing but the plasmonic modes [117]. Calculations based on classical models of the electron liquid give the following dispersion relations for the plasmons in three and two dimensions [117],¹

$$\omega_p(q) = \sqrt{\frac{nq^2 V_c(q)}{m}} = \begin{cases} \sqrt{\frac{4\pi n e^2}{m}} & 3D \\ \sqrt{\frac{2\pi n e^2 q}{m}} & 2D \end{cases}. \quad (5.23)$$

Obviously, the nature of the collective modes in 3D is different from 2D due to the q -dependence of the plasmon frequency. This means that, in contrast to 3D, plasmons can exist in a two-dimensional electron liquid even at very low frequencies and there is no gap in their spectrum.

The corresponding long-wavelength expansion of the RPA dielectric function ϵ^{RPA} ($v_F q \ll \omega$) is then given by

$$\epsilon^{RPA}(q, \omega) \simeq 1 - \frac{2\pi n e^2 q}{m\omega^2}. \quad (5.24)$$

Whereas the real part of the dielectric function is zero at the plasmon frequency, its imaginary part yields a delta function [117]

$$Im \left[\frac{1}{\epsilon^{RPA}(q, \epsilon_{\mathbf{k}+\mathbf{q}} - \omega)} \right] = -\frac{\pi}{2} \Omega_p(q) \delta(\omega + \Omega_p(q) - \epsilon_{\mathbf{k}+\mathbf{q}}). \quad (5.25)$$

For simplicity, we calculate only the imaginary part of the self energy at the Fermi surface and for negative frequencies which is given by

$$\begin{aligned} \Sigma''(\mathbf{k}_F, \omega) &= -\frac{e^2}{4} \int d^2 q \Omega_p(q) \delta(\omega + \Omega_p(q) - \epsilon_{\mathbf{k}_F+\mathbf{q}}) \\ &\quad \times [\Theta(\omega - \epsilon_{\mathbf{k}_F+\mathbf{q}}) - \Theta(-\epsilon_{\mathbf{k}_F+\mathbf{q}})]. \end{aligned} \quad (5.26)$$

Because $\omega < 0$ and $v_F q \ll |\omega|$, the first step function gives zero and $\Omega_p(q) \simeq \omega_p(q)$, which enormously simplifies the above integral

$$\Sigma''(\mathbf{k}_F, \omega) \simeq \frac{e^2}{4} \int dq \int d\theta \omega_p(q) \delta[\omega + \omega_p(q)] \Theta(-\epsilon_{\mathbf{k}_F+\mathbf{q}}), \quad (5.27)$$

where θ is the angle between \mathbf{k}_F and q . However, the angular integration is restricted to $\frac{\pi}{2} \leq \theta \leq \frac{3\pi}{2}$. Our final result for the electron self energy at the Fermi surface reads

$$\Sigma''(\mathbf{k}_F, \omega) = \frac{\pi e^2}{4} \int dq \omega_p(q) \delta[\omega + \omega_p(q)] = \frac{m}{4n} \omega^2. \quad (5.28)$$

¹The first quantum correction to the plasmon frequency yields $\Omega_p(q) = \omega_p(q)(1 + \frac{3a_B q}{8})$, where a_B is the Bohr radius. In our calculations, we neglect the (higher order) quantum corrections to the plasmonic spectrum because we are mainly interested in small momentum transfer q .

We note that the above result is valid for any frequency and, due to its positive sign, suppresses the same order correction which comes from the electron-hole bubble [121]. Another peculiar feature of the electron-plasmon coupling is that the self energy scales as the inverse of the density. Therefore, in low-density regimes this contribution becomes very important. However, this result can *not* be applied to *very* low density regimes, due to the breakdown of the RPA.

5.5 Non-analytic part of the self energy

Among three physically distinct bosonic non-analyticities in a generic Fermi liquid at zero temperature [121], we focus here on the non-analyticity in the particle-hole bubble (the response function), see Fig. 5.2, given by (in Matsubara representation) [57]

$$\Pi_{ph}(Q, i\Omega_m) \equiv - \int \frac{d^2p d\omega_n}{(2\pi)^3} G_0(\mathbf{p}, i\omega_n) G_0(\mathbf{p} + \mathbf{Q}, i\omega_n + i\Omega_m), \quad (5.29)$$

$$\Pi_{ph}^{Q \rightarrow 0}(Q, i\Omega_m) = \frac{m}{2\pi} \left(1 - \frac{|\Omega_m|}{\sqrt{v_F^2 Q^2 + \Omega_m^2}}\right), \quad (5.30)$$

at small frequency and momentum transfer. In the single particle-hole bubble approximation, see Fig. 5.2, the self energy reads

$$\begin{aligned} \Sigma(\mathbf{k}, i\omega_n) &= -k_B T U^2 \sum_{i\Omega_m} \int \frac{d^2Q}{(2\pi)^2} G_0(\mathbf{k} + \mathbf{Q}, i\omega_n + i\Omega_m) \\ &\quad \times \Pi_{ph}(Q, i\Omega_m), \end{aligned} \quad (5.31)$$

where k_B is the Boltzmann constant, and T is the temperature. U is the Fourier transform of the Coulomb interaction which we assumed to be momentum independent (the so-called contact interaction).

The non-analytic part of the self energy for the interacting electrons in two dimensions is given by the following equation ($\omega < 0$)

$$\Sigma''(\mathbf{k}, \omega) = -\frac{mU^2}{8\pi^3 v_F^2} \int_0^{|\omega|} d\Omega \Omega \ln \frac{4W}{|B|}, \quad (5.32)$$

$$B = (\epsilon_{\mathbf{k}} - \omega)(2\Omega + \omega - \epsilon_{\mathbf{k}}) + \frac{\Omega^2}{2E_F}(3\omega - \epsilon_{\mathbf{k}} + \Omega), \quad (5.33)$$

where $W \sim E_F$ is the upper cut-off in the integration over $v_F Q$. Note that the leading order on-shell self energy is then logarithmic in frequency ω , as shown before [121]

$$\Sigma''(\mathbf{k}, \omega_{\mathbf{k}}) = -\frac{3U^2 m}{16\pi^3 v_F^2} \omega_{\mathbf{k}}^2 \log \frac{W}{\omega_{\mathbf{k}}}. \quad (5.34)$$

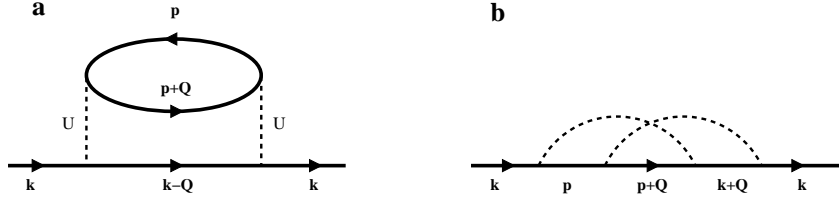


Figure 5.2: Electron-hole (a) and electron-electron (b) bubble diagrams.

We need to stress that linearizing the electron dispersion relation leads to an on-shell singularity in the electron self energy, however, it is an artificial singularity and can be removed either by introducing the curvature of the Fermi surface (as we did here) or by replacing the contact interaction U with a dynamical interaction, e.g. RPA interaction [121]. To calculate the momentum distribution, we need to know both on- and off-shell expressions for the self energy and that is why the simple form in Eq. (5.34) is not sufficient.

To go further, we approximate the form of the spectral function for low frequencies and momentum and calculate its contribution to the total momentum distribution function

$$\begin{aligned} n_{\mathbf{k}} &\simeq \frac{1}{2\pi} \int_{-\omega_c}^0 A(\mathbf{k}, \omega) d\omega \\ &= -\frac{1}{\pi} \text{Im} \int_{-\omega_c}^0 \frac{d\omega}{(1 + \alpha)\omega - (1 + \beta)\epsilon_{\mathbf{k}} - i\Sigma''(\mathbf{k}, \omega)}, \end{aligned} \quad (5.35)$$

where ω_c is a small frequency cut-off and $\alpha = -\frac{\partial}{\partial \omega} \Sigma'$ and $\beta = \frac{\partial}{\partial k} \Sigma'$ are the coefficients of the linear expansion of the real part of self energy at the Fermi surface and zero frequency. Moreover, they are both positive and normally $\alpha \gtrsim \beta$ [118].

The numerical evaluation of the integral is given in Figs. 5.3, 5.4, and 5.5, for different densities, where the size of the step (the renormalization factor Z_F), and α and β are estimated from RPA calculations [118, 123]. The parameters of the system are chosen for two-dimensional electrons in GaAs heterostructures. Evidently, the graphs follow the true behavior of the distribution function for interacting fermions, however, their energy (momentum) dependence is smaller compare to previous calculation. In particular, the jump at the Fermi surface is shifted downwards. We address this discrepancy to the absence of exchange and correlation corrections to the self energy. Moreover, we approximated Coulomb interaction with a momentum-independent contact interaction. However, better approximation can be achieved by introducing charge and density fluctuations in the calculation of the self energy, which through local field factors, lead to an effective momentum and frequency dependent interaction between the electrons [118, 119].

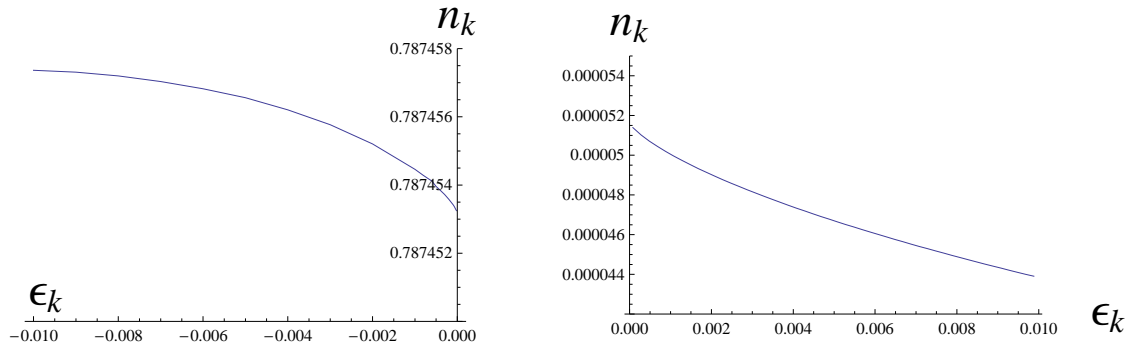


Figure 5.3: Momentum distribution function for $r_s = 0.5$. The origin of the axis is at the Fermi surface where we have linearized the energy spectrum (shown in Fermi energy units) for small energies around the Fermi energy.

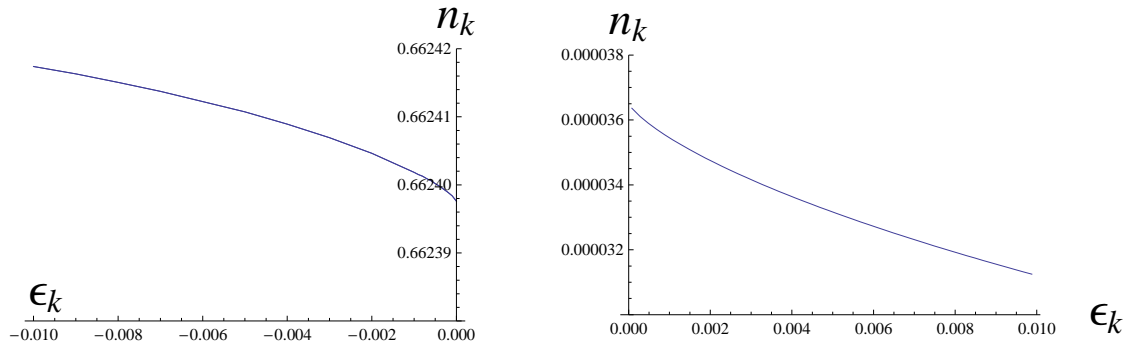


Figure 5.4: Momentum distribution function for $r_s = 1$.

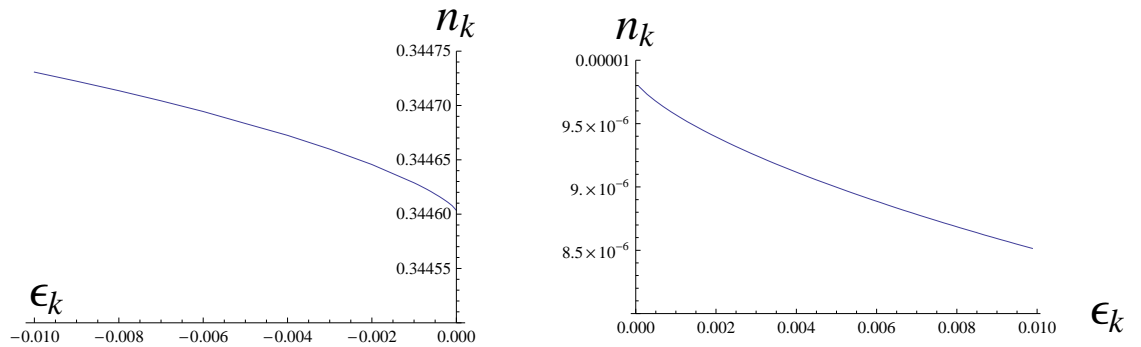


Figure 5.5: Momentum distribution function for $r_s = 5$.

5.6 Electron tunneling from a 2DEG into a quantum dot

The usual approach in charge transport models is to treat the leads as non-interacting electron gas with the corresponding Fermi distribution. Although this picture is a good approximation for high density electron leads, however, it fails in the regime of low density which the Coulomb interaction plays a crucial role. In this section, we calculate the electron tunneling from a correlated electron lead into a single-level quantum dot which is given by [57]

$$\Gamma_L = \int \langle \dot{N}_L(\mathbf{r}) \rangle d\mathbf{r}, \quad (5.36)$$

$$\dot{N}_L(\mathbf{r}) = i[H, N_L] = i[H_T, N_L], \quad (5.37)$$

$$H_T = \sum_{\sigma} t_{\sigma}(\mathbf{r}) d_{\sigma}^{\dagger} \psi_{\sigma}(\mathbf{r}) + c.c., \quad (5.38)$$

$$N_L(\mathbf{r}) = \sum_{\mathbf{k}\sigma} c_{\mathbf{k}\sigma}^{\dagger} c_{\mathbf{k}\sigma}, \quad \psi_{\sigma}(\mathbf{r}) = \sum_{\mathbf{k}} e^{i\mathbf{k}\cdot\mathbf{r}} c_{\mathbf{k}\sigma}, \quad (5.39)$$

where Γ_L is the electron tunneling rate from the left lead, N_L is the corresponding number operator, $t_{\sigma}(\mathbf{r})$ is the coordinate dependent tunneling amplitude for an electron possessing spin σ , and $c_{\mathbf{k}\sigma}$ and $\psi_{\sigma}(\mathbf{r})$ are the annihilation operators for the electrons in the leads and the quantum dot, respectively. Using the commutation relations for Fermionic operators yields

$$\dot{N}_L(\mathbf{r}) = i \sum_{\mathbf{k}\sigma} t_{\sigma}(\mathbf{r}) e^{i\mathbf{k}\cdot\mathbf{r}} d_{\sigma}^{\dagger} c_{\mathbf{k}\sigma} - t_{\sigma}^*(\mathbf{r}) e^{-i\mathbf{k}\cdot\mathbf{r}} c_{\mathbf{k}\sigma}^{\dagger} d_{\sigma}. \quad (5.40)$$

Next, we expand the S matrix in the interaction picture and retain only first order term in the tunneling probability [57]

$$\langle \dot{N}_L \rangle = i \int \int \int_{-\infty}^t \langle [N_L(t, \mathbf{r}), H_T(t', \mathbf{r}')] \rangle dt' d\mathbf{r}' d\mathbf{r} \quad (5.41)$$

$$\begin{aligned} &= - \int d\mathbf{r} \int d\mathbf{r}' \int_{-\infty}^{\infty} dt' \Theta(t - t') \\ &\quad \times \{ e^{i\Delta\mu(t-t')} \langle [M(t, \mathbf{r}), M^{\dagger}(t', \mathbf{r}')] \rangle \\ &\quad - e^{i\Delta\mu(t-t')} \langle [M^{\dagger}(t, \mathbf{r}), M(t', \mathbf{r}')] \rangle \}. \end{aligned} \quad (5.42)$$

It is more convenient to introduce here the retarded Green's function for the operator $M(t, \mathbf{r})$ and its corresponding Fourier transform

$$\mathcal{G}_{ret}(t) = -i \Theta(t) \langle [M(t), M^{\dagger}(0)] \rangle, \quad (5.43)$$

$$\tilde{\mathcal{G}}_{ret}(-\Delta\mu) = \int_{-\infty}^{\infty} e^{-i\Delta\mu t} \mathcal{G}_{ret}(t) dt. \quad (5.44)$$

It can be shown that the average tunneling rate is proportional to $\tilde{\mathcal{G}}_{ret}(-\Delta\mu)$

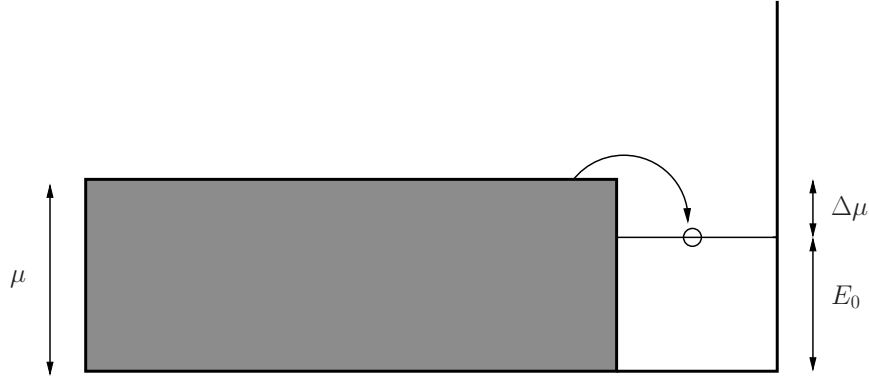


Figure 5.6: Electron tunneling from a correlated lead onto a single-level quantum dot. It is assumed that the quantum dot is empty before tunneling occurs.

[57]. To this end, we employ the Matsubara formalism for the imaginary (bosonic) frequencies. The corresponding retarded Green's function will be given by the analytic continuation

$$\begin{aligned} \tilde{\mathcal{G}}(i\omega) = & - \sum_{\mathbf{k}\sigma\mathbf{k}'\sigma'} \int d\mathbf{r} \int d\mathbf{r}' t_{\sigma}(\mathbf{r}) t_{\sigma'}^*(\mathbf{r}') e^{i(\mathbf{k}\cdot\mathbf{r}-\mathbf{k}'\cdot\mathbf{r}')} \\ & \times \int_0^{\beta} e^{i\omega\tau} \langle \mathcal{T}_{\tau} d_{\sigma}^{\dagger}(\tau) c_{\mathbf{k}\sigma}(\tau) c_{\mathbf{k}'\sigma'}^{\dagger} d_{\sigma'} \rangle, \end{aligned} \quad (5.45)$$

where $\beta = k_B T$. The correlator in the above equation factors into a product of Green's functions for the lead G_L and the quantum dot G_D

$$\langle \mathcal{T}_{\tau} d_{\sigma}^{\dagger}(\tau) c_{\mathbf{k}\sigma}(\tau) c_{\mathbf{k}'\sigma'}^{\dagger} d_{\sigma'} \rangle = \langle \mathcal{T}_{\tau} c_{\mathbf{k}\sigma}(\tau) c_{\mathbf{k}'\sigma'}^{\dagger} \rangle \langle \mathcal{T}_{\tau} d_{\sigma'} d_{\sigma}^{\dagger}(\tau) \rangle, \quad (5.46)$$

$$\langle \mathcal{T}_{\tau} c_{\mathbf{k}\sigma}(\tau) c_{\mathbf{k}'\sigma'}^{\dagger} \rangle = \delta_{\sigma\sigma'} \delta_{\mathbf{k}\mathbf{k}'} G_L^{\sigma}(\mathbf{k}, \tau), \quad (5.47)$$

$$\langle \mathcal{T}_{\tau} d_{\sigma'} d_{\sigma}^{\dagger}(\tau) \rangle = \delta_{\sigma\sigma'} G_D^{\sigma}(-\tau), \quad (5.48)$$

$$\begin{aligned} \tilde{\mathcal{G}}(i\omega) = & \sum_{\mathbf{k}\sigma} \int d\mathbf{r} \int d\mathbf{r}' e^{i\mathbf{k}\cdot(\mathbf{r}-\mathbf{r}')} t_{\sigma}(\mathbf{r}) t_{\sigma'}^*(\mathbf{r}') \\ & \times \frac{1}{\beta} \sum_{ip} G_L^{\sigma}(\mathbf{k}, ip) G_D^{\sigma}(ip - i\omega), \end{aligned} \quad (5.49)$$

where we consider only a single-orbital-level quantum dot. To simplify further, we assume that the tunneling is local and spin-independent $t_{\sigma}(\mathbf{r}) = t \delta(\mathbf{r})$, where the origin of the coordinate system is located at the barrier between the lead and the quantum dot. Using the Matsubara sum rules and performing

the analytic continuation yields ($\omega < 0$)

$$\begin{aligned}
\text{Im } \tilde{\mathcal{G}}_{ret}(\omega) &= \sum_{\mathbf{k}\sigma} |t_\sigma|^2 \int \frac{d\epsilon}{2\pi} n_F(\epsilon) [A_L^\sigma(\mathbf{k}, \epsilon) \text{Im } G_D^\sigma(\epsilon - \omega - i\eta) \\
&\quad + A_D^\sigma(\epsilon) \text{Im } G_L^\sigma(\mathbf{k}, \epsilon + \omega + i\eta)] \\
&= \sum_{\mathbf{k}} |t|^2 \int d\epsilon n_F(\epsilon) [A_L(\mathbf{k}, \epsilon) \delta(\epsilon - \omega) \\
&\quad - A_L(\mathbf{k}, \epsilon + \omega) \delta(\epsilon)] \\
&= |t|^2 \sum_{\mathbf{k}} A_L(\mathbf{k}, \omega) [n_F(\omega) - \frac{1}{2}], \tag{5.50}
\end{aligned}$$

$$\Gamma_L = 2 \text{Im } \tilde{\mathcal{G}}_{ret}(\omega) = |t|^2 \sum_{\mathbf{k}} A_L(\mathbf{k}, \omega) \quad T = 0. \tag{5.51}$$

Note that for noninteracting electrons, the spectral function $A_L(\mathbf{k}, \omega)$ reduces to a delta function $\delta(\omega - \epsilon_{\mathbf{k}})$ and one can replace the sum over k by integral over frequencies

$$\sum_{\mathbf{k}} \rightarrow \int \frac{d^2k}{(2\pi)^2} \rightarrow N_L \int d\epsilon_{\mathbf{k}}, \tag{5.52}$$

$$\Gamma_L = N_L |t|^2. \tag{5.53}$$

Physically, it means that the quantum dot acts as an energy filter, picking only those electrons which have the same energy as of the dot, see Fig. 5.6, and the sum over k gives the total number of such electrons available in the lead. Consequently, our scheme can be used to scan the spectral function for different frequencies for a wide range of energies as long as the bias voltage is smaller than the quantum dot orbital level spacing. It has been shown that the current through bilayer quantum wells is linear in voltage V ($\Delta\mu$), for small voltages across the barrier [124]. Here, in contrary to the usual tunneling between two leads, there is no linear voltage-dependence of the tunneling rate for small bias voltages, due to the energy conservation and the very narrow phase space available for the electrons to scatter into.

Appendix A

Transformation matrix S

To derive the expression for the Schrieffer-Wolff transformation matrix S in Chapter (2), we note that applying $\frac{1}{L_d^n}$ on $\boldsymbol{\xi}$ yields linear combinations of momentum and position operators. Therefore, we make an ansatz for S , like we did in Eq. (2.14), with

$$\boldsymbol{\xi}_1 = ((\alpha_1 p_{y'} + \alpha_2 x')/\lambda_-, (\tilde{\alpha}_1 p_{x'} + \tilde{\alpha}_2 y')/\lambda_+, 0), \quad (\text{A.1})$$

$$\boldsymbol{\xi}_2 = ((\beta_1 p_{x'} + \beta_2 y')/\lambda_-, (\tilde{\beta}_1 p_{y'} + \tilde{\beta}_2 x')/\lambda_+, 0). \quad (\text{A.2})$$

Then by inserting this ansatz into the relation $[H_d + H_Z, S] = H_{SO}$, we obtain a set of algebraic equations for the coefficients α_i , β_i , $\tilde{\alpha}_i$, and $\tilde{\beta}_i$ ($i = 1, 2$). We find that

$$\tilde{\alpha}_1 = \alpha_1, \quad \tilde{\alpha}_2 = -\alpha_2, \quad (\text{A.3})$$

$$\tilde{\beta}_1 = -\beta_1, \quad \tilde{\beta}_2 = \beta_2, \quad (\text{A.4})$$

with the coefficients α_i and β_i given in Eqs. (2.17)-(2.20).

Appendix B

QPC transmission coefficients: k -dependent coupling constants, $k_F^{-1}, \lambda_{sc} \ll a$

The coupling constants ϵ_{ee} , ϵ_{oo} and ϵ_{eo} , presented in Section (2.5) of Chapter (2), are generally k -dependent. In the regime where $k_F^{-1}, \lambda_{sc} \ll a$ we obtain the following relations

$$\begin{aligned} \epsilon_{ee} = & \frac{e}{4\kappa a^4 k^3} \{2k^3 \lambda_{sc} (4a^2 + 3\lambda_d^2 - 2\lambda_{sc}^2) + 6k \lambda_{sc} \cos 2(k\lambda_{sc} + \delta) \\ & - (3 + 4a^2 k^2 + 3k^2 \lambda_d^2 - 6k^2 \lambda_{sc}^2) \sin 2(k\lambda_{sc} + \delta) \\ & + (3 + 4a^2 k^2 + 3k^2 \lambda_d^2) \sin(2\delta)\} \mathbf{e}_Y, \end{aligned} \quad (\text{B.1})$$

$$\begin{aligned} \epsilon_{oo} = & \frac{e}{4\kappa a^4 k^3} \{2k^3 \lambda_{sc} (4a^2 + 3\lambda_d^2 - 2\lambda_{sc}^2) + 6k \lambda_{sc} \cos(2k\lambda_{sc}) \\ = & - (3 + 4a^2 k^2 + 3k^2 \lambda_d^2 - 6k^2 \lambda_{sc}^2) \sin(2k\lambda_{sc})\} \mathbf{e}_Y, \end{aligned} \quad (\text{B.2})$$

$$\begin{aligned} \epsilon_{oe} = & \frac{e}{8\kappa a^5 k^4} \{-(9 + 4a^2 k^2 + 3k^2 \lambda_d^2 - 18k^2 \lambda_{sc}^2) \cos(2k\lambda_{sc} + \delta) \\ & (9 + 4a^2 k^2 + 3k^2 \lambda_d^2 - 6k^4 \lambda_{sc}^4 + 6k^4 \lambda_d^2 \lambda_{sc}^2 + 8a^2 k^4 \lambda_{sc}^2) \cos \delta \\ & - (9 + 4a^2 k^2 + 3k^2 \lambda_d^2 - 6k^2 \lambda_{sc}^2) 2k \lambda_{sc} \sin(2k\lambda_{sc} + \delta)\} \mathbf{e}_X, \end{aligned} \quad (\text{B.3})$$

with δ being the relative scattering phase. The transformation to the Left-Right basis is given by

$$\epsilon_{LL} = \frac{1}{2}(\epsilon_{ee} + \epsilon_{oo} - 2\epsilon_{eo} \cos \delta), \quad (\text{B.4})$$

$$\epsilon_{RR} = \frac{1}{2}(\epsilon_{ee} + \epsilon_{oo} + 2\epsilon_{eo} \cos \delta), \quad (\text{B.5})$$

$$\epsilon_{LR} = \epsilon_{RL}^* = \frac{1}{2}(\epsilon_{ee} - \epsilon_{oo} + 2i\epsilon_{eo} \sin \delta). \quad (\text{B.6})$$

Here, as before, we have assumed that $\hbar v_F \Delta k \leq E_Z \ll \hbar v_F \lambda_{sc}^{-1} \ll E_F$. Note that the coupling constants ϵ_{LR} and ϵ_{RL} in Eq. (B.6) have both real and imaginary parts. Therefore, the last term in Eq. (2.46) does not vanish in general.

Nevertheless, we find that for an in-plane magnetic field $\mathbf{B} = (B_x, B_y, 0)$ this term vanishes, because only a single component of $\delta\mathbf{B}(t)$ (namely $\delta B_z(t)$, see Eq. (2.22)) is present for in-plane fields, which leads to $\varepsilon_{kij}n_k\mathcal{J}_{ij}^-(\omega_Z) = 0$ (see also Eqs. (2.47) and (2.60)).

Appendix C

Spin relaxation rate

To calculate the spin decay rate, we will need the master equation for the dynamics of the system. The time evolution of the combined system-bath density matrix can be written in the following form ($\hbar = 1$)

$$\dot{\rho}_{tot} = -i[H, \rho_{tot}], \quad (\text{C.1})$$

$$H = H_S + H_B + H_{SB}, \quad (\text{C.2})$$

where ρ_{tot} is the total density matrix of the system-bath in the Schrödinger picture and the dot stands for the time derivative. In Eq. (C.2), H_S , H_B , and H_{SB} denote the system, bath, and interaction Hamiltonians, respectively. Integrating over the bath degrees of freedom and using the Born-Markov approximation, one arrives at the Bloch-Redfield equations for the reduced density matrix of the system [59]

$$\begin{aligned} \dot{\rho}_{nm} = & -i\epsilon_{nm}\rho_{nm} - \sum_{kl} [\Gamma_{nllk}^{(+)}\rho_{km} + \Gamma_{lkkm}^{(-)}\rho_{nl} \\ & - \Gamma_{kmnl}^{(-)}\rho_{lk} - \Gamma_{kmnl}^{(+)}\rho_{lk}], \end{aligned} \quad (\text{C.3})$$

where $\epsilon_{km} = \epsilon_k - \epsilon_m$, with ϵ_m being the energy eigenstate of the system, $H_S|m\rangle = \epsilon_m|m\rangle$. The coefficients $\Gamma_{kmnl}^{(\pm)}$ are time-independent in this approximation and are given by the following correlators of the system-bath coupling

$$\Gamma_{kmnl}^{(-)} = \int_0^\infty dt e^{-i\epsilon_{km}t} \overline{\langle k|H_{SB}|m\rangle \langle n|H_{SB}(t)|l\rangle}, \quad (\text{C.4})$$

$$\Gamma_{kmnl}^{(+)} = [\Gamma_{lnmk}^{(-)}]^*, \quad (\text{C.5})$$

where $H_{SB}(t) = \exp(iH_B t) H_{SB} \exp(-iH_B t)$ and the overbar denotes averaging over the bath.

For our spin-1/2 system coupled to fluctuating (quantum) magnetic fields, we have (see Eqs. (2.21) and (2.22))

$$H_S = \frac{1}{2} g \mu_B \mathbf{B} \cdot \boldsymbol{\sigma}, \quad (\text{C.6})$$

$$H_{SB}(t) = \frac{1}{2} g \mu_B \delta \mathbf{B}(t) \cdot \boldsymbol{\sigma}. \quad (\text{C.7})$$

Substituting these expressions into Eq. (C.4), we obtain

$$\Gamma_{kmnl}^{(-)} = \langle k|\sigma_i|m\rangle\langle n|\sigma_j|l\rangle J_{ij}(\epsilon_{km}), \quad (\text{C.8})$$

$$J_{ij}(\omega) = \frac{g^2\mu_B^2}{2} \int_0^\infty e^{-i\omega t} \langle \delta B_i(0)\delta B_j(t)\rangle dt. \quad (\text{C.9})$$

where in the above and the following equations, we imply summation over repeating indices (like i) but not for spin indices (like m). Next we relate the spin-1/2 density matrix ρ in Eq. (C.3) to the average spin $\langle \mathbf{S} \rangle$, using the following expression

$$\rho = \frac{\mathbb{1}}{2} + \langle \mathbf{S} \rangle \cdot \boldsymbol{\sigma}, \quad (\text{C.10})$$

where $\mathbb{1}$ is the unity matrix in the spin space. Multiplying Eq. (C.3) on both sides by $\boldsymbol{\sigma}$ and tracing over the spin, we arrive at the Bloch-Redfield equation for the average spin,

$$\langle \dot{\mathbf{S}} \rangle \equiv \frac{1}{2} \text{Tr}_S(\dot{\rho}\boldsymbol{\sigma}) = \boldsymbol{\omega} \times \langle \mathbf{S} \rangle - \overleftrightarrow{\Gamma} \langle \mathbf{S} \rangle + \boldsymbol{\Upsilon}, \quad (\text{C.11})$$

where $\boldsymbol{\omega}$ stands for the spin precession frequency, defined as follows $\boldsymbol{\omega} = \sum_n \epsilon_n \boldsymbol{\sigma}_{nn}$, the tensor $\overleftrightarrow{\Gamma}$ denotes the spin relaxation tensor, and the vector $\boldsymbol{\Upsilon}$ is the inhomogeneous part of the Bloch-Redfield equation. From the Born-Markov approximation we obtain

$$\begin{aligned} \overleftrightarrow{\Gamma} \langle \mathbf{S} \rangle &= \frac{1}{2} \sum_{nm} [(\sigma_i)_{mn} J_{ij}^*(\epsilon_{nm}) \{ \langle \mathbf{S} \rangle \cdot \boldsymbol{\sigma} [\boldsymbol{\sigma}, \sigma_j] \}_{nm} \\ &\quad + (\sigma_i)_{mn} J_{ij}(\epsilon_{mn}) \{ [\sigma_j, \boldsymbol{\sigma}] \langle \mathbf{S} \rangle \cdot \boldsymbol{\sigma} \}_{nm}], \end{aligned} \quad (\text{C.12})$$

$$\begin{aligned} \boldsymbol{\Upsilon} &= -\frac{1}{4} \sum_{nm} [(\sigma_i)_{mn} J_{ij}^*(\epsilon_{nm}) \{ [\boldsymbol{\sigma}, \sigma_j] \}_{nm} \\ &\quad + (\sigma_i)_{mn} J_{ij}(\epsilon_{mn}) \{ [\sigma_j, \boldsymbol{\sigma}] \}_{nm}], \end{aligned} \quad (\text{C.13})$$

where $n, m = \pm$ refer to the spin indices. The relaxation tensor $\overleftrightarrow{\Gamma}$ can be generally divided into two parts: (i) a pure relaxation part $\overleftrightarrow{\Gamma}^r$, which originates from processes of energy exchange with the bath ($\epsilon_{mn} \neq 0$), and (ii) a dephasing part $\overleftrightarrow{\Gamma}^d$, which originates from energy conserving scattering ($\epsilon_{mn} = 0$). Setting $n = m$ in the sum of Eq. (C.12), we obtain for the dephasing part

$$\begin{aligned} \overleftrightarrow{\Gamma}^d \langle \mathbf{S} \rangle &= \sum_n (\sigma_i)_{nn} [J_{ij}^*(0) + J_{ij}(0)] \\ &\quad \times \{ \langle \mathbf{S} \rangle (\sigma_j)_{nn} - (\boldsymbol{\sigma})_{nn} \langle S_j \rangle \}, \\ &= n_i [J_{ij}^*(0) + J_{ij}(0)] \{ \langle \mathbf{S} \rangle n_j - \mathbf{n} \langle S_j \rangle \}. \end{aligned} \quad (\text{C.14})$$

Differentiating the i -th component of the latter expression with respect to $\langle S_j \rangle$, we arrive at the tensor [34]

$$\Gamma_{ij}^d = \delta_{ij} n_p n_q J_{pq}^+(0) - n_i n_p J_{pj}^+(0). \quad (\text{C.15})$$

Here and below, we use the following notations

$$J_{ij}^\pm(\omega) = \text{Re} [J_{ij}(\omega) \pm J_{ij}(-\omega)], \quad (\text{C.16})$$

$$I_{ij}^\pm(\omega) = \text{Im} [J_{ij}(\omega) \pm J_{ij}(-\omega)]. \quad (\text{C.17})$$

Note that both terms in Eq. (C.15) can be presented as scalar products of \mathbf{n} with $\delta \mathbf{B}$, as it can be seen by taking \mathbf{n} inside the time integral and averaging sign in Eq. (C.9) for any terms of the type $\sum_i n_i J_{ij}$. Therefore, for $\delta \mathbf{B}(t)$ in Eq. (2.22), the tensor $\overleftarrow{\Gamma}^d$ is identically zero, due to the transverse nature of the fluctuating field.

Setting now $n = -m$ in the sum of Eq. (C.12), we obtain for the pure relaxation part

$$\begin{aligned} \overleftarrow{\Gamma}^r \langle \mathbf{S} \rangle &= \sum_n (\sigma_i)_{-n,n} [J_{ij}^*(\epsilon_{n,-n}) + J_{ij}(\epsilon_{-n,n})] \\ &\times \{ \langle \mathbf{S} \rangle (\sigma_j)_{n,-n} - (\boldsymbol{\sigma})_{n,-n} \langle S_j \rangle \}. \end{aligned} \quad (\text{C.18})$$

Differentiating with respect to $\langle S_j \rangle$ as before and introducing $\omega = |\boldsymbol{\omega}|$, we arrive at the following expression [34]

$$\begin{aligned} \Gamma_{ij}^r &= \delta_{ij} (\delta_{pq} - n_p n_q) J_{pq}^+(\omega) - (\delta_{ip} - n_i n_p) J_{pj}^+(\omega) \\ &\quad - \delta_{ij} \varepsilon_{kpq} n_k I_{pq}^-(\omega) + \varepsilon_{ipq} n_p I_{qj}^-(\omega). \end{aligned} \quad (\text{C.19})$$

The inhomogeneous part of the Bloch-Redfield equation Υ_i is calculated in the same way,

$$\begin{aligned} 2\Upsilon_i &= n_j J_{ij}^-(\omega) - n_i J_{jj}^-(\omega) + \varepsilon_{ipq} I_{pq}^+(\omega) \\ &\quad + \varepsilon_{iqk} n_k n_p [I_{pq}^+(\omega) - I_{pq}^+(0)]. \end{aligned} \quad (\text{C.20})$$

In the secular approximation, $\Gamma_{ij} \ll \omega$, the solution of Eq. (C.11) reads

$$\begin{aligned} \langle S_X(t) \rangle &= S_\perp^0 e^{-t/T_2} \sin(\omega t + \varphi_0), \\ \langle S_Y(t) \rangle &= S_\perp^0 e^{-t/T_2} \cos(\omega t + \varphi_0), \\ \langle S_Z(t) \rangle &= S_T + (S_Z^0 - S_T) e^{-t/T_1}, \end{aligned} \quad (\text{C.21})$$

where $\langle S_Z(t) \rangle \equiv \mathbf{n} \cdot \langle \mathbf{S}(t) \rangle$ is the spin projection along the magnetic field, $\langle S_X(t) \rangle$ and $\langle S_Y(t) \rangle$ are complementary spin projections in the plane perpendicular to \mathbf{n} . Note that, here, the axes X and Y do not refer to the electron position in the QPC, as used in Chapter 2. The electron spin is initialized repeatedly in one and the same state, which is characterized by the average

spin value $\langle \mathbf{S}(0) \rangle = (S_{\perp}^0 \sin \varphi_0, S_{\perp}^0 \cos \varphi_0, S_Z^0)$. Each time, the spin is left to evolve in the presence of the magnetic field and the Markovian bath, relaxing in the long-time limit to the equilibrium value

$$\mathbf{S}_T = \frac{\mathbf{n}(\mathbf{n} \cdot \boldsymbol{\Upsilon})}{(\mathbf{n} \cdot \overleftrightarrow{\Gamma} \cdot \mathbf{n})} = -\frac{\mathbf{n}g}{2|g|} \tanh\left(\frac{\hbar\omega}{2k_B T}\right). \quad (\text{C.22})$$

The relaxation time T_1 and the decoherence time T_2 in Eq. (C.21) are defined as follows [34]

$$\frac{1}{T_1} = n_i n_j \Gamma_{ij} = n_i n_j \Gamma_{ij}^r, \quad (\text{C.23})$$

$$\frac{1}{T_2} = \frac{1}{2} (\delta_{ij} - n_i n_j) \Gamma_{ij}. \quad (\text{C.24})$$

Note that from Eq. (C.15) it follows that $n_i n_j \Gamma_{ij}^d = 0$, and therefore the relaxation time T_1 is determined solely by the pure relaxation part Γ_{ij}^r . In contrast, the decoherence time T_2 is determined by the total relaxation tensor $\Gamma_{ij} = \Gamma_{ij}^r + \Gamma_{ij}^d$. Separating the contributions of Γ_{ij}^r and Γ_{ij}^d in Eq. (C.24), we arrive at

$$\frac{1}{T_2} = \frac{1}{2T_1} + \frac{1}{T_{\varphi}}, \quad (\text{C.25})$$

where $1/T_{\varphi}$ is the dephasing contribution to the decoherence rate,

$$\frac{1}{T_{\varphi}} = \frac{1}{2} (\delta_{ij} - 2n_i n_j) \Gamma_{ij}^d = n_i n_j J_{ij}^+(0). \quad (\text{C.26})$$

As mentioned above, for $\delta \mathbf{B}(t)$ in Eq. (2.22) we have $1/T_{\varphi} = 0$, which results in $T_2 = 2T_1$, provided no other dephasing mechanism is present.

Finally, substituting Eq. (C.19) into Eq. (C.23), we obtain

$$\frac{1}{T_1} = (\delta_{ij} - n_i n_j) J_{ij}^+(\omega_Z) - \varepsilon_{kij} n_k J_{ij}^-(\omega_Z). \quad (\text{C.27})$$

Note that the tensors $J_{ij}^{\pm}(\omega)$ present in Eq. (C.27) are expressed in terms of the tensor $J_{ij}(\omega)$ given in Eq. (C.9). Furthermore, the time integration from 0 to $+\infty$ in Eq. (C.9) can be extended to an integration from $-\infty$ to $+\infty$, provided one calculates relaxation rates. Indeed, in all sums over repeating indices in Eq. (C.27), one can rearrange the terms in such a way that only integrals from $-\infty$ to $+\infty$ appear. As a result, from Eq. (C.27), we arrive at Eq. (2.46), in which the quantities $\mathcal{J}_{ij}^{\pm}(\omega)$, given in Eq. (2.47), contain only symmetric time integrals, which is convenient for calculation.

Appendix D

Schrieffer-Wolff transformation and fine structure

In this Appendix, we first work out the Schrieffer-Wolff transformation to the third order of perturbation theory and for a general weak perturbation. Then, we consider an example Hamiltonian and use the Schrieffer-Wolff transformation to partly diagonalize the Hamiltonian. Finally, we analyze the fine structure of the transformed Hamiltonian and complete its diagonalization by an additional unitary transformation.

As in standard perturbation theory, we consider a Hamiltonian $H = H_0 + H_1$, where H_1 is a weak perturbation with respect to H_0 . For the matrix elements of H_1 , we assume

$$\langle n|H_1|m\rangle = 0, \quad \text{for } E_n = E_m, \quad (\text{D.1})$$

$$\langle n|H_1|m\rangle \ll E_n - E_m, \quad \text{for } E_n \neq E_m, \quad (\text{D.2})$$

where $|n\rangle$ and E_n are, respectively, the eigenstates and eigenvalues of H_0 , and are obtained from $H_0|n\rangle = E_n|n\rangle$.

The projector \mathcal{P} , defined as follows

$$\mathcal{P}A = \sum_{\substack{nm \\ E_n = E_m}} A_{nm} |n\rangle \langle m|, \quad \forall A \quad (\text{D.3})$$

projects onto the diagonal or degenerate part of H_0 . In the particular case, when the spectrum of H_0 is non-degenerate, \mathcal{P} assumes $\mathcal{P}A = \sum_n A_{nn} |n\rangle \langle n|$, $\forall A$. From Eq. (D.1) and the definition (D.3), it follows that

$$\mathcal{P}H_1 = 0, \quad (\text{D.4})$$

$$\mathcal{P}H_0 = H_0. \quad (\text{D.5})$$

Next we look for a unitary transformation that brings the Hamiltonian $H = H_0 + H_1$ to a partly diagonal form,

$$\tilde{H} = e^{S'} (H_0 + H_1) e^{-S'} = H_0 + \Delta H, \quad (\text{D.6})$$

where the operator ΔH obeys $\mathcal{P}\Delta H = \Delta H$. Here, $S' = -S'^{\dagger}$ is the transformation matrix. The unitary transformation in Eq. (D.6) is called the Schrieffer-Wolff transformation [56]. We expand S' and ΔH in terms of the perturbation H_1 :

$$S' = S'^{(1)} + S'^{(2)} + S'^{(3)} + \dots, \quad (\text{D.7})$$

$$\Delta H = \Delta H^{(1)} + \Delta H^{(2)} + \Delta H^{(3)} + \dots, \quad (\text{D.8})$$

where the superscripts give the order of perturbation theory. Substituting Eqs. (D.7) and (D.8) into Eq. (D.6), we find a set of equations for S' ,

$$[H_0, S'^{(1)}] = H_1, \quad (\text{D.9})$$

$$[H_0, S'^{(2)}] = \frac{\mathcal{Q}}{2}[S'^{(1)}, H_1], \quad (\text{D.10})$$

$$[H_0, S'^{(3)}] = \frac{\mathcal{Q}}{2}[S'^{(2)}, H_1] + \frac{\mathcal{Q}}{12}[S'^{(1)}, [S'^{(1)}, H_1]] + \frac{\mathcal{Q}}{4}[S'^{(1)}, \mathcal{P}[S'^{(1)}, H_1]], \quad (\text{D.11})$$

where $\mathcal{Q} \equiv 1 - \mathcal{P}$. It is important to note that S is defined in Eqs. (D.9)-(D.11) up to terms $\mathcal{P}M$, where M is arbitrary. Such terms drop out on the left-hand side in Eqs. (D.9)-(D.11) because $[H_0, \mathcal{P}S'] = 0$. Thus, $\mathcal{P}S'$ can be chosen arbitrarily, which shows that there are infinitely many transformation matrices S' that satisfy Eq. (D.6). For simplicity, we choose $\mathcal{P}S' = 0$ and address the fine structure of $\tilde{H} = H_0 + \Delta H$ later on. For the operator ΔH , we obtain

$$\Delta H^{(1)} = 0, \quad (\text{D.12})$$

$$\Delta H^{(2)} = \frac{\mathcal{P}}{2}[S'^{(1)}, H_1], \quad (\text{D.13})$$

$$\Delta H^{(3)} = \frac{\mathcal{P}}{3}[S'^{(1)}, [S'^{(1)}, H_1]]. \quad (\text{D.14})$$

Introducing the Liouvillean \hat{L}_0 : $\hat{L}_0 A = [H_0, A]$, $\forall A$, we can formally solve Eqs. (D.9)-(D.11) one by one. For example, the transformation matrix at the lowest order reads $S'^{(1)} = \mathcal{Q}\hat{L}_0^{-1}H_1$. For ΔH , we recover then the perturbation theory expansion in a more familiar form,

$$\Delta H = -\mathcal{P}H_1\hat{L}_0^{-1}H_1 + \mathcal{P}H_1\hat{L}_0^{-1}H_1\hat{L}_0^{-1}H_1 + \dots, \quad (\text{D.15})$$

with the usual convention, $\mathcal{P}\hat{L}_0^{-1}A = 0$, $\forall A$, adopted.

Next, we remark that the fine structure of $\tilde{H} = H_0 + \Delta H$ can be addressed in each particular case by means of degenerate perturbation theory. As an example, we consider here the Hamiltonian $H = H_0 + H_1$, with $H_0 = H_d + H_Z$ and $H_1 = H_{SO}$. Here, H_d is given in Eq. (3.5), with $U(\mathbf{r}) = m_e\omega_0^2 r^2/2$, H_Z

is given in Eq. (3.6), and H_{SO} is given in Eq. (4.3). Using the transformation matrix $S' = S$, with S given in Eq. (3.12), we obtain a diagonal Hamiltonian, $\tilde{H} = H_d + H_Z$, at the first order of H_{SO} . At the second order of H_{SO} , however, a fine structure in the energy spectrum arises. At $B = 0$, the transformed Hamiltonian reads

$$\tilde{H} = \frac{p^2}{2m_e} + \frac{m_e\omega_0^2}{2}r^2 + \frac{1}{2}\Delta_{SO}\ell_z\sigma_z, \quad (\text{D.16})$$

where $\ell_z = -i(x\partial/\partial y - y\partial/\partial x)$ is the electron rotational momentum and $\Delta_{SO} = 2m_e(\beta^2 - \alpha^2)$. The Kramers doublets are identified, in this case, as the pairs of states with quantum numbers (ℓ_z, σ_z) and $(-\ell_z, -\sigma_z)$. For $\ell_z > 0$, the two-fold orbital degeneracy is lifted and a splitting $\Delta_{SO}\ell_z$ arises. Note that the ground orbital state, which has $\ell_z = 0$, remains doubly degenerate in this case.

At $B \neq 0$, the fine-structure interaction in Eq. (D.16) is modified by both the Zeeman energy E_Z and the cyclotron frequency ω_c . For simplicity, we omit terms $\sim \Delta_{SO}E_Z/\hbar\omega_0$, but keep terms $\sim \Delta_{SO}\omega_c/\omega_0$, assuming that $E_Z \ll \hbar\omega_c$. Then, the Hamiltonian (D.16) acquires two extra terms

$$\frac{E_Z}{2}\mathbf{n} \cdot \boldsymbol{\sigma} + \frac{\Delta_{SO}}{4\lambda^2}\sigma_z\mathcal{P}r^2, \quad (\text{D.17})$$

where $\lambda = \sqrt{\hbar/m_e\omega_c}$ is the magnetic length and we use the symmetric gauge, $\mathbf{A}(\mathbf{r}) = B_z(-y/2, x/2, 0)$. The last term in Eq. (D.17) can be viewed as a renormalization of the electron g -factor. Allowing for an anisotropic Zeeman interaction,

$$H_Z^{\text{eff}} = \frac{1}{2}\mu_B \sum_{ij} g_{ij}\sigma_i B_j, \quad (\text{D.18})$$

we obtain that the tensor g_{ij} is diagonal in the main crystallographic frame, with

$$\begin{aligned} g_{xx} &= g_{yy} = g, \\ g_{zz} &= g + \frac{m\Delta_{SO}}{\hbar^2}\langle\psi_n|r^2|\psi_n\rangle, \end{aligned} \quad (\text{D.19})$$

where m is the electron mass in vacuum and ψ_n is the electron orbital state. For the ground orbital state, the corrected g -factor reads $g_{zz} = g + m\Delta_{SO}/m_e\hbar\omega$, where $\omega = \sqrt{\omega_0^2 + \omega_c^2/4}$. Note that the sign of the correction is given by the sign of $\beta^2 - \alpha^2$ contained in Δ_{SO} . The spin quantization axis does not, in general, coincide with the magnetic field direction \mathbf{n} and is given by the following unit vector

$$\tilde{\mathbf{n}} = \frac{\mathbf{n} + \zeta\mathbf{n}_z}{\sqrt{1 + \zeta(2 + \zeta)n_z^2}}, \quad (\text{D.20})$$

where $\zeta = (g_{zz} - g)/g$. An additional unitary transformation can be used to diagonalize the 2×2 blocks of Zeeman-split Kramers doublets,

$$\tilde{H}_Z^{\text{eff}} = e^{S''} H_Z^{\text{eff}} e^{-S''} = \frac{1}{2} \tilde{E}_Z \mathbf{n} \cdot \boldsymbol{\sigma} \quad (\text{D.21})$$

where $\tilde{E}_Z = E_Z \sqrt{1 + \zeta(2 + \zeta)n_z^2}$ is the renormalized Zeeman energy and

$$e^{-S''} = \sqrt{\frac{1 + \mathbf{n} \cdot \tilde{\mathbf{n}}}{2}} - i \frac{\zeta[\mathbf{n} \times \mathbf{n}_z] \cdot \boldsymbol{\sigma}}{\sqrt{\zeta^2 n_z^2 (1 - n_z^2)}} \sqrt{\frac{1 - \mathbf{n} \cdot \tilde{\mathbf{n}}}{2}}. \quad (\text{D.22})$$

So far, we have considered a given orbital state ψ_n , for which the tensor g_{ij} is given in Eq. (D.19). The transformation above is also valid in general, provided ζ is understood as a diagonal operator, $\zeta = (m\Delta_{SO}/g\hbar^2)\mathcal{P}r^2$.

We summarize by mentioning that the unitary transformation in Eq. (D.6) can, in principle, be adjusted to give a fully diagonal $\tilde{H} = H_0 + \Delta H$, i.e. we had not to require $\mathcal{P}S' = 0$ in the first place. However, in practice, it is more convenient first to apply the non-degenerate perturbation theory, Eqs. (D.9)-(D.15), and then, at the end, complete the diagonalization of $H_0 + \Delta H$ by a second unitary transformation. The latter is specific to each particular case and amounts, in general, to applying the degenerate perturbation theory. For the sake of simplicity, we shall refer to S in the main text of the thesis as to the full transformation matrix, despite the fact that the respective unitary transformation comes, in practice, as a product of two unitary transformations. Thus, we denote the product $e^{-S'} e^{-S''}$ by e^{-S} in the main text. Finally, we remark that $e^{-S''} \approx 1 + \mathcal{O}(H_{SO}^2)$.

Appendix E

The non-Abelian spin rotation generator

The transformation matrix $S = -S^\dagger$ in Eq. (4.4) can be evaluated by perturbation theory in H_{SO} or by diagonalizing the Hamiltonian H for a specific potential $U(\mathbf{r})$. At the leading order in H_{SO} , S satisfies the operator equation

$$[H_d + H_Z, S] = H_{SO}, \quad (\text{E.1})$$

whereas the energy levels of H coincide, at this order, with the energy levels of $H_d + H_Z$. A detailed analysis of the transformation in Eq. (4.4) is given in Refs. [86, 105].

Next we consider the Schrödinger equation,

$$i\hbar \frac{\partial \Psi(\mathbf{r}, t)}{\partial t} = H(t) \Psi(\mathbf{r}, t), \quad (\text{E.2})$$

in the presence of a time-dependent displacement-vector $\mathbf{r}_0(t)$. At each moment in time, the Hamiltonian $H(t)$ has an instantaneous basis of states, which we denote by $|\Phi_{ns\mathbf{r}_0}\rangle$, where the index \mathbf{r}_0 indicates that the dot is centered at \mathbf{r}_0 . Obviously, the states $|\Phi_{ns\mathbf{r}_0}\rangle$ can be obtained from Eq. (4.4) by means of a displacement by the vector $-\mathbf{r}_0$. In the presence of a magnetic field, the instantaneous eigenstates read

$$\Phi_{ns\mathbf{r}_0}(\mathbf{r}) = e^{(ie/\hbar c)f(\mathbf{r}, \mathbf{r}_0)} T_{-\mathbf{r}_0} \psi_{ns}(\mathbf{r}), \quad (\text{E.3})$$

where $f(\mathbf{r}, \mathbf{r}_0)$ is a gauge function satisfying the equation

$$-\frac{\partial f(\mathbf{r}, \mathbf{r}_0)}{\partial \mathbf{r}} = \mathbf{A}(\mathbf{r} - \mathbf{r}_0) - \mathbf{A}(\mathbf{r}). \quad (\text{E.4})$$

In Eq. (E.3), $T_{\mathbf{a}} = \exp(\mathbf{a} \cdot \partial / \partial \mathbf{r})$ denotes the translation operator by a vector \mathbf{a} and for the cylindric gauge $\mathbf{A}(\mathbf{r}) = B_z (-y/2, x/2, 0)$, we can choose $f(\mathbf{r}, \mathbf{r}_0) = \mathbf{r}_0 \cdot \mathbf{A}(\mathbf{r})$.

The solutions of the Schrödinger equation (E.2) can be looked for in terms of the instantaneous basis in Eq. (E.3),

$$\Psi(\mathbf{r}, t) = \sum_{ns} a_{ns}(t) \Phi_{ns\mathbf{r}_0(t)}(\mathbf{r}, t), \quad (\text{E.5})$$

where the coefficients $a_{ns}(t)$ satisfy the normalization condition $\sum_{ns} |a_{ns}(t)|^2 = 1$ and we have used the notation $\Phi_{ns\mathbf{r}_0(t)}(\mathbf{r}, t) = \exp(-iE_{ns}t/\hbar) \Phi_{ns\mathbf{r}_0(t)}(\mathbf{r})$ for the Schrödinger picture of Eq. (E.3). By substituting Eq. (E.5) into Eq. (E.2) we obtain a set of equations for $a_{ns}(t)$

$$\frac{da_{ns}}{dt} = \frac{i}{\hbar} \sum_{n's'} \mathbf{v}_0(t) \cdot \langle \psi_{ns} | \tilde{\mathbf{p}}(t) | \psi_{n's'} \rangle e^{i\omega_{nsn's'}t} a_{n's'}, \quad (\text{E.6})$$

where $\mathbf{v}_0(t) = d\mathbf{r}_0(t)/dt$ is the velocity of the slipping dot and $\omega_{nsn's'} = (E_{ns} - E_{n's'})/\hbar$. The quantity $\tilde{\mathbf{p}}(t)$ depends on t only through $\mathbf{r}_0(t)$ and is defined as follows

$$\tilde{\mathbf{p}} = -i\hbar \frac{\partial}{\partial \mathbf{r}} - \frac{e}{c} T_{\mathbf{r}_0} \frac{\partial f(\mathbf{r}, \mathbf{r}_0)}{\partial \mathbf{r}_0} T_{-\mathbf{r}_0}. \quad (\text{E.7})$$

For our choice of gauge, i.e. cylindrical gauge, we obtain $\tilde{\mathbf{p}} = -i\hbar \partial/\partial \mathbf{r} - (e/c) \mathbf{A}(\mathbf{r} + \mathbf{r}_0)$. Note that the choice of $f(\mathbf{r}, \mathbf{r}_0)$ is not unique; In general, one can also include terms of the form $g_0(\mathbf{r}_0) + sg_3(\mathbf{r}_0) |\psi_{ns}\rangle \langle \psi_{ns}|$ and, at $B = 0$, additionally terms of the form $g_1(\mathbf{r}_0) |\psi_{ns}\rangle \langle \psi_{n,-s}| + isg_2(\mathbf{r}_0) |\psi_{ns}\rangle \langle \psi_{n,-s}|$, where $g_j(\mathbf{r}_0)$ are arbitrary real functions of \mathbf{r}_0 .

Next we consider a specific situation for which we can further simplify Eq. (E.6).

We can further define a resting qubit at a position \mathbf{r}_0 using the transformation in Eq. (E.3). Let the quantum dot be driven along a trajectory $\mathbf{r}_0(t)$ between two points $\mathbf{r}_A = 0$ and \mathbf{r}_B during a time interval T , such that

$$\mathbf{r}_0(0) = \mathbf{r}_A, \quad \mathbf{r}_0(T) = \mathbf{r}_B, \quad (\text{E.8})$$

$$\mathbf{v}_0(0) = 0, \quad \mathbf{v}_0(T) = 0. \quad (\text{E.9})$$

The probability for the qubit to leak out of its subspace by the end of the pulse is given by

$$P_{\text{leak}} = \sum_{\substack{n \neq 0 \\ s = \pm 1/2}} |a_{ns}(T)|^2. \quad (\text{E.10})$$

The coefficients $a_{ns}(T)$ can, therefore, be found by solving Eq. (E.6) with the initial condition $\sum_s |a_{0s}(0)|^2 = 1$. At the leading order in the driving, we have

$$a_{ns}(T) \simeq \frac{i}{\hbar} \int_0^T dt \mathbf{v}_0(t) \cdot \langle \psi_{ns} | \tilde{\mathbf{p}}(t) | \sigma \rangle e^{i\omega_{ns0\sigma}t}, \quad (\text{E.11})$$

where $|\sigma\rangle = |\psi_{0\sigma}\rangle$ denotes the qubit state at $t = 0$. Since the matrix elements $\langle \psi_{ns} | \tilde{\mathbf{p}}(t) | \sigma \rangle$ do not depend on time for $n \neq 0$, the coefficients $a_{ns}(T)$ in

Eq. (E.11) are, thus, proportional to the Fourier transform of the quantum dot velocity $\mathbf{v}_0(t)$ evaluated at the orbital transition frequency $\omega_{ns0\sigma} \simeq \omega_0$. It is, therefore, sufficient to devise pulses of $\mathbf{v}_0(t)$ with the spectral weight below the orbital frequency ω_0 in order to avoid leakage from the qubit subspace.

It is convenient to have an adiabaticity criterion based on the differential properties of $\mathbf{v}_0(t)$. We note that Eq. (E.6) can be rewritten in terms of the new unknowns $\tilde{a}_{ns} = a_{ns} \exp(-itE_{ns}/\hbar)$ as follows

$$\frac{d\tilde{a}_{ns}}{dt} = -\frac{i}{\hbar} \sum_{n's'} \mathcal{H}_{nsn's'}(t) \tilde{a}_{n's'}, \quad (\text{E.12})$$

$$\mathcal{H}_{nsn's'}(t) = E_{ns} \delta_{ns,n's'} - \mathbf{v}_0(t) \cdot \langle \psi_{ns} | \tilde{\mathbf{p}}(t) | \psi_{n's'} \rangle. \quad (\text{E.13})$$

One can identify Eq. (E.13) with $\mathcal{H}(t) = H(t) - i\hbar\partial/\partial t$, expressed in the time-dependent basis (E.3). For the case of $B = 0$, Eq. (E.13) has been previously obtained in Ref. [108]. The virtue of Eq. (E.13) is that $\mathcal{H}_{nsn's'}(t)$ depend on time only through a perturbation $\propto v_0(t)$, which vanishes at $t = 0, T$. Applying the adiabaticity criterion to the Hamiltonian in Eq. (E.13) for the orbital transitions out of the qubit subspace, we obtain that the condition

$$\left| \frac{d\mathbf{v}_0}{dt} \cdot \langle \psi_{ns} | \tilde{\mathbf{p}} | \sigma \rangle \right| \ll \hbar\omega_0^2 \quad (\text{E.14})$$

must be satisfied at any moment in time in order for the pulse to be adiabatic.

If $\mathbf{r}_0(t)$ changes adiabatically with respect also to the Zeeman energy E_Z , then $|a_s(t)|$ is independent of time, i.e. the qubit follows adiabatically the change of its basis states. In the opposite case, when $B = 0$, the states $|\psi_{ns}\rangle$ in Eq. (4.4) are degenerate with respect to the spin index s to all orders of H_{SO} , due to the Kramers theorem. In this case, the change of the instantaneous basis can be interpreted as a unitary operation on the qubit. In order to tell what is the qubit instantaneous basis at $B = 0$, one has, in principle, to consider a finite B and follow the energy levels of the quantum dot in the limit of $B \rightarrow 0$. Here, it is important to note that the spin-orbit interaction gives rise to an anisotropic Zeeman interaction at the second order of H_{SO} [105]. As a result, the spin quantization axis and the magnetic field are not necessarily aligned with each other. To avoid the need of state finding, we denote $\langle ns | e^{-S} | n, -s \rangle$ by α_{ns} and remark that $\alpha_{ns} = \mathcal{O}(H_{SO}^2)$.

Returning now to Eq. (E.5), we consider an infinitesimal displacement of the quantum dot in the (x,y) -plane by $\delta\mathbf{r}_0$ and derive the corresponding generators of the qubit transformation under translations. We encode the qubit into the instantaneous states of the n -th orbital level of the Hamiltonian (4.1).

Let $\mathbf{r}_0(t) = \mathbf{r}_0$ be the position of the quantum dot center at time t and $\mathbf{r}_0(t + \delta t) = \mathbf{r}_0 + \delta\mathbf{r}_0$ be the new position at time $t + \delta t$. The infinitesimal transformation that takes the state $\Psi(t)$ to a new state $\Psi(t + \delta t)$ is given in Eq. (E.2). Starting from a basis state $\Phi_{ns}(t)$ at time t , we obtain the following

state at time $t + \delta t$,

$$\Psi_{ns}(t + \delta t) = \Phi_{ns}(t) - \frac{i}{\hbar} H(t) \Phi_{ns}(t) \delta t. \quad (\text{E.15})$$

The overlap of this state with the basis state $\Phi_{ns'}(t + \delta t)$, generates an infinitesimal transformation of the Kramers doublet, where from Eq. (E.3), we find the basis state at time $t + \delta t$,

$$\Phi_{ns'}(t + \delta t) = \Phi_{ns'}(t) - \frac{i}{\hbar} \left[\frac{d\mathbf{r}_0}{dt} \cdot \tilde{\mathbf{p}} + H(t) \right] \Phi_{ns'}(t) \delta t. \quad (\text{E.16})$$

Thus, the desired infinitesimal transformation reads

$$\langle \Phi_{ns'}(t + \delta t) | \Psi_{ns}(t + \delta t) \rangle = \delta_{s's} + \frac{i}{\hbar} \delta \mathbf{r}_0 \cdot \langle \Phi_{ns'}(t) | \tilde{\mathbf{p}} | \Phi_{ns}(t) \rangle. \quad (\text{E.17})$$

For a qubit that is encoded into the instantaneous states of the n -th orbital level of the Hamiltonian (4.1), the infinitesimal transformation (E.17) can be rewritten as

$$|s(t)\rangle \rightarrow \exp(\mathcal{G} \cdot \delta \mathbf{r}_0) |s(t)\rangle. \quad (\text{E.18})$$

Here, $|s(t)\rangle$ denotes the qubit state at time t and the 2×2 matrices and

$$\mathcal{G}_{ss'} = \frac{i}{\hbar} \langle \psi_{ns} | \tilde{\mathbf{p}} | \psi_{ns'} \rangle \quad (\text{E.19})$$

are the corresponding generators of the transformations that take place on the qubit under parallel translations of the quantum dot on the substrate. In deriving Eq. (E.19) we made use of our choice of gauge, see the text below Eq. (E.3).

It is important to note that, along with spin-orbit interaction-induced SU(2) transformations on the qubit, Eqs. (E.18) and (E.19) account also for the Aharonov-Bohm phase due to the orbital magnetic field. It is, therefore, convenient to subdivide \mathcal{G} into Abelian and non-Abelian parts,

$$\mathcal{G}_{ss'} = \mathcal{G}_{ss'}^a + \mathcal{G}_{ss'}^{na}, \quad (\text{E.20})$$

$$\mathcal{G}_{ss'}^a = \delta_{ss'} \sum_p \frac{1}{2} \mathcal{G}_{pp}. \quad (\text{E.21})$$

For a point-like quantum dot, we obtain the Abelian generators

$$\mathcal{G}_{ss'}^a = (-ie/\hbar c) \delta_{ss'} \mathbf{A}(\mathbf{r}_0), \quad (\text{E.22})$$

recovering, thus, the usual expression for the Aharonov-Bohm phase ($e^{i\varphi_{\text{AB}}}$)

$$\varphi_{\text{AB}} = -\frac{e}{\hbar c} \int_c \mathbf{A}(\mathbf{r}_0) \cdot d\mathbf{r}_0 \quad (\text{E.23})$$

in going around a closed path \mathcal{C} . Note that it is always possible to sum up independently the phase due to the Abelian generators, because $[\mathcal{G}^a, \mathcal{G}^{na}] = 0$. In what follows, we focus on the non-Abelian generators \mathcal{G}^{na} since they give rise to useful unitary operations on the qubit.

To calculate the matrix elements $\langle \Phi_{ns'}(t) | \tilde{\mathcal{P}} | \Phi_{ns}(t) \rangle$, we make use of Eq. (E.3) and the following property $e^{-ief/\hbar c} \tilde{\mathcal{P}} e^{ief/\hbar c} = \mathcal{P}$, and obtain that

$$\langle \Phi_{ns'}(t) | \tilde{\mathcal{P}} | \Phi_{ns}(t) \rangle = e^{\frac{i}{\hbar}(E_{ns'} - E_{ns})t} \langle \psi_{ns'} | T_{\mathbf{r}_0} \mathcal{P} T_{-\mathbf{r}_0} | \psi_{ns} \rangle, \quad (\text{E.24})$$

where $|\psi_{ns}\rangle$ are the states in Eq. (4.4) and E_{ns} are the energies corresponding to these states. Obviously, if the Zeeman energy is large, the exponential factor in Eq. (E.24) oscillates rapidly as a function of time and the transformation in Eq. (E.17) averages out to unity. For the latter to take place, it is sufficient that

$$\left| \frac{d\mathbf{r}_0}{dt} \cdot \frac{\langle \psi_{ns} | T_{\mathbf{r}_0} \mathcal{P} T_{-\mathbf{r}_0} | \psi_{n,-s} \rangle}{E_{ns} - E_{n,-s}} \right| \ll 1. \quad (\text{E.25})$$

Estimating further $|\langle \psi_{ns} | T_{\mathbf{r}_0} \mathcal{P} T_{-\mathbf{r}_0} | \psi_{n,-s} \rangle| \sim \hbar/\lambda_{SO}$ and $E_{ns} - E_{n,-s} \approx E_Z$, we obtain that the spin rotator is inefficient at small speeds of the dot,

$$\hbar \dot{r}_0 \ll E_Z \lambda_{SO}. \quad (\text{E.26})$$

In the absence of magnetic fields, the transformation in Eq. (E.17) acquires the form

$$\Delta = \mathbb{1} + \delta\mathbf{r}_0 \cdot \langle \psi_{ns'} | \frac{\partial}{\partial \mathbf{r}} | \psi_{ns} \rangle. \quad (\text{E.27})$$

Note that Eq. (E.27) can as well be derived from the infinitesimal version of the identity $|\Phi_{ns}(t)\rangle = T_{\delta\mathbf{r}_0} T_{-\delta\mathbf{r}_0} |\Phi_{ns}(t)\rangle = T_{\delta\mathbf{r}_0} |\Phi_{ns}(t + \delta t)\rangle$. Thus, the spin rotation takes place (at least at $B = 0$), because the confinement defines local Kramers states, which differ from each other along the dot trajectory. An illustration of the dot trajectory is given in Fig. 4.2. The radius-vector $\mathbf{r}_0(t)$ describes a curve as a function of time and, as the dot is moved along that curve, the local Kramers state changes. The infinitesimal transformation in Eq. (E.27), or more generally in Eq. (E.17), has to be ordered along the path of integration when integrated over $\delta\mathbf{r}_0$. This ordering occurs because the spin matrices in Eq. (E.27) do not always commute with each other at different points of the path due to generally different directions of $\delta\mathbf{r}_0$ at these points.

Further, it is convenient to refer to the Kramers doublets $|\Phi_{ns}(t)\rangle$ as to spin states that are locally defined at each point of the dot trajectory. Mathematically, we perform a mapping given by the following canonical transformation,

$$|\Phi_{ns, \mathbf{r}_0}\rangle = e^{ief/\hbar c} T_{-\mathbf{r}_0} e^{-S} |\psi_n\rangle |\chi_s\rangle, \quad (\text{E.28})$$

which is obtained by substituting Eq. (4.4) into Eq. (E.3) and omitting the free evolution factor $e^{-(i/\hbar)E_{ns}t}$ from $\psi_{ns}(\mathbf{r}, t)$. For a given quantum number n , this transformation, obviously, maps the Kramers doublet at position \mathbf{r}_0 onto

a spin-1/2 space: $|\chi_s\rangle$, ($s = \pm 1/2$). Equation (E.27) can then be rewritten in an operator form

$$\Delta = \mathbb{1} + \delta\mathbf{r}_0 \cdot \langle\psi_n|e^S \frac{\partial}{\partial\mathbf{r}} e^{-S}|\psi_n\rangle, \quad (\text{E.29})$$

where S contains Pauli matrices, which should now be regarded as effective operators in the Hilbert space of a local Kramers doublet (n, \mathbf{r}_0) .

For a small quantum dot the transformation matrix S is small, because $\lambda_d \ll \lambda_{SQ}$ [86]. In this case, one can expand the transformation to the first order, $e^{\pm S} \approx 1 \pm S$. Then, Eq. (E.29) acquires the form ($B = 0$)

$$\Delta = \mathbb{1} - \delta\mathbf{r}_0 \cdot \langle\psi_n|\frac{\partial S}{\partial\mathbf{r}}|\psi_n\rangle, \quad (\text{E.30})$$

where we used $\langle\psi_n|\partial/\partial\mathbf{r}|\psi_n\rangle = 0$.

Bibliography

- [1] M. A. Nielsen and I. L. Chuang, *Quantum Computation and Quantum Information* (Cambridge University Press, New York, 2000).
- [2] H.-J. Briegel and R. Raussendorf, Phys. Rev. Lett. **86**, 910 (2001).
- [3] K. Huang, *Statistical Mechanics, second edition* (John Wiley, Singapore, 1987).
- [4] R. Raussendorf and H.-J. Briegel, Phys. Rev. Lett. **86**, 5188 (2001).
- [5] D. Loss and D. P. DiVincenzo, Phys. Rev. A **57**, 120 (1998).
- [6] R. Raussendorf, D. E. Browne, and H.-J. Briegel, Phys. Rev. A **68**, 022312 (2003).
- [7] N. W. Ashcroft and N. D. Mermin, *Solid State Physics* (Saunders, Philadelphia, 1976).
- [8] G. Burkard, D. Loss, and D. P. DiVincenzo, Phys. Rev. B **59**, 2070 (1999).
- [9] D. D. Awschalom, D. Loss, and N. Samarth (eds.), *Semiconductor Spintronics and Quantum Computation* (Springer, Berlin, 2002).
- [10] A. Barenco *et al.*, Phys. Rev. A **52**, 3457 (1995).
- [11] G. Burkard, D. Loss, D. DiVincenzo, and J. A. Smolin, Phys. Rev. B **60**, 11404 (1999).
- [12] J. Schliemann, D. Loss, and A. H. MacDonald, Phys. Rev. B **63**, 085311 (2001).
- [13] R. Requist, J. Schliemann, A. G. Abanov, and D. Loss, Phys. Rev. B **71**, 115315 (2005).
- [14] J. I. Cirac and P. Zoller, Phys. Rev. Lett. **74**, 4091 (1995).
- [15] J. E. Mooij *et al.*, Science **285**, 1036 (1999).

- [16] S. A. Wolf *et al.*, *Science* **294**, 1488 (2001).
- [17] I. Žutić, J. Fabian, and S. D. Sarma, *Rev. Mod. Phys.* **76**, 323 (2004).
- [18] V. Cerletti, W. A. Coish, O. Gywat, and D. Loss, *Nanotechnology* **16**, R27 (2005).
- [19] M. Field *et al.*, *Phys. Rev. Lett.* **70**, 1311 (1993).
- [20] E. Buks, R. Schuster, M. Heiblum, D. Mahalu, and V. Umansky, *Nature* **391**, 871 (1998).
- [21] M. Avinun-Kalish, M. Heiblum, A. Silva, D. Mahalu, and V. Umansky, *Phys. Rev. Lett.* **92**, 156801 (2004).
- [22] J. M. Elzerman *et al.*, *Nature* **430**, 431 (2004).
- [23] R. Hanson *et al.*, *Phys. Rev. Lett.* **94**, 196802 (2005).
- [24] J. Petta, A. Johnson, C. Marcus, M. Hanson, and A. Gossard, *Phys. Rev. Lett.* **93**, 186802 (2004).
- [25] S. Gustavsson *et al.*, *Phys. Rev. Lett.* **96**, 076605 (2006).
- [26] S. Tarucha, D. G. Austing, T. Honda, R. J. van der Hage, and L. P. Kouwenhoven, *Phys. Rev. Lett.* **77**, 3613 (1996).
- [27] M. Ciorga *et al.*, *Phys. Rev. B* **61**, R16315 (2000).
- [28] J. M. Elzerman *et al.*, *Phys. Rev. B* **67**, R161308 (2003).
- [29] R. Hanson *et al.*, *Phys. Rev. Lett.* **91**, 196802 (2003).
- [30] Y. Levinson, *Europhys. Lett.* **39**, 299 (1997).
- [31] I. L. Aleiner, N. S. Wingreen, and Y. Meir, *Phys. Rev. Lett.* **79**, 3740 (1997).
- [32] A. Silva and S. Levit, *Europhys. Lett.* **62**, 103 (2003).
- [33] H.-A. Engel *et al.*, *Phys. Rev. Lett.* **93**, 106804 (2004).
- [34] V. N. Golovach, A. Khaetskii, and D. Loss, *Phys. Rev. Lett.* **93**, 016601 (2004).
- [35] A. V. Khaetskii and Y. V. Nazarov, *Phys. Rev. B* **64**, 125316 (2001).
- [36] M. Kroutvar *et al.*, *Nature* **432**, 81 (2004).
- [37] G. Burkard, D. Loss, and D. P. DiVincenzo, *Phys. Rev. B* **59**, 2070 (1999).

- [38] A. V. Khaetskii, D. Loss, and L. Glazman, *Phys. Rev. Lett.* **88**, 186802 (2002).
- [39] A. V. Khaetskii, D. Loss, and L. Glazman, *Phys. Rev. B* **67**, 195329 (2003).
- [40] I. A. Merkulov, A. L. Efros, and M. Rosen, *Phys. Rev. B* **65**, 205309 (2002).
- [41] S. I. Erlingsson and Y. V. Nazarov, *Phys. Rev. B* **66**, 155327 (2002).
- [42] J. Schliemann, A. V. Khaetskii, and D. Loss, *Phys. Rev. B* **66**, 245303 (2002).
- [43] R. de Sousa and S. D. Sarma, *Phys. Rev. B* **67**, 033301 (2003).
- [44] W. A. Coish and D. Loss, *Phys. Rev. B* **70**, 195340 (2004).
- [45] W. A. Coish and D. Loss, *Phys. Rev. B* **72**, 125337 (2005).
- [46] D. Klauser, W. A. Coish, and D. Loss, *Phys. Rev. B* **73**, 205302 (2006).
- [47] A. S. Bracker *et al.*, *Phys. Rev. Lett.* **94**, 047402 (2005).
- [48] F. H. L. Koppens *et al.*, *Science* **309**, 1346 (2005).
- [49] J. R. Petta *et al.*, *Nature* **435**, 925 (2005).
- [50] J. R. Petta *et al.*, *Science* **309**, 2180 (2005).
- [51] H.-A. Engel and D. Loss, *Phys. Rev. Lett.* **86**, 4648 (2001).
- [52] O. Gywat *et al.*, *Phys. Rev. B* **69**, 205303 (2004).
- [53] O. Gywat, H.-A. Engel, and D. Loss, *J. Supercond.* **69**, 18 (2005).
- [54] Y. Bychkov and E. I. Rashba, *J. Phys. C* **17**, 6039 (1984).
- [55] G. Dresselhaus, *Phys. Rev.* **100**, 580 (1955).
- [56] J. R. Schrieffer and P. A. Wolff, *Phys. Rev.* **149**, 491 (1966).
- [57] G. Mahan, *Many Particle Physics, third edition* (Plenum Press, New Yor, 2000).
- [58] S. Gustavsson *et al.*, *Phys. Rev. Lett* **96**, 076605 (2006).
- [59] C. P. Slichter, *Principles of Magnetic Resonance* (Springer-Verlag, Berlin, 1980).
- [60] D. P. DiVincenzo and D. Loss, *Phys. Rev. B* **71**, 035318 (2005).

- [61] Y. M. Blanter and M. Büttiker, Phys. Rep. **336**, 1 (2000).
- [62] N. M. Atherton, *Electron Spin Resonance* (Ellis Horwood Limited, New York, 1973).
- [63] H.-A. Engel and D. Loss, Phys. Rev. B **65**, 195321 (2002).
- [64] Y. Kato *et al.*, Science **299**, 1201 (2003).
- [65] R. C. Miller, A. C. Gossard, D. A. Kleinman, and O. Munteanu, Phys. Rev. B **29**, 3740 (1984).
- [66] G. Salis *et al.*, Nature **414**, 619 (2001).
- [67] E. I. Rashba and A. L. Efros, Phys. Rev. Lett. **91**, 126405 (2003).
- [68] E. I. Rashba and A. L. Efros, Appl. Phys. Lett. **83**, 5295 (2003).
- [69] E. I. Rashba, J. Supercond. **18**, 137 (2005).
- [70] R. L. Bell, Phys. Rev. Lett. **9**, 52 (1962).
- [71] B. D. McCombe, S. G. Bishop, and R. Kaplan, Phys. Rev. Lett. **18**, 748 (1967).
- [72] M. Dobrowolska *et al.*, Phys. Rev. Lett. **49**, 845 (1982).
- [73] M. Dobrowolska *et al.*, Phys. Rev. B **29**, 6652 (1984).
- [74] M. Schulte, J. G. S. Lok, G. Denninger, and W. Dietsche, Phys. Rev. Lett. **94**, 137601 (2005).
- [75] M. Duckheim and D. Loss, Nature Physics **2**, 195 (2006).
- [76] Y. Kato, R. C. Myers, A. C. Gossard, and D. D. Awschalom, Nature **427**, 50 (2004).
- [77] J. Nitta, T. Akazaki, H. Takayanagi, and T. Enoki, Phys. Rev. Lett. **78**, 1335 (1997).
- [78] L. P. Kouwenhoven, D. G. Austing, and S. Tarucha, Rep. Prog. Phys. **64**, 701 (2001).
- [79] A. V. Khaetskii and Y. V. Nazarov, Phys. Rev. B **61**, 12639 (2000).
- [80] B. I. Halperin *et al.*, Phys. Rev. Lett. **86**, 2106 (2001).
- [81] I. L. Aleiner and V. I. Fal'ko, Phys. Rev. Lett. **87**, 256801 (2001).
- [82] M. I. D'yakonov and V. Y. Kachorovskii, Sov. Phys. Semicond. **20**, 110 (1986).

- [83] S. Amasha *et al.*, cond-mat/0607110 (unpublished) .
- [84] J. D. Jackson, *Classical Electrodynamics* (John Wiley & Sons, Inc., New York, 1999).
- [85] F. H. L. Koppens *et al.*, Nature **442**, 766 (2006).
- [86] M. Borhani, V. N. Golovach, and D. Loss, Phys. Rev. B **73**, 155311 (2006).
- [87] F. Bloch, Phys. Rev. **70**, 460 (1946).
- [88] R. K. Wangsness and F. Bloch, Phys. Rev. **89**, 728 (1953).
- [89] F. Bloch, Phys. Rev. **105**, 1206 (1957).
- [90] C. Cohen-Tannoudji, B. Diu, and F. Laloë, *Quantum Mechanics, Vol. II* (John Wiley & Sons, New York, 1977).
- [91] F. Meier and B. P. Zakharchenya (eds.), *Optical orientation* (North-Holland, Amsterdam, 1984).
- [92] F. Bayen, M. Flato, C. Fronsdal, A. Lichnerowicz, and D. Sternheimer, Ann. Phys. (N.Y.) **111**, 61 (1978).
- [93] F. Bayen, M. Flato, C. Fronsdal, and a. D. S. A. Lichnerowicz, Ann. Phys. (N.Y.) **111**, 111 (1978).
- [94] M. Trif, V. N. Golovach, and D. Loss, Phys. Rev. B **75**, 085307 (2007).
- [95] M. Berry, Proc. Roy. Aca. A **392**, 45 (1984).
- [96] B. Simon, Phys. Rev. Lett. **51**, 2167 (1983).
- [97] F. Wilczek and A. Zee, Phys. Rev. Lett. **52**, 2111 (1984).
- [98] Y. Aharonov and J. Anandan, Phys. Rev. Lett. **58**, 1593 (1987).
- [99] A. S. F. Wilczek (eds.), *Geometric Phases in Physics* (World Scientific, Singapore, 2002).
- [100] P. Zanardi and M. Rasetti, Phys. Lett. A **264**, 94 (1999).
- [101] E. Sjöqvist, Physics **1**, 35 (2008).
- [102] L.-M. Duan, J. I. Cirac, and P. Zoller, Science **292**, 1695 (2001).
- [103] J. A. Jones, V. Vedral, A. Ekert, and G. Castagnoli, Nature **403**, 869 (2000).

- [104] W. A. Coish, V. N. Golovach, J. C. Egues, and D. Loss, *Physica Status Solidi (b)* **243**, 3658 (2006).
- [105] V. N. Golovach, M. Borhani, and D. Loss, *Phys. Rev. B* **74**, 165319 (2006).
- [106] C. Flindt, A. S. Sorensen, and K. Flensberg, *Phys. Rev. Lett.* **97**, 240501 (2006).
- [107] D. V. Bulaev and D. Loss, *Phys. Rev. Lett.* **98**, 097202 (2007).
- [108] P. San-Jose, B. Scharfenberger, G. Schön, A. Shnirman, and G. Zarand, *Phys. Rev. B* **77**, 045305 (2008).
- [109] M. Nakahara, *Geometry, Topology and Physics* (IOP Publishing Ltd., 1990).
- [110] R. Held *et al.*, *Appl. Phys. Lett.* **73**, 262 (1998).
- [111] A. Fuhrer *et al.*, *Nature* **413**, 822 (2001).
- [112] R. Hanson and G. Burkard, *Phys. Rev. Lett.* **98**, 050502 (2007).
- [113] M. Borhani and D. Loss, *Phys. Rev. A* **71**, 034308 (2005).
- [114] H. J. Briegel, D. E. Browne, W. Dür, R. Raussendorf, and M. V. den Nest, *Nature Physics* **5**, 19 (2009).
- [115] L. D. Landau, *Sov. Phys. JETP* **3**, 920 (1957).
- [116] D. Pines and P. Nozieres, *The Theory of Quantum Liquids* (Benjamin, New York, 1966).
- [117] G. F. Giuliani and G. Vignale, *Quantum Theory of the Electron Liquid* (Cambridge University Press, Cambridge, England, 2005).
- [118] H.-J. Schulze, P. Schuck, and N. V. Giai, *Phys. Rev. B* **61**, 8026 (2000).
- [119] R. Asgari *et al.*, *Phys. Rev. B* **71**, 045323 (2005).
- [120] M. Holzmann, B. Bernu, V. Olevano, R. M. Martin, and D. M. Ceperley, arXiv:0810.2450 (unpublished) .
- [121] A. V. Chubukov and D. L. Maslov, *Phys. Rev. B* **68**, 155113 (2003).
- [122] J. J. Quinn and R. A. Ferrell, *Phys. Rev.* **112**, 812 (1958).
- [123] G. Burkard, D. Loss, and E. V. Sukhorukov, *Phys. Rev. B* **61**, R16303 (2000).
- [124] S. Q. Murphy, J. P. Eisenstein, L. N. Pfeiffer, and K. W. West, *Phys. Rev. Lett.* **52**, 14825 (1995).

Curriculum vitae

for Massoud Borhani

Born: 8 June 1980

Nationality: Iranian

Education

- 1986 - 1990 Elementary School, Yazd, Iran
- 1990 - 1993 Shahed Secondary School, Yazd, Iran
- 1993 - 1997 Nemooneh Malek Sabet High School, Yazd, Iran
- 1997 - 2002 Bachelor of Physics, Sharif University, Tehran, Iran
- 2004 - 2004 Master of Physics, University of Basel, Basel, Switzerland
- 2004 - 2008 Ph.D. of Physics, University of Basel, Basel, Switzerland
- Aug. 2002 B.Sc. in Theoretical Physics
- Bachelor project under the supervision of Prof. R. Mansouri
- “ Spherically Symmetric Thick Branes in Vacuum ”
- Oct. 2004 M.Sc. in Theoretical Physics
- Master thesis under the supervision of Prof. Dr. D. Loss
- “ Cluster States From Heisenberg Interaction ”
- 2004 - 2008 Ph.D. student under the supervision of Prof. Dr. D. Loss

Publications

- Massoud Borhani, Daniel Loss
Plasmonic Corrections to the Electron Self Energy in Two Dimensional Electron Liquid
(in preparation)
- Vitaly N. Golovach, Massoud Borhani, Daniel Loss
Holonomic Quantum Computation with Electron Spins in Quantum Dots
Phys. Rev. A **81**, 022315 (2010) (arXiv:0908.2800v2)
- Björn Trauzettel, Massoud Borhani, Mircea Trif, Daniel Loss
Theory of Spin Qubits in Nanostructures
JPSJ, Special Topics: Advances in Spintronics.
J. Phys. Soc. Jpn. **77**, 031012 (2008) (arXiv:0707.4622)
- Vitaly N. Golovach, Massoud Borhani, Daniel Loss
Electric Dipole Induced Spin Resonance in Quantum Dots
Phys. Rev. B **74**, 165319 (2006) (cond-mat/0601674)
- Massoud Borhani, Vitaly N. Golovach, Daniel Loss
Spin Decay in a Quantum Dot Coupled to a Quantum Point Contact
Phys. Rev. B **73**, 155311 (2006) (cond-mat/0510758)
- Massoud Borhani, Daniel Loss
Cluster States From Heisenberg Interaction
Phys. Rev. A **71**, 034308 (2005) (quant-ph/0410145)
- Massoud Borhani, Reza Mansouri, Samad Khakshournia
Spherically Symmetric Thick Branes in Vacuum
Int. J. Mod. Phys. A **19**, 4687 (2004) (hep-th/0301228)